

Chapter 3: Understanding the mechanism of insecticide resistance in *Callosobruchus chinensis* via transcriptomic approach

3.1 Introduction

Callosobruchus chinensis (Coleoptera: Bruchidae) is a highly destructive pest of stored grains that is widely distributed worldwide. It is a major feeder and infests a range of commodities and stored items that are vital to both global food security and human nutrition. Furthermore, it has main colonisation characteristics, enabling larvae and adults to readily infiltrate kernels even when moisture levels are low, ultimately culminating in their life cycle being fulfilled within intact whole grain kernels. Consequently, the majority of life stages, particularly the larvae, remain unaffected by contact pesticides that are administered topically to the outer surface of the grain kernel. Significantly, *C. chinensis* exhibits a considerable increase in population size, leading to severe levels of infestation, particularly under conditions of ideal temperatures. The global investigation of *C. chinensis* management in stored grain and other commodities has been documented by Kumar (2017), Nayak and Daglish (2018), Yaseen et al. (2019), and Guru et al. (2022).

The use of synthetic chemical pesticides has been crucial in the management of insect pests in agricultural sites (Damalas and Koutroubas 2016; Ebadollahi et al., 2020). Nevertheless, the extensive use of pesticides can result in the development of insecticide resistance, deterioration of the ecosystem, pollution of subsurface water and soil, and unintended damage to non-target species. For instance, methyl bromide and phosphine are often employed as pesticide chemicals due to their exceptional efficacy in pest management. However, the use of methyl bromide has been gradually discontinued due to its detrimental impact on the ozone layer, while phosphine has experienced a decline in efficacy due to the development of insect resistance in a number of countries (Wang et al., 2020; Oppert et al., 2015; Pimentel et al., 2010). Fields and White (2002) argue that the use of alternative pesticides, such as sulfuryl fluoride, ethyl formate, and hydrogen cyanide, is accompanied by several drawbacks. As a result, there has been a growing inclination towards employing disinfestation strategies that are both less toxicologically and environmentally harmful in the control of stored-grain pests.

According to a recent study conducted by Zhou et al. (2017), it has been observed that introduction to sub-lethal levels of insecticides can have significant impacts on the

reproductive capacity, developmental processes, and chemical susceptibility of insects. These effects have the potential to contribute to the resurgence of pest populations. The process of detoxification in insects may be broadly categorized into three distinct phases: phase I, phase II, and phase III, as described by Xu et al. (2005). Phase I involves the first metabolic reactions, phase II encompasses the involvement of metabolising enzymes, and phase III pertains to the participation of transporters. The enzymes that play a key role in the phase I and phase II detoxification pathways include P450 monooxygenase, glutathione S-transferase (GST), and carboxylesterase (CarE) (Xiao et al., 2018). Conversely, the principal constituents of phase III are the ATP-binding cassette (ABC) transporters (Ferreira et al., 2014).

The enzymes responsible for detoxification, including *care*, *gst*, and *cest*, play a crucial role in the processes of insect resistance. It is imperative to note that an elevation in the activity of these enzymes is essential for effective pesticide metabolism (Qi et al., 2016). In a previous study conducted by Wang and Liu, (2014), it was shown that the levels of GST and MFO activity in two different colour morphs of the pea aphid *Acyrtosiphon pisum* exhibited an increase when exposed to escalating sublethal doses of abamectin for a duration beyond 24 hours. According to Ru et al., (2017), the expression levels of CarE, GST, and MFO in *Tetranychus urticae* were notably increased 12 hours after being exposed to abamectin. In a similar manner, the application of avermectin led to a considerable increase in the activity of CarE, GST, and MFO in *S. furcifera*. This induction was observed at 6, 12, and 24 hours after treatment. The results of this study suggest that insects have the ability to adjust to the stress caused by avermectin through the activation of their detoxifying enzymes.

Furthermore, following the administration of thiamethoxam and buprofezin, the enzymatic activity of CarE exhibited a general pattern of early upregulation followed by suppression. Notably, the maximum level of activity was seen at the 6-hour time point. The application of thiamethoxam and buprofezin resulted in a notable increase in GST activity in *S. furcifera*. Conversely, these insecticides were seen to typically limit the action of MFO. In a previous study conducted by Wu et al., (2016), it was observed that the activities of GST and P450 in *Aphis craccivora* were significantly increased following a 48-hour treatment with cyclozaprid and imidacloprid. However, the activity of CarE was found to be inhibited, although the difference observed was

not statistically significant. Furthermore, Shang et al., (2017) reported that the application of imidacloprid to *Cydia pomonella* resulted in a notable increase in the activity of CarE and GST enzymes. Conversely, the activity of MFO enzymes was greatly suppressed. The results of this study indicate that the involvement of MFO in the insect's reaction to stress caused by neonicotinoid pesticides may not be significant. Instead, the principal detoxification enzymes responsible for this response are CarE and GST. The aforementioned findings suggest that insects possess detoxification enzymes that allow them to effectively cope with the stress caused by low levels of pesticide exposure. However, it is important to note that the induction of protective enzymes such as CarE, GST, and MFO varies across various insect species and occurs at varied time intervals. Furthermore, it has been observed that the primary enzymes engaged in the process of detoxification exhibit a dependence on the specific species involved.

Multiple studies have demonstrated that insects with resistance tend to have elevated levels of P450 dependent monooxygenases, which are enzymes that play a role in catalysing reactions involving hazardous substances (Gilbert et al., 2005; Feyereisen, 2006). Several investigations have demonstrated that the amplification of transferase gene has a role in the sequestration and detoxification of several endogenous and xenobiotic chemicals, including insecticides (Raymond al., 1989; Field et al., 1988; Sanilet al., 2014). The examination of the mechanism behind metabolic resistance to carbamates, organophosphates, and pyrethroids has provided insights into the involvement of esterases, particularly carboxylesterases, in insect species that exhibit resistance (Hemingway et al., 2004; Liu et al., 2019; Li et al., 2007; Lilly 2016; Bass et al., 2014; Puntaet al., 2012). These enzymes possess the ability to sequester pesticide substrates through two primary processes. There are two factors that have been seen to contribute to the phenomenon under investigation: the overexpression of one or more esterases, and mutations in the gene responsible for encoding esterase (Hemingway et al., 2004).

The primary mechanism implicated in pesticide resistance of *T. castaneum* is the augmentation of detoxification processes mediated by cytochrome P450 enzymes. The CYP450 gene CYP6BQ9 exhibited a 200-fold increase in expression in the QTC279 strain of *T. castaneum* that is resistant to deltamethrin. This upregulation implies that CYP6BQ9 plays a substantial role in the metabolism of deltamethrin in *T.*

castaneum (Zhu et al., 2010). The use of functional genomic and quantitative reverse transcription polymerase chain reaction (qRT-PCR) techniques has facilitated the identification of a noteworthy upregulation of CYP6BQ9 expression in the brain. This heightened expression potentially augments the brain cells' capacity to efficiently catalyse deltamethrin, so fortifying the defences of the target location. This finding was reported in a study by Zhu et al., (2010).

Furthermore, an experimental approach involving RNA interference (RNAi) was employed to investigate the potential involvement of transcription factors in the regulatory mechanism behind the upregulation of the CYP6BQ9 gene. Among the seven transcription factors that were examined, it has been determined that the CncC and Maf transcription factors play a crucial role in the activation of CYP6BQ genes and are accountable for the development of deltamethrin resistance in *T. castaneum* (Kalsi and Palli, 2015). In a separate investigation, the utilisation of RNA sequencing, RNA interference knockdown, and quantitative real-time polymerase chain reaction (qRT-PCR) techniques provided evidence for the participation of CncC in the control of gene expression related to various detoxification processes. These processes encompass phase I (P450s), phase II (GSTs), and phase III (ABC transporters) detoxification mechanisms in a strain of *T. castaneum* that exhibits resistance to pyrethroid insecticides (Kalsi and Palli, 2017). Both investigations indicate that the presence of the transcription factor CncC is necessary for the activation of genes that encode proteins involved in the breakdown of xenobiotics. Numerous investigations conducted on flies and beetles have documented the role of CncC in regulating the expression of genes that encode proteins engaged in phase I (P450s) and phase II (GSTs) detoxification processes (Sykiotis et al., 2010; Misra et al., 2011). The glutathione S transferase (GSTs) represents a superfamily of multifunctional enzymes that play a crucial role in the development of pesticide resistance (Lewis et al., 1988). The enzymes facilitate the metabolic process of insecticides by a conjugation reaction with reduced glutathione, resulting in the formation of hydrophobic xenobiotics. Consequently, water-soluble metabolites are generated, which may be readily eliminated from the body. The classification of insect GSTs was determined by their cellular localization, namely as cytosolic, microsomal, or mitochondrial entities. (Ladner et al., 2004; Shi et al., 2012). These GSTs belong to several protein classes in arthropods, including Delta, Epsilon, Sigma, Theta, Omega, and Zeta (Friedman et al.,

2011). The act of sequencing the genome of the insect presented a valuable chance to detect and analyse the genome-wide distribution of GSTs (Shi et al., 2012; Han et al., 2016; Zhou et al., 2019). This platform facilitates a more comprehensive comprehension of the evolutionary process of pesticide resistance in arthropods. Previous research has indicated that the Epsilon class of glutathione S-transferases (GSTs) encodes enzymes that play a crucial role in the degradation of certain pesticides, including DDT and pyrethroids, in *Aedes aegypti* (Ortelli et al., 2003) and *Anopheles gambiae*. The existence of increased epsilon GSTs in *T. castaneum* suggests that this insect species retains better pesticide resistance and tolerance, as evidenced by the detoxifying capabilities of the Epsilon class of GSTs in other insects (Shi et al., 2012). Furthermore, it has been shown that the delta class of glutathione S-transferases (GSTs) in *T. castaneum* plays a crucial role in the defence against toxic substances and the acquisition of resistance to certain insecticides (Chen et al., 2016). Understanding the mechanism by which GST mediates detoxification is crucial for early detection of resistance, pre-emptively eliminating the specific insecticide prior to the fixation of resistance alleles in populations, and facilitating the development of potent insecticidal molecules.

Carboxylesterases are a class of enzymes that exhibit a broad distribution throughout several biological systems and have a pivotal function in the detoxification of xenobiotics, namely esters. The enzymes in question belong to the esterase family and have been identified in several creatures across the biological spectrum. These entities, as indicated by their nomenclature, participate in hydrolysis processes, facilitating the conversion of carboxyl esters into carboxylic acid and alcohol. The process of hydrolyzing the ester bond encompasses the hydrolysis of a wide variety of ester substrates, including phospho, thio, carboxylic, and other esters. The hydrolysis reaction of carboxylesterases involves a two-stage process. In the first phase, the oxygen of a serine residue performs a nucleophilic assault on the carbonyl group of the substrate, resulting in the removal of the alcohol product. This step also leads to the formation of acyl enzymes, which are generally stable. Furthermore, it should be noted that a water molecule assumes the role of an intermediate agent, facilitating a nucleophilic assault that results in the removal of the acid product generated during the reaction and afterwards yielding the liberated enzyme. The aforementioned response mechanism is responsible for the development of pesticide resistance in

several insect species. Esterases have been extensively studied in the context of xenobiotic metabolism and resistance, since they play a crucial role in the detoxification mechanism. The level of carboxylesterase expression was found to be notably higher in the *Aphis gossypii* resistant to organophosphorus compounds compared to the susceptible strain (Cao et al., 2008). The pyrethroid-resistant species *Musca domestica* was shown to have increased carboxylesterase activity and expression (Zhang et al., 2017). Furthermore, the heightened enzymatic activity of CarE was seen to confer tolerance to cypermethrin in *Musca domestica*. In a study conducted by Small and Hemingway, (2000), it was observed that the rise of CarE activity in both OP resistant and susceptible species of *Nilaparvata lugens*, together with the corresponding increase in CarE mRNA expression, indicated a potential association between CarE mRNA and OP resistance in *Nilaparvata lugens*. The potential of carboxylesterases to detoxify harmful substances and the capacity of certain carboxylesterases to be induced can serve as biomarkers for evaluating tolerance to certain xenobiotics.

The ABC transporters encompass a diverse group of proteins that facilitate the transportation of many substances, including inorganic ions, carbohydrates, amino acids, lipids, lipopolysaccharides, peptides, metals, and xenobiotics (Zhou et al., 2019). In the realm of insects, this particular family may be further categorised into eight prominent subfamilies denoted by the letters A through H (Helmkamp et al., 2015). Research on ABC transporters has demonstrated their ability to transport molecules that are structurally unrelated. As a result, there is a growing emphasis on investigating the functions of these proteins in the transportation of foreign drugs and in the development of pesticide resistance in insects. Recent research has indicated a clear correlation between the expression of ABC transporters and the emergence of pesticide resistance (Pohl et al., 2012; Dermauw and Van Leeuwen, 2014).

It has been previously observed that the expression levels of an ABCG gene and an ABCC gene were increased in *S. furcifera* when exposed to a high concentration (LC₈₅) of cycloxyaprid. Conversely, the expression levels of two ABCG genes were increased when exposed to a low concentration (LC₁₅) of this insecticide (Yang et al., 2016). According to Bariami et al. (2012), the use of transcriptome sequencing has provided insights into the expression patterns of the ABCB, ABCC, and ABCG subfamily genes in a pyrethroid-resistant *Aedes aegypti*, indicating their high levels of

expression. In a similar vein, previous studies have demonstrated that there is a notable upregulation of gene expression in resistant species of *Myzus persicae* belonging to the ABCG and ABCH subfamilies, as evidenced by microarray experiments (Silva et al., 2012). Additionally, it has been observed that the expression levels of ABCG subfamily genes are elevated in DDT-resistant strains of *Anopheles arabiensis* (Jones et al., 2012). The involvement of ABCG subfamily genes in conferring resistance to insecticides has been extensively documented in several insect species (You et al., 2013; Yang et al., 2016; Sun et al., 2017; Xiao et al., 2018). In the case of *S. fuscifera*, it has been observed that highly expressed ABCG genes are closely linked to the development of cross-resistance in this insect. Nevertheless, it is imperative to validate these deductions by empirical investigations. In a study conducted by Xiao et al. (2018), it was shown that the application of malathion, abamectin, and beta-cypermethrin in *Bactrocera dorsalis* resulted in a substantial upregulation of 4, 10, and 14 ABC genes, respectively. The study conducted by Sun et al. (2017) utilised quantitative polymerase chain reaction (qPCR) analysis to examine the expression levels of eight ABC transporters belonging to the ABCB/C/D/G subfamilies in *Laodelphax striatellus*. The findings indicated that these transporters were significantly upregulated in species resistant to chlorpyrifos, deltamethrin, and imidacloprid, in comparison to a susceptible species. According to a study conducted by You et al. (2013), RNA sequencing (RNA-seq) analysis revealed an upregulation of ABC transporters belonging to the subfamilies ABCA/C/G/H/F in chlorpyrifos-resistant species of *Plutella xylostella*. However, despite the valuable knowledge acquired from these aforementioned investigations, our present comprehension of the involvement of ABC transporters in pesticide resistance among insects, particularly in the case of *C. chinensis*, remains constrained.

The numerous impacts of pesticides on insects encompass several sublethal effects, such as alterations in insect behaviour, reproduction, development, and the development of resistance to insecticides. Furthermore, the adaptation of insects to stress caused by insecticides involves a multifaceted metabolic detoxification process that encompasses the involvement of several enzymes. The examination of the genome and transcriptome of *C. chinensis* has the potential to offer valuable knowledge on the intricate regulatory networks involved in its evolutionary processes. Additionally, such studies may contribute to the development of strategies to enhance

resistance to xenobiotics (Kolawole and Kolawole, 2014). The scarcity of available literature on *C. chinensis* poses significant challenges in comprehending the molecular mechanisms involved in investigating the developmental, physiological, and biochemical features of this insect species. In recent years, there has been a noticeable advancement in sequencing technology, characterised by an augmentation in the length of sequence reading. Additionally, significant progress has been made in the development of de novo transcriptome assembly software tools, enabling the assembly of transcriptomes in the absence of a reference genome. The aforementioned methodology has been recently employed for the purpose of constructing transcriptomes de novo in a limited number of beetle species (Sayadi et al., 2016; Raghavan et al., 2022). The sequencing and publication of the transcriptome of *C. maculatus* by Sayadi et al. (2016) has provided a valuable resource for conducting gene expression research and investigating the functional properties of genes involved in several biological processes inside this organism at the molecular level.

Hence, the objective of this work was to get a deeper understanding of the functions performed by these enzymes and genes in the reaction of C. chinensis when subjected to deltamethrin.

3.2 Materials and Methodology

Experimental regime

As discussed in chapter 2, two sublethal concentration of deltamethrin were given to *C. chinensis* for 7 days. The insects were sacrificed on the 8th day and were used for further applications.

Gene Identification

The transcriptome database of *C. chinensis* was sequenced and annotated using the Rna-seq method, as detailed in a recent study by Sayadi et al. (2016). The transcriptome data was assembled using Geneious R9 software (Kearse et al., 2012), with the published gene of *C. maculatus* serving as a reference, in order to retrieve the matching sequences for *C. chinensis*. Furthermore, each of the purported sequences was employed as a query in order to conduct a search on the protein database of the National Centre for Biotechnology Information (NCBI) (<http://www.ncbi.nlm.nih.gov>) in order to further corroborate their authenticity.

RNA isolation

Total RNA was isolated from 40mg dissected tissues (pulling out the tissue from the insects). Tissues were homogenized using homogenizer in 500µl TRIzol reagent (Invitrogen). The homogenate was taken into 2 ml micro centrifuge tubes (Tarsons). After successful homogenization, equal volume of Trizol reagent was added. For complete dissociation of nucleoprotein complexes, homogenized samples were incubated for 5 minutes at room temperature. The incubation was followed by the addition of 400ul chloroform and was vigorously shaken for effective mixing of both the solutions. The samples were kept at room temperature for 5 minutes till the aqueous and organic layers are distinct. Thereafter, the tubes were subjected to centrifugation at 12,000x g for 15 minutes at 4°C. The mixture was separated into a lower red phenol-chloroform phase, an interphase, and a colourless upper aqueous phase. An aliquot of upper aqueous phase will then be transferred into a new 1.5 ml micro centrifuge tube. Precipitation was done by adding 500 µl of isopropanol to the transferred supernatant. The samples were kept in -20°C for 10 minutes, centrifuged at 12,000x G for 15 minutes at 4°C. After precipitation the supernatant was discarded without disturbing the pellet and was washed in 1000µl of 75% ethanol and then 300 µl absolute ethanol was added to the pellet. Effective mixing was done by gentle inversion and was further subjected to centrifugation at 7,500 x g for 7 minutes at

4°C. The pellets were air dried and was resuspended by adding 50 µl of DEPC water (Diethylpyrocarbonate) and was incubated at room temperature for 10mins (**Fig. 3.1**).

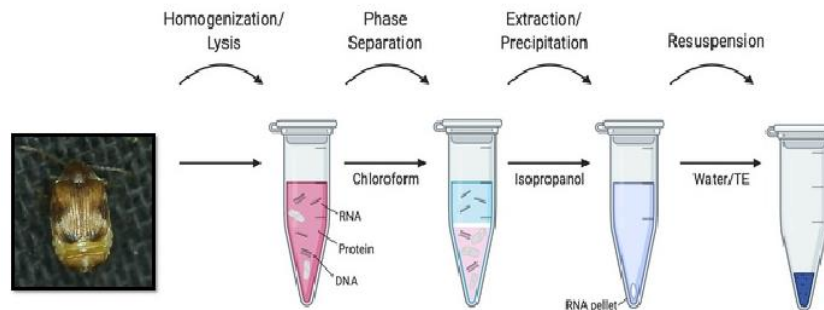


Figure 3.1 Depicts the steps in RNA isolation

Quantification of RNA:

Prior to quantification, DNAase (Thermo Scientific) treatment was performed. 1 µg of 10X RNA reaction buffer with MgCl₂ was added to the tube and incubated at 37 °C for 30 min. Then after 20 µl chelating agent EDTA added in 50 mM concentration and will incubate at 65°C for 10 min in water bath as RNA get hydrolyzed during heating with divalent cations in the absence of a chelating agent. RNA quantification was done by taking A₂₆₀/A₂₈₀ ratio using Perkin Elmer spectrophotometer. This ratio reveals the presence of contaminants and gives evidence of possible degradation. An A₂₆₀/A₂₈₀ ratio of 1.8 is considered acceptable for RNA. 5µl of template RNA was aliquoted and added to 1.5ml micro centrifuge tube. To the aliquot, 995µl of nuclease free water was added and absorbance was measured at the mentioned ratio against the blank having 1000µl of nuclease free water.

The concentration of RNA was done using following standard formula:

1 OD₂₆₀ corresponds to 40 µg/mL of RNA.

$$\text{Amount of DNA } (\mu\text{g/mL}) \text{ (ng/}\mu\text{L)} = \text{OD at } 260\text{nm} \times 40 \times \text{dilution factor}$$

Dilution Factor generally taken is 200.

Illumina PE library preparation

The RNA-Seq paired end sequencing libraries were prepared from the QC passed RNA samples using illumina TruSeq Stranded mRNA sample Prep kit. Briefly, mRNA was enriched from the total RNA using Poly-T attached magnetic beads, followed by enzymatic fragmentation, 1st strand cDNA conversion using SuperScript II and Act-D mix to facilitate RNA dependent synthesis. The 1st strand cDNA was

then synthesized to second strand using second strand mix. The dscDNA was then purified using AMPureXP beads followed by A-tailing, adapter ligation and then enriched by limited no of PCR cycles.

Transcriptome Assembly and Comparative Expression Analyses

The assemblies utilised in our ultimate analysis were generated using Trinity version 2013_08_14 (Grabherr et al., 2011) with no modifications to the default parameters, save for adjusting the minimum contig length to 200. The research conducted by Song et al. (2015) employed the Trimmomatic programme, specifically for the purpose of performing the Illuminaclip test (Illuminaclip Leading:3 Trailing:3 Sliding window: 4:15 Minlen:36). The procedure of generating comprehensive assemblies involved including readings from all temporal intervals, whereas individual assemblies were built just utilising the data collected from each respective sampling time point. The DeconSeq standalone version 0.4.3 was utilised to do the analysis of the whole assemblies, following the methodology outlined by Schmieder and Edwards (2011). The investigation was carried out with the use of certain characteristics, namely an identification threshold of 95% and a classification threshold of 95%. The databases that were examined as part of the inquiry encompassed the bacterial, fungal, viral, and protozoan databases. The comparative expression analyses were conducted by aligning reads from each time point to the combined assemblies using RSEM, which is a tool included in the Trinity module (Li & Dewey, 2011). The alignment and estimation of abundance were performed using the align_and_estimate_abundance.pl script. The research employed the RSEM methodology, which is founded on the RNA-Seq by Expectation-Maximization approach, in conjunction with the Bowtie alignment tool. The aforementioned methodology was utilised to conduct a comparative study of RNA samples at various stages, as well as the compiled dataset. The script abundance_estimates_to_matrix.pl was subsequently executed, employing cross-sample normalisation using the Trimmed Mean of M-values technique. The run_DE_analysis.pl script was utilised to conduct edgeR analysis, afterwards followed by the analyze_diff_expr.pl script to extract the transcripts demonstrating the greatest differential expression and group them into clusters. To control the false discovery rate (FDR), a significance threshold of 0.001 was utilised. Additionally, a minimum absolute $\log_2(a/b)$ change of 2, which corresponds to a 4-fold change, was implemented. The Euclidean metric was employed for gene_dist, whilst the full

method was utilised for gene_clust. The study presents data about the "as-isoform," with more information on the "as-gene" available in the Supporting Information files. The assessment of gene completeness was performed with the BUSCO v1.1b1 software, following the methodology outlined by Hara et al. (2015) and González-Aravena et al. (2019). The research utilised the Ortholog Hit Ratio approach to ascertain the percentage of orthologous sequences that had the greatest level of resemblance when compared to the *T. castaneum* Tcas3.31.pep.all.fa peptide collection. The study was performed use a BlastX threshold of E-5, following the methodology outlined in O'Neil et al. (2010).

Bioinformatic analysis

The assembled unigenes were searched against the NCBI nr sequence database (<ftp://ncbi.nih.gov>), the Swiss-Prot database (http://web.expasy.org/docs/swiss-prot_guideline.html), kyoto encyclopedia of genes and genome (KEGG, <http://www.genome.jp/kegg/>), cluster of orthologous groups (COG) and eukaryotic orthologous groups (KOG) (<ftp://ncbi.nih.gov/pub/COG/COG>) with the BLASTX algorithm (accessed in Sept 2012). The E-value cut-off was set at 10^{-5} . Genes were tentatively identified based on the best hits against known sequences. Blast2GO was used to predict the functions of the sequences, to assign gene ontology (GO) terms (<http://www.geneontology.org/>), and to predict the metabolic pathways in COG and KEGG databases. Amino acid sequences were deduced by using ORF Finder (<http://www.ncbi.nlm.nih.gov/gorf/gorf.html>) and GENSCAN (<http://genes.mit.edu/GENSCAN.html>). The putative protein sequences were used for alignment by ClustalX (v1.83) program. Using ORF finder2, we identified the open reading frames (ORFs) of the genes and determined the amino acid sequences of the encoded proteins. The Pfam program³ and a search of the NCBI Conserved Domain Database⁴ were used to identify the conserved domains (nucleotide-binding and transmembrane domains) of all putative genes.

Quality trimming

The quality assessment of RNA reads acquired from sequencing was performed using FastQC v.0.11.2 (Andrews, 2015). The removal of Illumina adapter sequences from the reads was performed using cutadapt v.1.2.1, as described by Martin (2011). The Cutadapt software will do a search for a provided set of adapters within all the reads. It is necessary for there to be a minimum overlap of 15 base pairs between the adapter

and the read. The process of searching for adaptors is performed twice during each reading in order to eliminate adaptors in a consecutive manner. In order to improve the quality of the scans, Trimmomatic v.0.3 was used to trim the poor-quality reads located at the 3' and 5' ends. This was achieved by scanning the reads using a sliding window of 4 bases, and removing any leading or trailing bases that had an average phred quality score below 20. Reads of a length less than 50 base pairs (Bolger et al., 2014) were also excluded from the analysis. The process of de novo assembly of the transcriptome. The process of digital normalisation and transcriptome de novo assembly was performed using the Trinity 2.0.6 programme, employing a default k-mer size of 25. The Trinity system is comprised of three distinct modules, namely Inchworm, Chrysalis, and Butterfly. The Inchworm algorithm constructs a K-mer dictionary using the reads, facilitating the subsequent assembly of contigs. The Chrysalis algorithm employs a de Bruijn network methodology to merge overlapping contigs into cohesive components. As a concluding measure, Butterfly streamlines the entirety of the produced graphs to present comprehensive transcripts and their alternatively spliced counterparts (Haas et al., 2013). DeconSeq standalone version 0.4.3 (Schmieder and Edwards, 2011) was used to detect and eliminate sequence contaminations from the assembled transcriptome, utilising bacterial, fungal, plant, viral and other databases. The DeconSeq tool was executed with an alignment identity threshold of 95% (-i 95) and an alignment coverage criterion of 90% (-c 90). The clustering of assembled transcripts was performed using CD-HIT-EST version 4.6.1 (2012-08-27) with the default parameters. Two sequence identity thresholds were applied, namely 100% and 98%. To evaluate the quality of the assembled transcriptomes, we conducted an assessment of the quantity of paired-end reads that were detected within the assembled transcripts. In order to accomplish this, the Bowtie software (version 0.12.6) developed by Langmead et al. in 2009 was employed to align all the unprocessed reads with the assemblies. To mitigate the risk of overestimating transcriptome quality during the mapping process, only a single position was given for reads that mapped to several sites.

The procedure of assigning functional annotations to the transcriptome. The annotation procedure was performed with Blast2go version 3.2 (Conesa et al., 2005) and the Trinotate pipeline (<https://trinotate.github.io/>). The putative genes that were built underwent queries against several databases, such as the NCBI protein database

(Nr), Swissprot-Uniprot database, Kyoto Encyclopaedia of Genes and Genomes (KEGG), Gene Ontology (GO), EggNog, and InterproScan. The search was performed with BlastX, employing an E-value threshold of 10^{-5} , as described by Altschul et al. (1990) and Kanehisa et al. (2012).

The process of predicting open reading frames (ORFs) in genes was carried out using Transdecoder v.2.0.1, a software application accessible at <http://transdecoder.sourceforge.net/>. We specifically chose projected open reading frames (ORFs) that had a minimum length of 100 amino acids, irrespective of their completeness as partial or full sequences. The Open Reading Frames (ORFs) underwent a BlastP analysis against the NCBI Uniref90 database, with an E-value threshold of 10^{-6} as outlined by Altschul et al. (1990). The subsequent functional annotation was carried out using Blast2GO and Trinotate. The Trinotate pipeline utilises a multitude of software tools: The software tools employed in this investigation consist of Hmmer v.3.1b1, a software programme designed for protein domain identification known as PFAM (Finn et al., 2011). The software Tmhmm v.2.0c, developed by Krogh et al. (2001), is utilised for the purpose of predicting transmembrane helices in proteins. The software tool Rnammer v.1.2, developed by Finn et al. (2011), is utilised for the purpose of forecasting ribosomal RNA. The software SignalP v.4.1 is employed to forecast the locations where signal peptides are cleaved (Lagesen et al., 2007; Petersen et al., 2011). Gene ontology prediction is performed using GOseq (Young et al., 2010), and orthologous group search is conducted using eggNog v.3.0 (Powell et al., 2012). The assessment of gene integrity in the assembled transcriptome was performed utilising the BUSCO (Benchmarking Universal Single-Copy Orthologs) library, as outlined in the study by Hara et al. (2015). The library may be accessible using the following URL: <http://busco.ezlab.org/>. The use of the KEGG database and InterProScan software is a key aspect of Blast2GO's operations (Zdobnov et al., 2001). Figure 3.2 illustrates the visual representation of the several stages involved in the assembly of the transcriptome. This depiction offers a comprehensive picture of the whole process. The overall workflow, summarizing the transcriptome assembly steps, is presented graphically in **Fig 3.2**

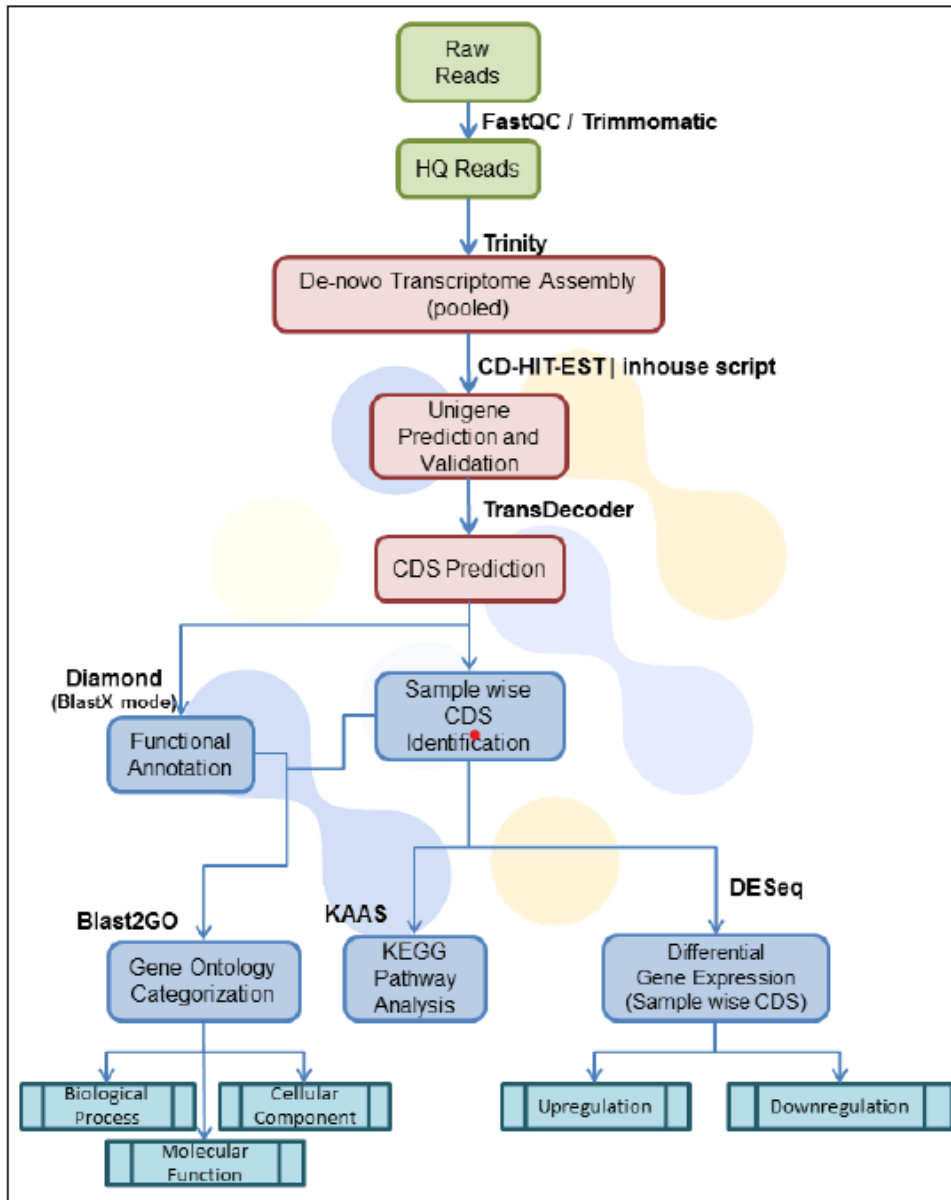


Figure 3.2: Depicts summary of the transcriptome assembly steps

Validation of few differentially expressed genes

To identify the common genes upregulated in response to treatment with the deltamethrin and to verify whether these genes show similar patterns of regulation qPCR was performed.

cDNA Synthesis:

After the purity check of RNA was validated using spectrophotometer, the RNA template then reversed transcribe to form cDNA from tissue. A cDNA kit employed from Thermo scientific- AB-1453/A. Briefly, fresh nuclease free PCR tubes (Tarsons) was taken, in which 4µl of 5X cDNA synthesis buffer, 2µl dNTP mix, 1µl of RNA

primer (oligonucleotides), 1 µl of RT enhancer, 1 µl of verso enzyme mix, 1-2 µl of RNA template (according to the spectroscopic quantification i.e., 1 ng) and the final assay volume was made to 20 µl using nuclease free water. The tubes effectively mix by giving a short centrifuge spin for 30s at around 2000 xg. The tubes containing the kit mixture was PCR amplified by 2 step reaction process. Firstly, the 1 cycle of cDNA synthesis was carried out at 42°C for 30 mins followed by 1 cycle of inactivation at 95°C for 2mins.

Table 3.1: Reaction mix for cDNA synthesis

	Volume
5X cDNA synthesis buffer	4 µL
dNTP Mix	2 µL
anchored oligo dT /random hexamers	1 µL
RT Enhancer	1 µL
Verso Enzyme Mix	1 µL
Template (RNA)	1-5 µL
Molecular grade nuclease-free Water	To 20 µL
Total Volume	20 µL

Table 3.2: Reverse transcription cycling program for cDNA synthesis

	Temperature	Time	Number of cycles
cDNA synthesis	42 °C	30 min	1 cycle
Inactivation	95 °C	2 min	1 cycle

PCR Reaction Mixture

Quantitative RT-PCR was performed of the few selected reference genes. Primer 3.0 software was used to design the gene-specific primers. OligoEvaluator™ sequence analysis tool was used to study the primer dimer, secondary structure as well as efficiency. RT-PCR was performed using PowerUp SYBR Green Master Mix (A25741, Applied Biosystems, USA) in Quant Studio 12K (Life technology) FAST real-time PCR machine with primers to detect selected messenger RNA (mRNA) targets. The melting curve of each sample was measured to ensure the specificity of the products. Beta Actin was used as an internal control to normalize the variability in

the expression levels and data was analyzed using $2^{-\Delta\Delta CT}$ method (Livak and Schmittgen, 2001).

Table 3.3: Real Time PCR Reaction mix

Component	Volume (10 μ L/well)
PowerUp SYBR Green Master Mix (2X)	5 μ L
Forward Primer (10uM)	0.5 μ L
Reverse Primer (10uM)	0.5 μ L
DNA Template	1 μ L
Molecular grade Nuclease free water	3 μ L
Total	10 μ L

Table 3.4: Real Time PCR condition

Step	Temperature	Duration	Cycles
UDG activation	94°C	5 seconds	Hold
Dual- Lock DNA polymerase	94°C	30 seconds	Hold
Denature	95°C	3 seconds	40
Anneal/extend	59 °C	30 seconds	

Table 3.5: Real time PCR primer sequences of selected genes.

Sr. No.	Accession no.	Gene Name	Primer type	Sequence	T _m (°C)
1.	NM_001170642.1	cncc	Forward	TGTAGTACCCGTA CTTCTTGGT	58.39
			Reverse	ATGCTACACATT CACAGGGAT	55.92
2.	NM_001190793.1	cyp6bq9	Forward	CGCGGTTTAGTCGCTGATG	58.82
			Reverse	GAAAGCTTGTGCTGCGAGTT	57.30
3.	NM_001114388.1	cyp4g7	Forward	CTTCGGGACGATTTGGACGA	59.35
			Reverse	TCGCCTCGACCATGAAATCC	59.35
4.	XM_023453981.1	cyp4c3	Forward	GCACGAGATGAAGGTTGTAATATCC	61.34
			Reverse	GTCTCCGCAGCCAATTCAAG	59.35
5.	XM_023156547.1	sod	Forward	TTCGTCATGTGGGTGACCTG	59.35
			Reverse	AGTCATCGGCTTCCGTTGTT	57.30

6.	GEUE01064616.1	gst	Forward	CAGTCCCTGTCAAGAGCACA	59.35
			Reverse	TGCATGGAGTGCAATTCCTA	59.35
7.	MK612043.1	gstd2	Forward	AGCCAAAAATGCCATGTCCAC	57.87
			Reverse	ACACTCCCGAAACCATTGGC	59.35
8.	MK612043.1	gstd3	Forward	AACCCACGGAAAAGACGACA	57.30
			Reverse	AGTCGAAGTACAGCCGTTGG	59.35
9.	NM_001170626.1	cest4/cest6	Forward	TCGGAGTTTTGTTCTGGGGG	59.35
			Reverse	CCTGGTCAGTAGTTGCCGTT	59.35
10.	MW664928.1	sult1	Forward	AAAGGGTGGATCAGACTGCAA	57.87
			Reverse	TGAAGGAATCTTCGCCCGTT	57.30
11.	XM_018711399.1	gpx	Forward	AGCTGTTGGTCTCGTACGTC	59.35
			Reverse	AGCGCTGAACTCGTAGATGG	59.35
12.	XM_005332668.3	pdi (p4hb)	Forward	GTTCTGCCCAAGAGTGTGT	59.35
			Reverse	GTGGTCGCTGTCGATGAAGA	59.35
13.	Contig_02154	abc9	Forward	TTTAGCAACCGATGTGACGCAAGC	62.72
			Reverse	TGACCCAGACGTTGTCAACACAGA	62.72
14.	Contig_05955	abc10	Forward	TCACAGCGGTCTTCCTGGATTCTT	62.72
			Reverse	AACTTCTGCGCGCACATTAGAACG	62.72
15.	NM_001039403.1	chs2	Forward	GGGACAATGTGGCACGAAAC	59.35
			Reverse	GTCCCAAATGCTCCCTCACA	59.35
16.	NM_001039398.2	lac2	Forward	GGTTCCTCCCAATTTCCCA	59.35
			Reverse	ACGAAGTTTCAGAGGAACGATCT	58.87

Data Analysis

Statistical analysis was done using Graphpad prism 9 software. The data was analyzed using one way and two-way ANOVA test followed by multiple comparison test (Tukey's). Results are presented as Mean±SEM. The level of significance was set as * $p < 0.05$, ** $p < 0.01$.

3.3 Results

The quality and quantity of the extracted RNA samples were checked on NanoDrop followed by Agilent Tape station using High Sensitivity RNA ScreenTape. A single distinct 18S peak was observed for both the extracted RNA samples confirm the quality of RNA, thus graded as ‘PASS’ in initial QC step and can be processed for library in regular process (**Fig. 3.3**). The QC passed RNA samples were processed for PE library preparation using TruSeq stranded mRNA Library Prep Kit as per the kit protocol. The quality of both the prepared libraries passed in our QC step and can be processed for sequencing on illumina platform using 2 x 150bp chemistry.

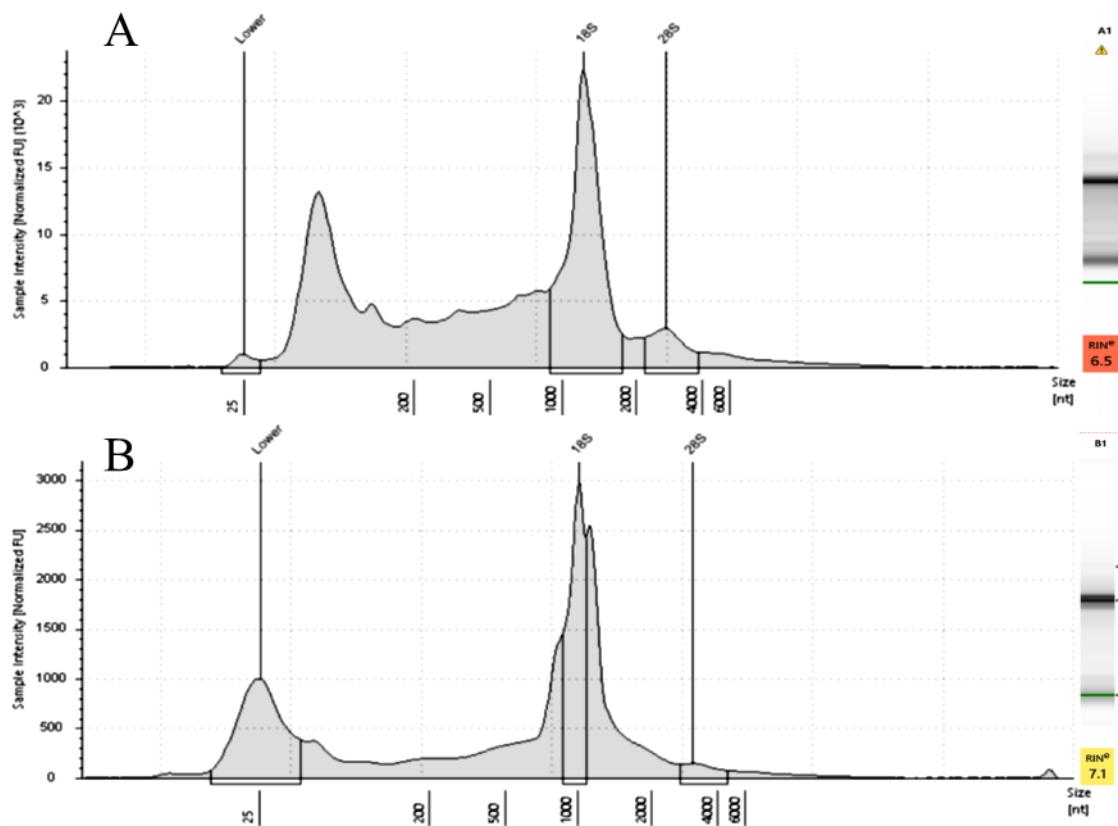


Figure 3.3: Depicts QC of Extracted RNA Samples on Agilent TapeStation

Quantity and quality check (QC) of library on Agilent 4200 Tape Station

The PCR enriched libraries were purified using AMPureXP beads and analyzed on 4200 Tape Station system (Agilent Technologies) using high sensitivity D1000 Screen tape as per manufacturer instructions (**Fig. 3.4**).

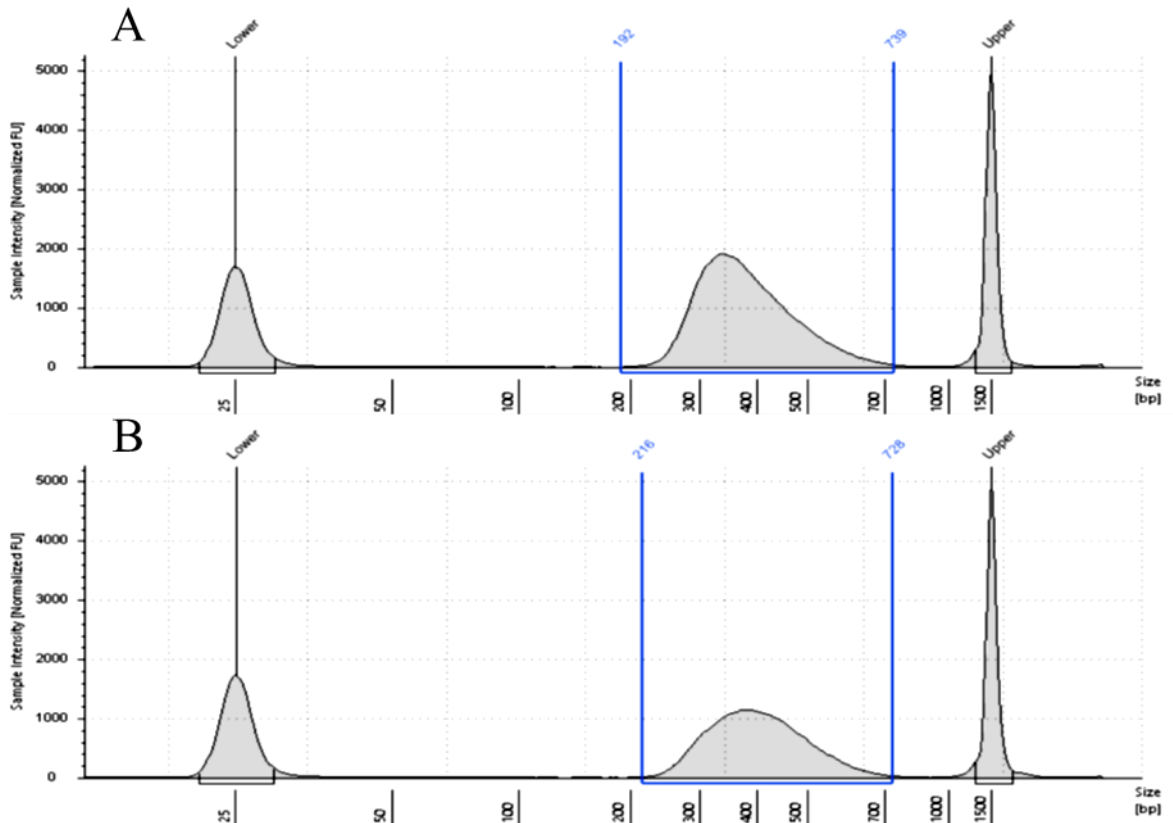


Figure 3.4: Depicts Library Profile of Samples: Control and Treated on Agilent TapeStation

De novo Transcriptome Assembly

The high-quality reads were assembled together into transcripts using Trinity de novo assembler (version 2.1.1) with a kmer of 25. Sequencing of *C. chinensis* transcriptome yielded 58,120 Transcripts (**Table 3.6**). The assembled transcripts were then further clustered together using CD-HIT-EST-4.8.1 to remove the isoforms produced during assembly. This resulted in sequences that can no longer be extended. Such sequences are defined as Unigenes. Only those unigenes which were found to have >85% coverage at 3X read depth were considered for downstream analysis. We combined the sequences into an assembly that generated 25,343 unigenes with an average length of 1,435 bp and an N50 of 2,045 bp (**Table 3.6**). The size distribution indicated that 13,336 (52.62 %) unigene lengths were longer than 1,000 bp (**Table 3.8**).

Table 3.6: Transcript (Pooled) summary

Description	Transcripts
No. of Transcripts	58,120
Total transcript length (bp)	64,282,882
N50 (bp)	1,760
Length of the longest transcript (bp)	20,096
Length of the shortest transcript (bp)	301
Mean transcript length (bp)	1,106

Table 3.7: Validated unigenes (Pooled) summary

Description	Unigenes
No. of Unigenes	25,343
Total unigenes length (bases)	36,367,379
N50	2,045
Length of the longest unigene (bp)	20,096
Length of the shortest unigene (bp)	301
Mean unigenes length (bp)	1,435

Table 3.8: Length distribution statistics of the validated unigenes (Pooled)

Range of unigenes	Unigenes
300 > unigene ≤ 400	3,001
400 > unigene ≤ 500	2,204
500 > unigene ≤ 600	1,725
600 > unigene ≤ 700	1,463
700 > unigene ≤ 800	1,348
800 > unigene ≤ 900	1,147
900 > unigene ≤ 1000	1,119
> 1000	13,336

Coding sequence (CDS) Prediction

TransDecoder-v5.3.0 was used to predict coding sequences (CDS) from the above mentioned unigenes. TransDecoder identifies candidate coding regions within

unigene sequences. TransDecoder identifies likely CDS based on the following criteria:

- A minimum length open reading frame (ORF) is found in a unigene sequence
- A log-likelihood score similar to what is computed by the GeneID software is > 0 .
- The above coding score is greatest when the ORF is scored in the 1st reading frame as compared to scores in the other 5 reading frames.

If a candidate ORF is found fully encapsulated by the coordinates of another candidate ORF, the longer one is reported. However, a single unigene can report multiple ORFs (allowing for operons, chimeras, etc.). A total 13,614 CDS were generated with a mean length of 1,190bp (**Table 3.9**). The size distribution indicated that 6,410 (47 %) unigene lengths were longer than 1,000 bp (**Table 3.10**).

Table 3.9: CDS (Pooled) Statistics

Description	CDS
No. of CDS	13,614
Total CDS length (bp)	16,206,501
Length of the longest CDS (bp)	17,022
Length of the shortest CDS (bp)	255
Mean CDS length (bp)	1,190

Table 3.10: Length distribution statistics of CDS (Pooled)

Range of CDSs	CDS
200 > CDS ≤ 300	23
300 > CDS ≤ 400	1,603
400 > CDS ≤ 500	1,139
500 > CDS ≤ 600	1,013
600 > CDS ≤ 700	1,008
700 > CDS ≤ 800	883
800 > CDS ≤ 900	750
900 > CDS ≤ 1000	785
> 1000	6,410

Functional Annotation

Functional annotation of the pooled CDS was performed using DIAMOND program, which is a BLAST-compatible local aligner for mapping translated DNA query sequences against a protein reference database. DIAMOND (BLASTX alignment mode) finds the homologous sequences for the genes against NR (non-redundant protein database) from NCBI. (Table 3.11). Majority of the blast hits were found to be against *Callosobruchus maculatus* (Fig.3.5).

Table 3.11: BlastX Data Distribution Statistics

Sample Name	Total no. of CDS	No. of CDS with Blast Hit	No. of CDS without Blast Hit
Pooled CDS	13,614	12,629	985

BLAST TOP HIT SPECIES DISTRIBUTION (TOP 25)

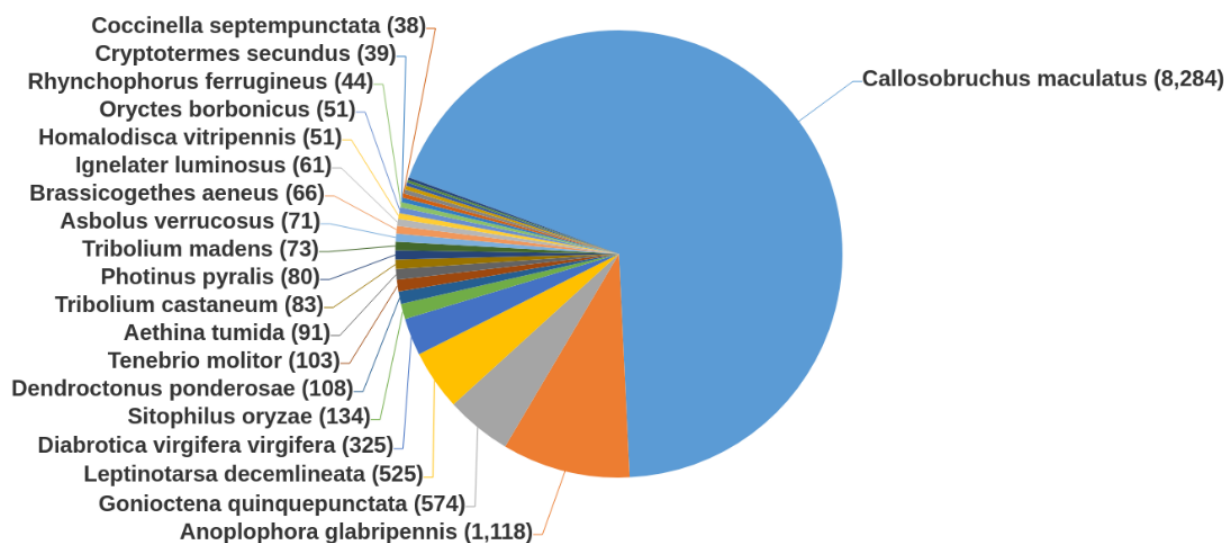


Figure 3.5: Depicts Top Blast Hit Species Distribution of pooled CDS.

Sample-wise CDS identification

To identify sample wise CDS from above mentioned pooled set of CDS, reads from each sample were mapped on the final set of pooled CDS. The read count (RC) values were calculated from the resulting mapping and those CDS having 85% coverage and 3X read depth were considered for downstream analysis for each of the samples. A total 6,596 CDS were generated with a mean length of 1,042 in control sample whereas in case of treated group (H_{LC50}) 11,622 CDS generated with a mean length of 1,257 (Table 3.12)

Table 3.12: Sample-wise CDS summary

Sr. No.	Sample Name	No. of CDS	Total CDS length (bp)	Longest CDS Length (bp)	Shortest CDS Length (bp)	Mean CDS Length(bp)
1	Control	6,596	6,875,946	17,022	276	1,042
2	H _{LC50}	11,622	14,611,353	17,022	276	1,257

Gene Ontology Analysis (GO)

Gene ontology (GO) analysis of the CDS identified for all samples were carried out using Blast2GO program. GO assignments were used to classify the functions of the predicted CDS. The GO mapping also provides ontology of defined terms representing gene product properties which are grouped into three main domains: In control group's Biological Process (BP) with 2,115 CDS, Molecular Function (MF) with 2,458 and Cellular Component (CC) with 2,048 while in treated group Biological Process (BP) with 3,608 CDS, Molecular Function (MF) with 4,112 and Cellular Component (CC) with 3,504. Molecular Function was found to have the highest number of CDS associated with it for all the samples. (Table 3.13 & Fig. 3.6) GO mapping was carried out in order to retrieve GO terms for all the functionally annotated CDS.

Table 3.13: GO category distribution of CDS

Sr. No.	Sample Name	Total No. of CDS	Total No. of Annotated CDS	Biological Process	Cellular Component	Molecular Function
1	Control	6,596	3,403	2,115	2,048	2,458
2	H _{LC50}	11,622	5,654	3,608	3,504	4,112

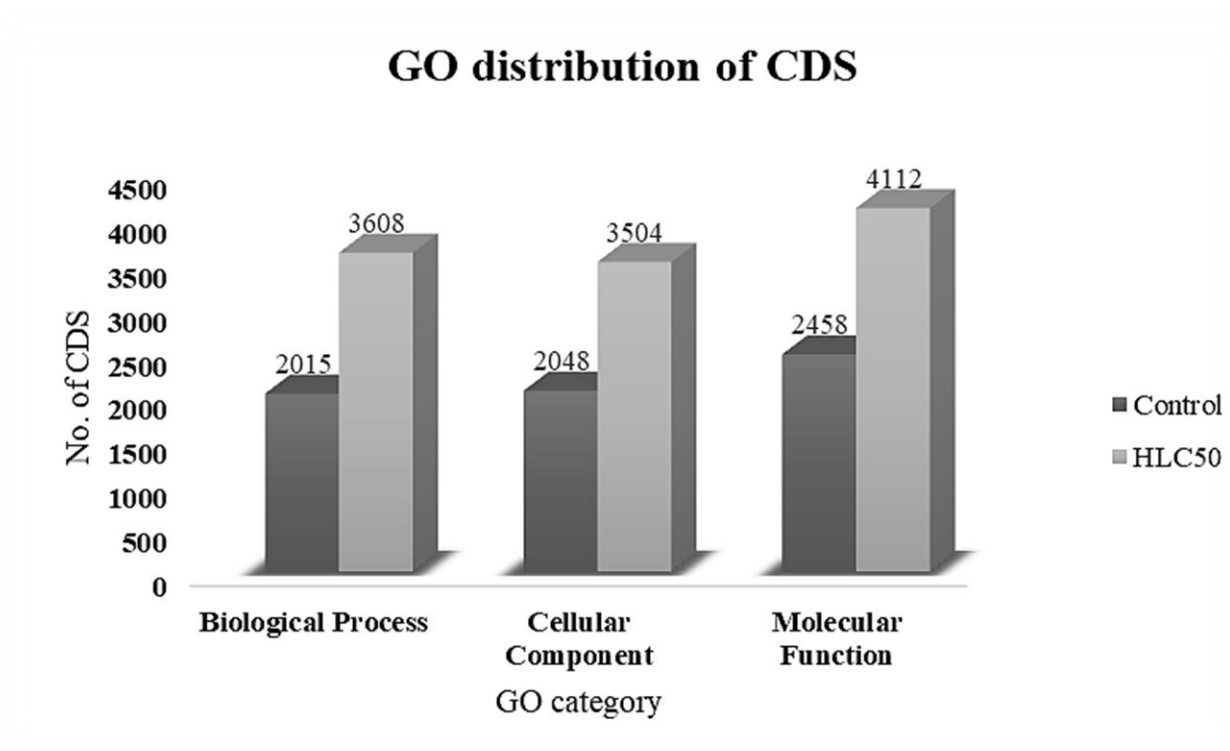


Figure 3.6: Depicts GO category distribution of CDS

Among the 9 GO categories in the Biological Process, the Organic substance metabolic process was having the maximum CDS (20.55% in control group 19.63% in treated group) (Table 3.14 and Fig. 3.7 & 3.8)

Table 3.14: Biological Process GO term distribution

Biological Process		
	Control	HLC50
Regulation of cellular process	213	504
Establishment of localization	387	706
Primary metabolic process	1264	2075
Organic substance metabolic process	1314	2154
Biogenesis	269	489
Biosynthetic process	518	387
Cellular metabolic process	1020	1635
Small molecule metabolic process	306	409
Nitrogen compound metabolic process	1104	1819

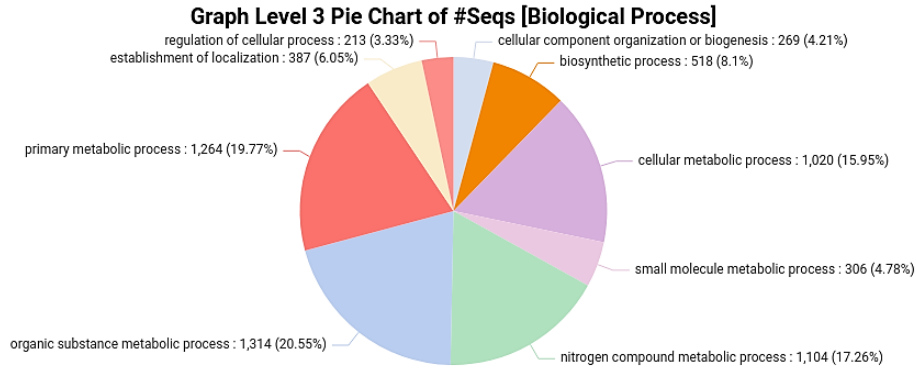


Figure 3.7: Depicts Biological Process GO term distribution for Control sample

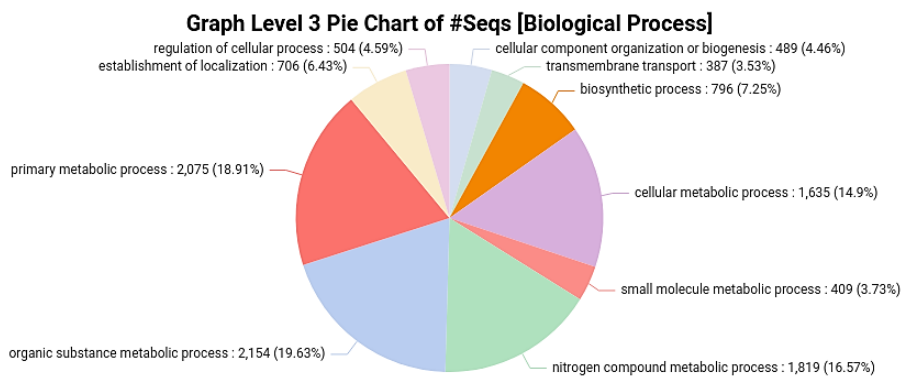


Figure 3.8: Depicts Biological Process GO term distribution for HLC50 sample

Among the 5 GO categories in the Cellular Component, the Intracellular anatomical structure was having the maximum CDS (30.77% in control group 30.52% in treated group) (Table 3.15 and Fig. 3.9 & 3.10)

Table 3.15: Cellular Component GO term distribution

Cellular Component		
	Control	HLC50
Organelle	1018	1671
Intracellular anatomical structure	1215	1973
Cytoplasm	707	1050
Membrane	1009	1771

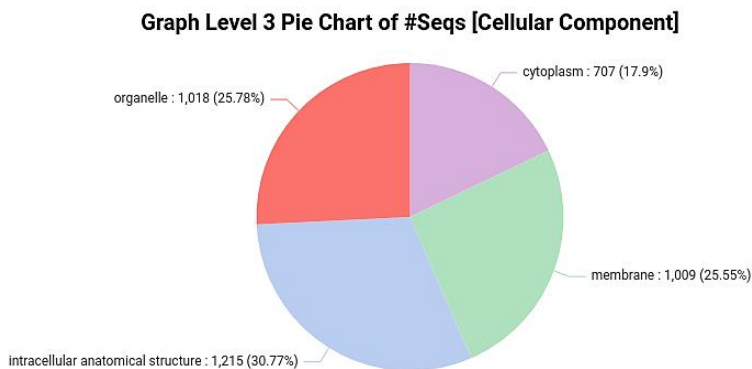


Figure 3.9: Depicts Cellular Component GO term distribution for Control sample

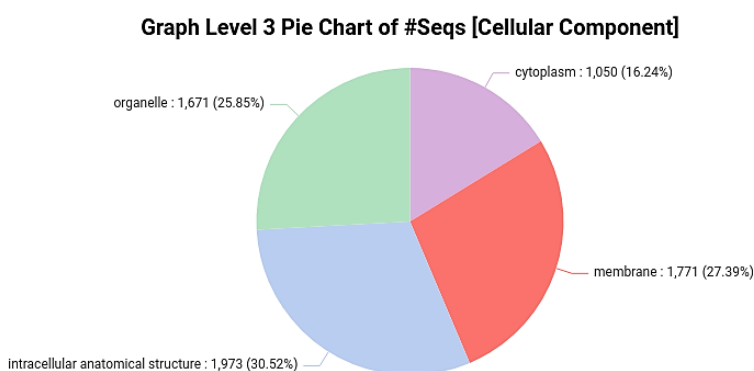


Figure 3.10: Depicts Cellular Component GO term distribution for H_{LC50} sample
Among the 8 GO categories in the Molecular Functions, the Ion binding and Heterocyclic compound binding was having the maximum CDS (17.23% in control group 18.5% in treated group) (Table 3.16 and Fig. 3.11 & 3.12)

Table 3.16: Molecular Function GO term distribution

Molecular Functions		
	Control	H _{LC50}
Catalytic activity	314	560
Heterocyclic compound binding	849	1484
Hydrolase activity	516	866
Carbohydrate derivative binding	365	685
Small molecule binding	456	822
Organic cyclic compound binding	849	1485
Ion binding	883	1516
Transferase activity	403	749

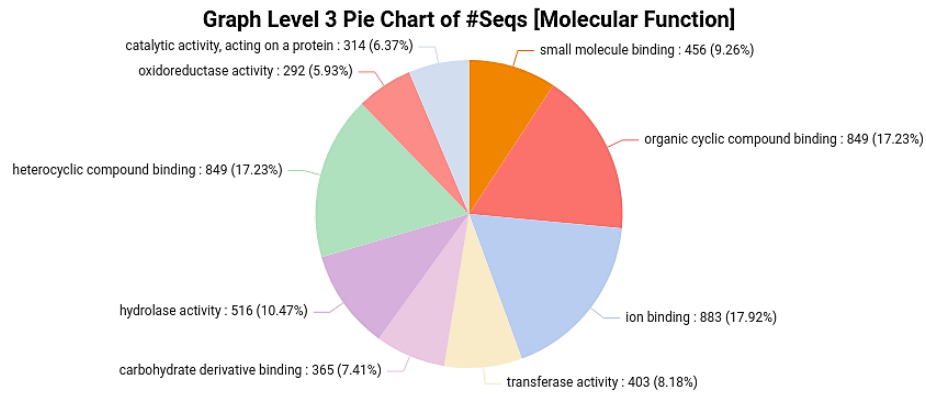


Figure 3.11: Depicts Molecular Function GO term distribution for Control sample

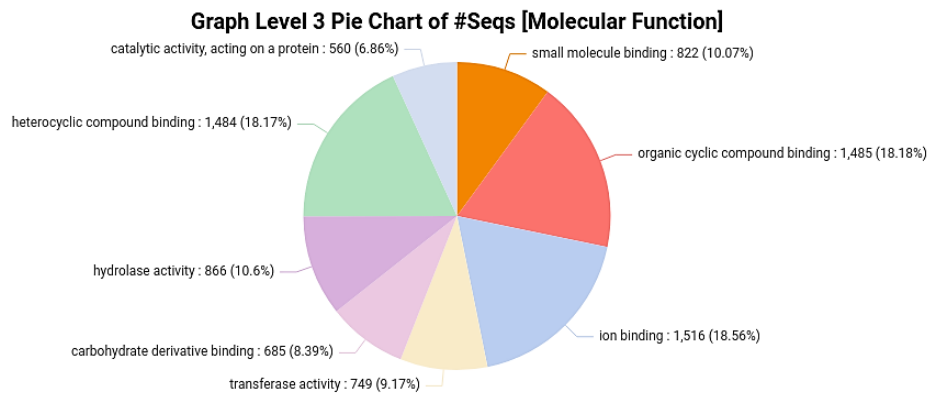


Figure 3.12: Depicts Molecular Function GO term distribution for H_{LC50} sample

Functional Annotation of KEGG Pathway

To identify the potential involvement of the predicted CDS in biological pathways, all the identified CDS of 2 samples were mapped to reference canonical pathways in KEGG (*Tribolium castaneum* (tca), *Dendrotonus ponderosae* (dpa), *Aethina tumida* (atd), *Nicrophorus vespilloides* (nvl), and *Drosophila melanogaster* (dme)) database. The identified CDS for all 2 samples were found to be categorized into 31 KEGG pathways under five main categories: Metabolism, Genetic information processing, Environmental information processing, Cellular processes and Organismal systems (Table 3.17). The output of KEGG analysis includes KEGG Orthology (KO) assignments and corresponding Enzyme Commission (EC) numbers and metabolic pathways of predicted CDS using KEGG automated annotation server, KAAS.

Table 3.17: KEGG Pathway annotation summary of CDS

Sample Name	No. of Identified CDS	No. of Annotated CDS	No. of Annotated Categories
Control	6,596	1,992	31
H _{LC50}	11,622	3,037	31

Differential Gene Expression Analysis

Differential expression analysis was performed on the CDS between control and treated samples by employing a negative binomial distribution model in DESeqpackage as mentioned below. The CDSs having log₂foldchange value greater than zero were considered as up-regulated whereas less than zero as down-regulated. P-value threshold of 0.05 was used to filter statistically significant results (**Table 3.18**).

Table 3.18: Statistics of differentially expressed Genes

Commonly Expressed	Upregulated (Significant)	Downregulated (Significant)
6,282	50	280

Heatmap

An average linkage hierarchical cluster analysis was performed on top 50 differentially expressed genes using multiple experiments viewer (MeV v4.9.0). The heatmap shows level of gene abundance. Levels of expression are represented as log₂ ratio of gene abundance between control and treated samples. Differentially expressed genes were analyzed by hierarchical clustering. A heat map was constructed using the log-transformed and normalized value of genes based on Pearson uncentered distance and average linkage method. In heatmap, each horizontal line refers to a gene. The color represents the logarithmic intensity of the expressed genes. Relatively high expression values are shown in red (Fig. 3.15).

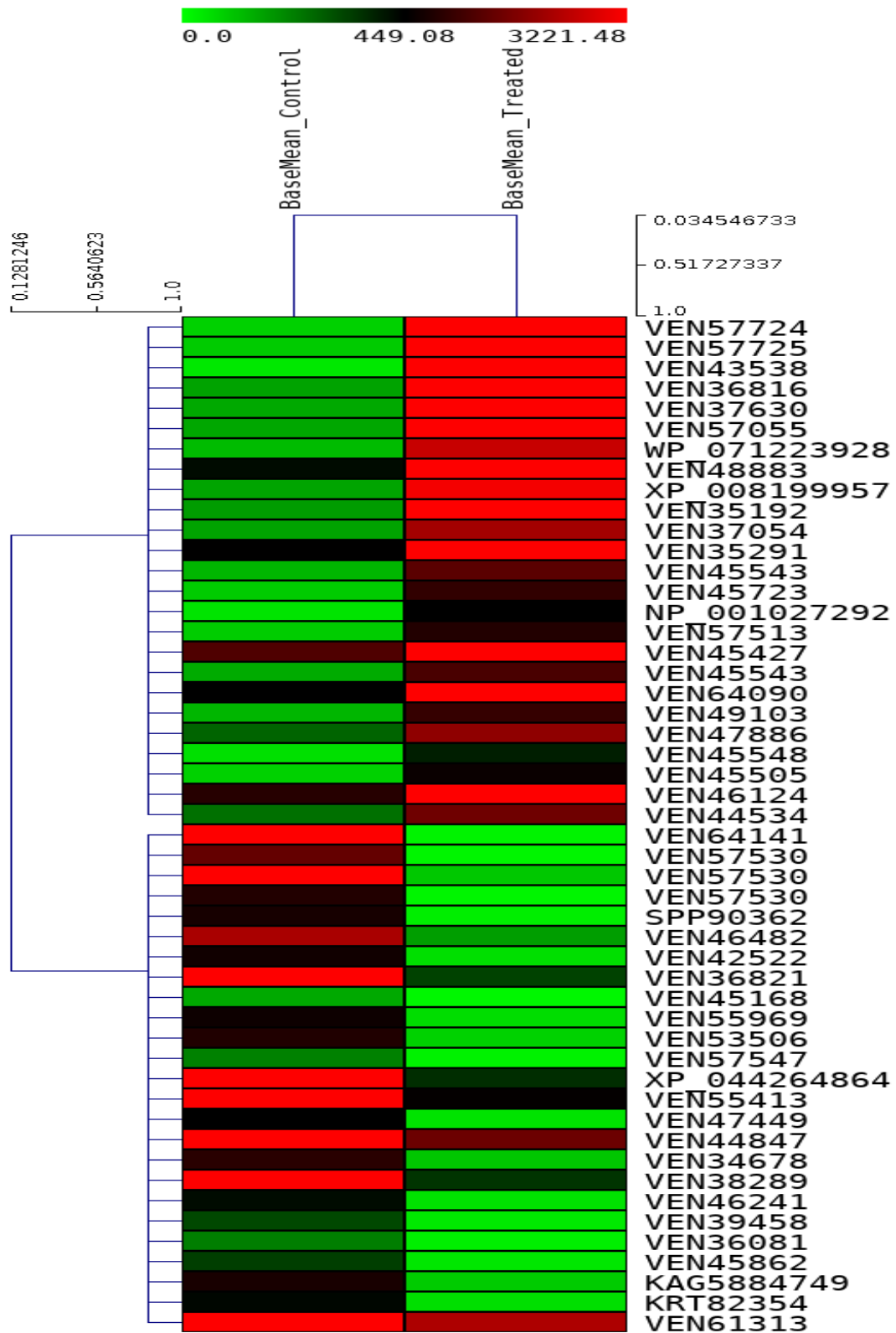


Figure 3.13: Depicts Heat map depicting the top 50 differentially expressed genes (significant); Basemean_Control represents the normalized expression values for Control sample and Basemean_Treated represents the normalized expression values for H_{LC50}sample for DGE Combination.

Scatter Plot

The Scatter Plot is useful for representing the expression of genes in two distinct conditions of each sample combinations. It helps to identify genes that are differentially expressed in one sample with respect to another and also allows comparing two values associated with genes. In scatter plot, each dot represents a gene. The vertical position of each gene represents its expression level in the Control samples while the horizontal position represents its expression level in the Treated samples. Thus, genes that fall above the diagonal are over-expressed and genes that fall below the diagonal are under-expressed as compared to their median expression level in experimental grouping of the experiment (Fig. 3.16).

Scatter Plot (Control vs. Treated)

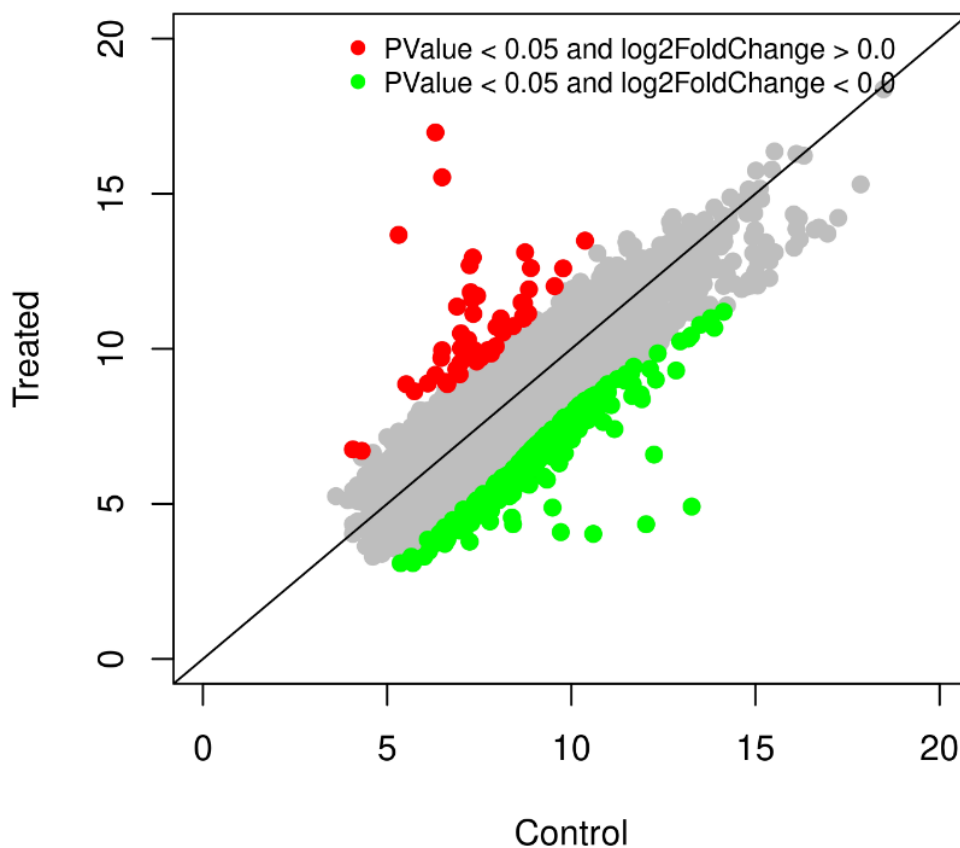


Figure 3.14: Depicts Scatterplot of differentially expressed genes; green dots represent the downregulated (significant) and red dots represent the upregulated (significant) genes in DGE Combination 1.

Volcano Plot

The Eurofins proprietary R script was used to depict the graphical representation and distribution of differentially expressed genes which were found in Control as well as Treated samples. The ‘volcano plot’ arranges expressed genes along dimensions of biological as well as statistical significance. The red block on the right side of zero represents the up regulated genes whereas green block on the left side of zero represents significant down regulated genes. While Y-axis represents the negative log of p-value (p value <0.05) of the performed statistical test, the data points with low p-values (highly significant) appears towards the top of the plot. Grey block shows the non-differentially expressed genes (Fig. 3.17).

Volcano Plot (Control vs. Treated)

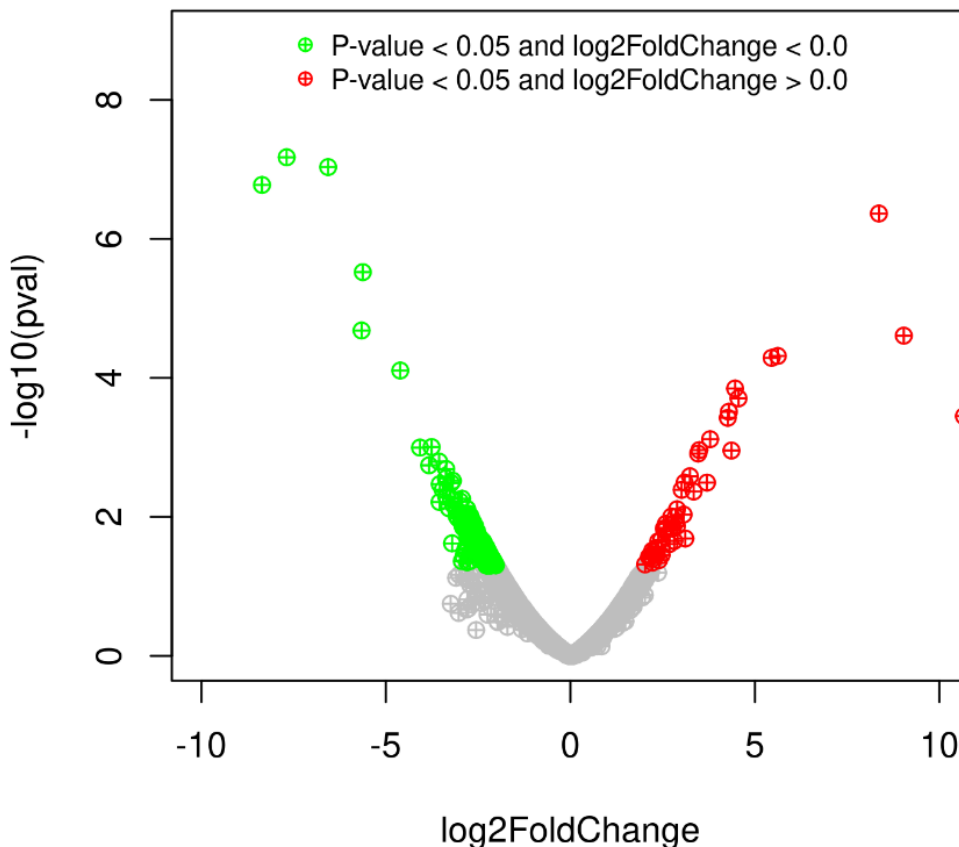


Figure 3.15: Depicts Volcano plot of differentially expressed genes; green dots represent the downregulated (significant) and red dots represent the upregulated (significant) genes for DGE Combination 1.

Metabolic pathways analysis

In this study, we conducted a comprehensive analysis of gene expression profiles in a treated group and a control group across 31 KEGG pathways. Our objective was to identify and quantify the differences in gene count between these two groups. Our analysis revealed significant differences in gene counts between the treated group and the control group across all 31 KEGG pathways. In each pathway, the treated group exhibited a higher gene count compared to the control group. This consistent pattern suggests a robust and widespread effect of the treatment on gene expression in multiple biological pathways.

Our analysis revealed a striking and uniform pattern of elevated gene counts in the treated group compared to the control group across all **metabolic pathways** studied (**Table 3.19**). Now, coming to specific metabolic pathways, 14 **amino acid syntheses and degradation** pathways (**Table 3.20**) were observed. Where, metabolism pertaining to aliphatic amino acid like valine, leucine and isoleucine breakdown and thiol group amino acid like Cysteine and methionine was found to be highest. Similar trend of increase in these metabolic pathways was also observed in treated group. In contrast the lowest gene count (1) was found in lysine biosynthetic pathway (**Fig. 3.17**). Additionally, 14 **Carbohydrate metabolic** pathways (**Table 3.21**) recorded where, metabolism pertaining to Glycolysis/Gluconeogenesis was maximum, it was followed by amino sugar and nucleotide sugar metabolism were more gene count in treated (28) compared to control (25). In contrast the lowest gene count (8) was found in Ascorbate and aldarate metabolic pathway (**Fig. 3.18**). In case of **energy metabolism**, the gene count was almost similar in control and treated group, there was a slight increase in case of treated group compared to control group. We recorded 6 metabolic pathways (**Table 3.22**) of energy where, metabolism pertaining to Oxidative phosphorylation was found to be maximum in both Treated (70) and control (69) groups respectively, while the lowest CDS count (3) was found in Nitrogen metabolism in both the groups (**Fig. 3.18**). In the present investigation, a comprehensive analysis was conducted to ascertain a collective count of 15 distinct **lipid metabolic** pathways (**Table 3.23**). Among the several pathways examined, it was observed that Glycerophospholipid metabolism had the most significant difference in gene count, with 34 genes identified in the treated group as opposed to 25 genes in the control group. In contrast, it was found that the gene count for Cutin,

suberine, wax biosynthesis, and metabolism of linoleic acid was consistently at its lowest value of 1 in both the treatment and control groups (**Fig. 3.18**). A significant discrepancy in gene count pertaining to **nucleotide metabolism** was observed, with a notable increase in gene count observed in the treated group as compared to the control group. In addition, we have identified the two main pathways that are crucial for nucleotide metabolism, namely Purine metabolism and Pyrimidine metabolism (**Table 3.24**). It was observed that both pathways showed an increase in the number of genes in the treated group compared to the control group. Specifically, there were 50 genes involved in Purine metabolism and 25 genes involved in Pyrimidine metabolism in the treated group, while the control group had 41 genes and 20 genes in these respective pathways (**Fig. 3.19**).

In the present study, an increase in the number of genes was detected in the treated group as compared to the control group in the metabolic pathways associated with **terpenoids and polyketides** (**Table 3.25**). In addition, a total of six metabolic pathways were found that are linked to the metabolism of terpenoids and polyketides. It is worth noting that the treated group had a higher gene count of 20 in the biosynthesis of terpenoid backbone, whereas the control group had 14 genes. Moreover, a notable disparity was seen in Zeatin biosynthesis, as the control group exhibited no gene count, while the treatment group displayed a count of 9 genes (**Fig. 3.20**). In the present study, it was shown that the number of genes related to **Xenobiotics biodegradation and metabolism** had a comparable range in both the control and treatment cohorts, but with a modest elevation in the treated group relative to the control group (**Table 3.25**). Nine primary metabolic pathways associated with the biodegradation and metabolism of Xenobiotics were identified. Among the several pathways examined, it was shown that Drug metabolism through other enzymes had the highest level of prominence in both experimental groups. Notably, the treated group displayed a somewhat greater number of genes (19) associated with this route compared to the control group (16). On the other hand, the remaining routes had similar gene counts in both groups, with the lowest count seen in the Naphthalene degradation pathway (1) (**Fig. 3.20**).

Table 3.19: Gene counts which are involved in different metabolic pathways.

Metabolism Pathways	Control	HLc50
Carbohydrate metabolism	218	261
Energy metabolism	150	154
Lipid metabolism	158	230
Nucleotide metabolism	64	93
Amino acid metabolism	156	188
Metabolism of other amino acids	81	97
Glycan biosynthesis and metabolism	76	141
Metabolism of cofactors and vitamins	133	173
Metabolism of terpenoids and polyketides	36	45
Biosynthesis of other secondary metabolites	32	38
Xenobiotics biodegradation and metabolism	62	72

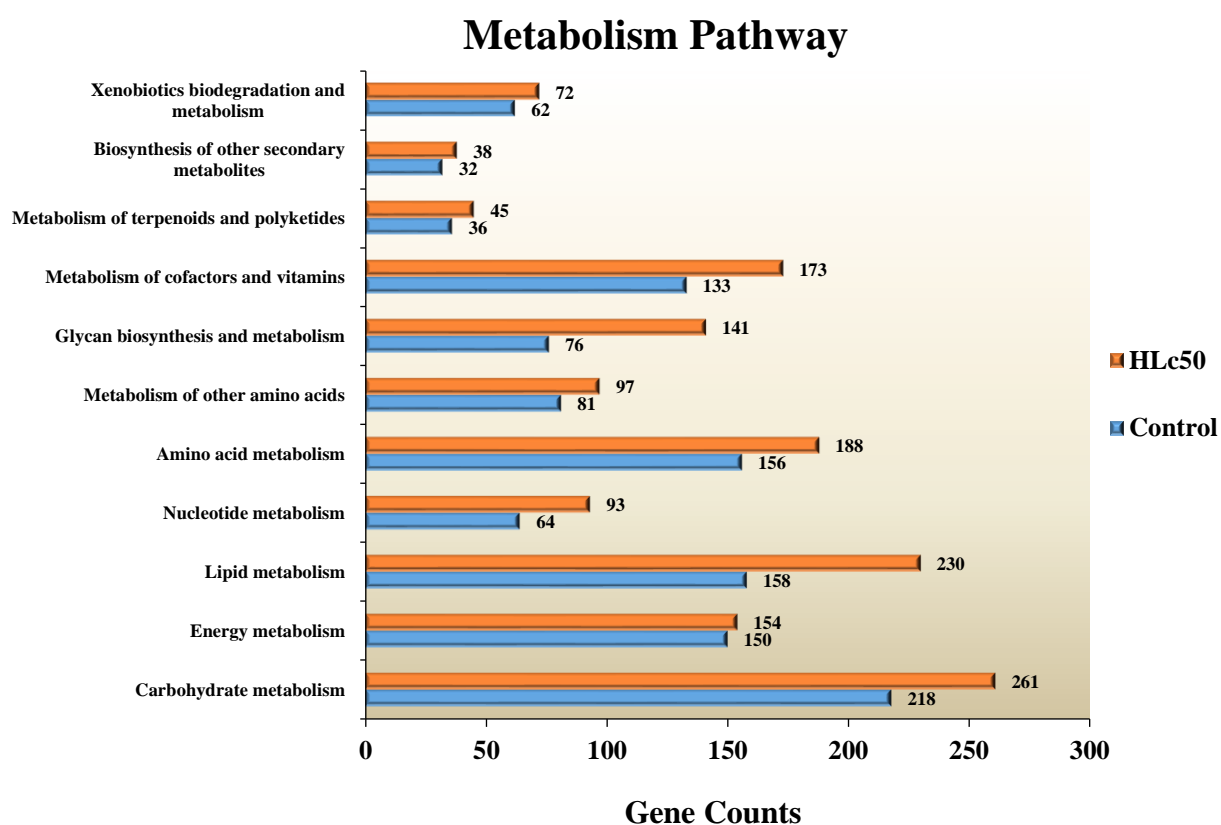


Figure 3.16: Depicts the total gene counts which are involved in different metabolic pathways.

Table 3.20: Gene counts involved in Amino Acid Metabolism: Pathway analysis

Amino acid metabolism	Control	HLc50
Alanine, aspartate and glutamate metabolism [PATH: ko00250]	17	21
Glycine, serine and threonine metabolism [PATH: ko00260]	20	21
Cysteine and methionine metabolism [PATH: ko00270]	27	29
Valine, leucine and isoleucine degradation [PATH: ko00280]	25	30
Valine, leucine and isoleucine biosynthesis [PATH: ko00290]	2	2
Lysine biosynthesis [PATH: ko00300]	1	1
Lysine degradation [PATH: ko00310]	18	27
Arginine biosynthesis [PATH: ko00220]	9	9
Arginine and proline metabolism [PATH: ko00330]	22	22
Histidine metabolism [PATH: ko00340]	6	7
Tyrosine metabolism [PATH: ko00350]	14	14
Phenylalanine metabolism [PATH: ko00360]	7	7
Tryptophan metabolism [PATH: ko00380]	17	18
Phenylalanine, tyrosine and tryptophan biosynthesis [PATH: ko00400]	4	4

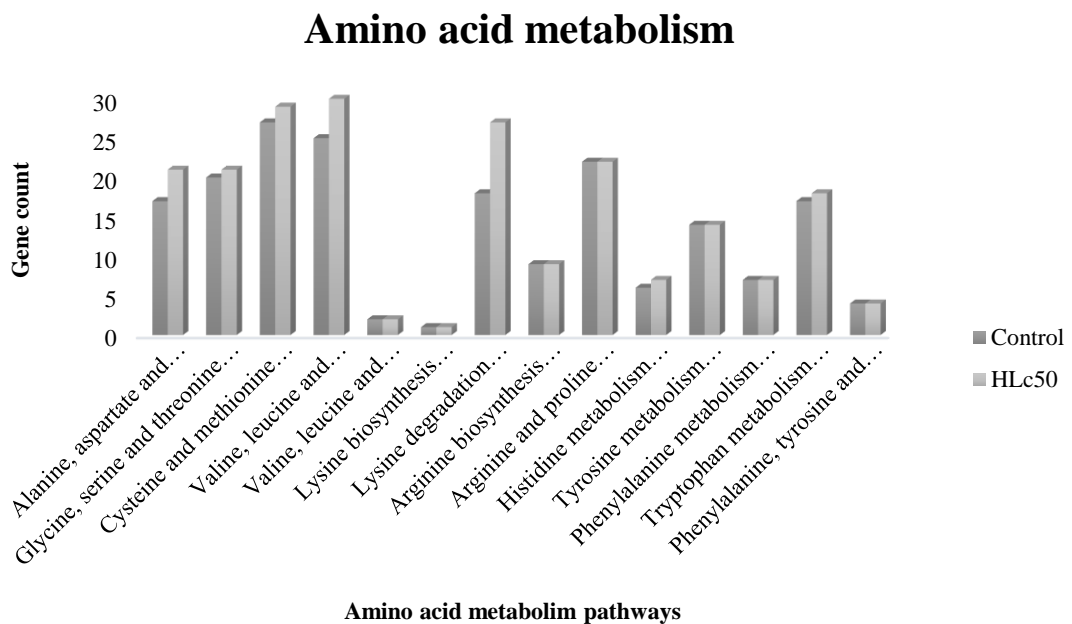


Figure 3.17: Depicts gene counts involved in different pathways of Amino Acid Metabolism

Table 3.21: Gene count involved in Carbohydrate Metabolism: Pathway analysis

Carbohydrate metabolism	Control	H _{Lc50}
Glycolysis / Gluconeogenesis [PATH: ko00010]	27	27
Citrate cycle (TCA cycle) [PATH: ko00020]	19	21
Pentose phosphate pathway [PATH: ko00030]	16	18
Pentose and glucuronate interconversions [PATH: ko00040]	15	15
Fructose and mannose metabolism [PATH: ko00051]	13	13
Galactose metabolism [PATH: ko00052]	12	13
Ascorbate and aldarate metabolism [PATH: ko00053]	8	8
Starch and sucrose metabolism [PATH: ko00500]	15	16
Amino sugar and nucleotide sugar metabolism [PATH: ko00520]	25	28
Pyruvate metabolism [PATH: ko00620]	21	22
Glyoxylate and dicarboxylate metabolism [PATH: ko00630]	18	21
Propanoate metabolism [PATH: ko00640]	18	20
Butanoate metabolism [PATH: ko00650]	10	12
Inositol phosphate metabolism [PATH: ko00562]	19	28

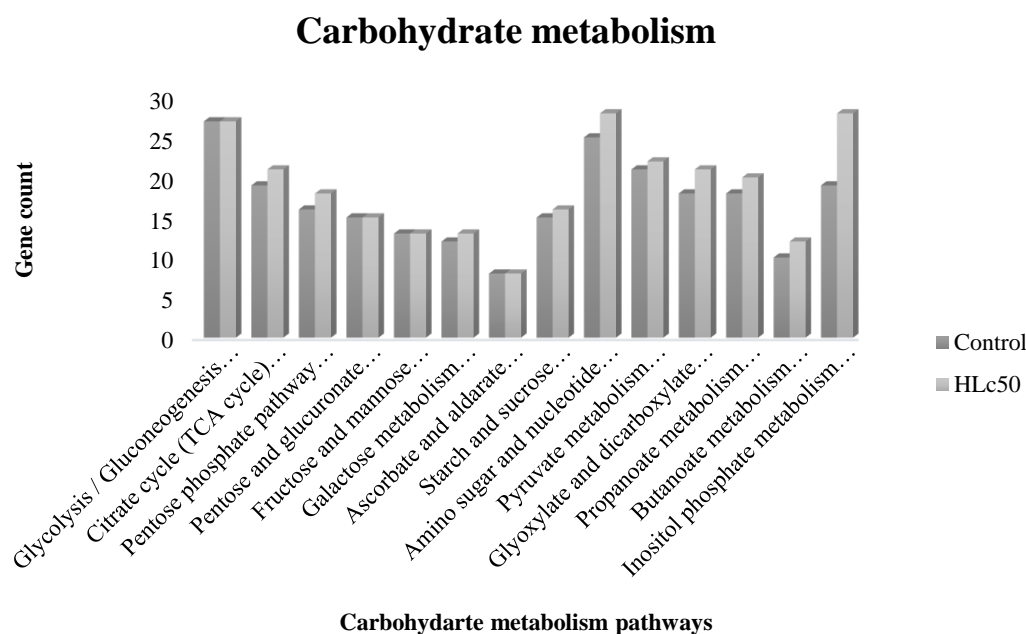


Figure 3.18: Depicts gene counts involved in different pathways of Carbohydrate Metabolism

Table:3.22: Gene count involved in Energy Metabolism: Pathway analysis

Energy metabolism	Control	HLc50
Oxidative phosphorylation [PATH: ko00190]	70	69
Carbon fixation in photosynthetic organisms [PATH: ko00710]	14	15
Carbon fixation pathways in prokaryotes [PATH: ko00720]	7	7
Methane metabolism [PATH: ko00680]	13	13
Nitrogen metabolism [PATH: ko00910]	3	3
Sulfur metabolism [PATH: ko00920]	7	7

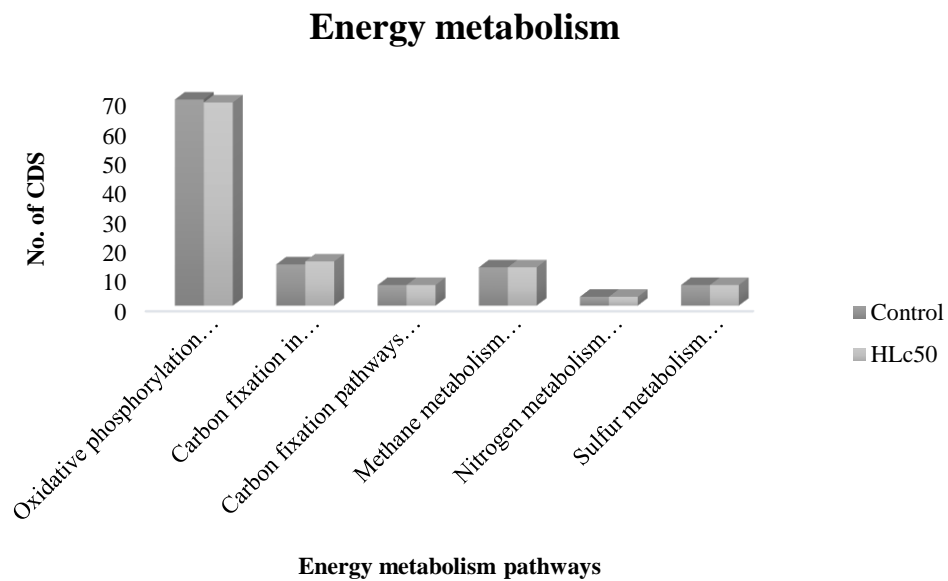


Figure 3.19: Depicts gene count involved in different pathways of Energy Metabolism

Table 3.23: Gene count involved in Lipid Metabolism: Pathway analysis

Lipid metabolism	Control	HLc50
Fatty acid biosynthesis [PATH: ko00061]	9	10
Fatty acid elongation [PATH: ko00062]	14	13
Fatty acid degradation [PATH: ko00071]	20	21
Cutin, suberine and wax biosynthesis [PATH: ko00073]	1	1
Steroid biosynthesis [PATH: ko00100]	3	4
Primary bile acid biosynthesis [PATH: ko00120]	3	3
Steroid hormone biosynthesis [PATH: ko00140]	5	4

Glycerolipid metabolism [PATH: ko00561]	18	22
Glycerophospholipid metabolism [PATH: ko00564]	25	34
Ether lipid metabolism [PATH: ko00565]	5	9
Sphingolipid metabolism [PATH: ko00600]	11	20
Arachidonic acid metabolism [PATH: ko00590]	10	10
Linoleic acid metabolism [PATH: ko00591]	1	1
alpha-Linolenic acid metabolism [PATH: ko00592]	2	2
Biosynthesis of unsaturated fatty acids [PATH: ko01040]	11	11

Lipid metabolism

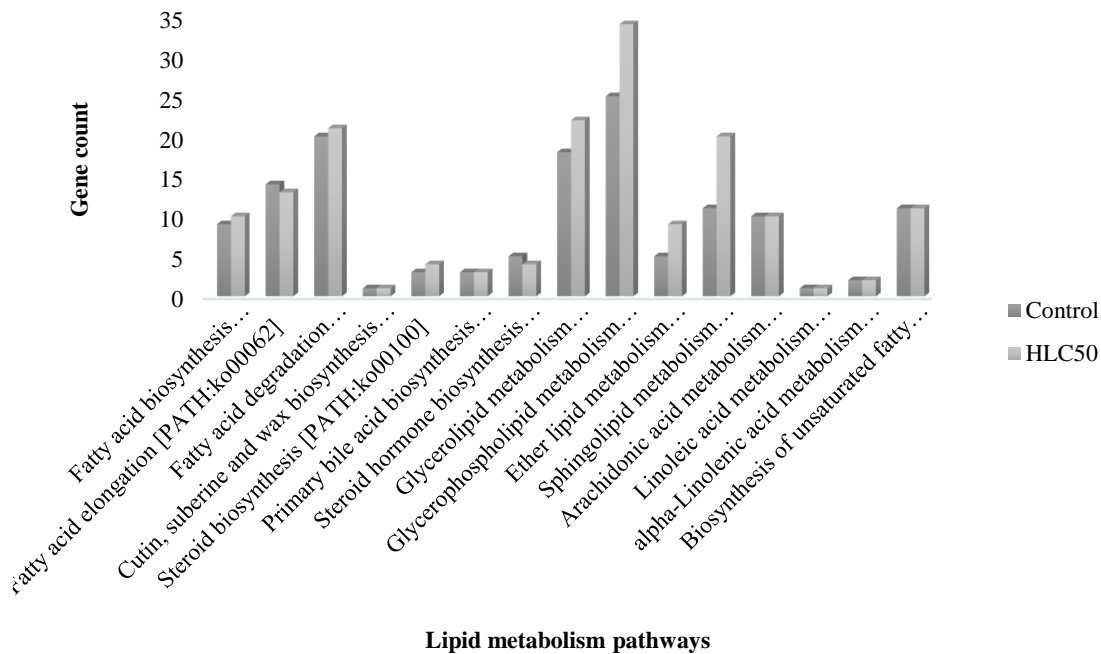


Figure 3.20: Depicts gene count involved in different pathways of Lipid Metabolism

Table 3.24: Gene count involved in Nucleotide Metabolism: Pathway analysis

Nucleotide metabolism	Control	H _{Lc50}
Purine metabolism [PATH: ko00230]	41	50
Pyrimidine metabolism [PATH: ko00240]	20	25

Nucleotide metabolism

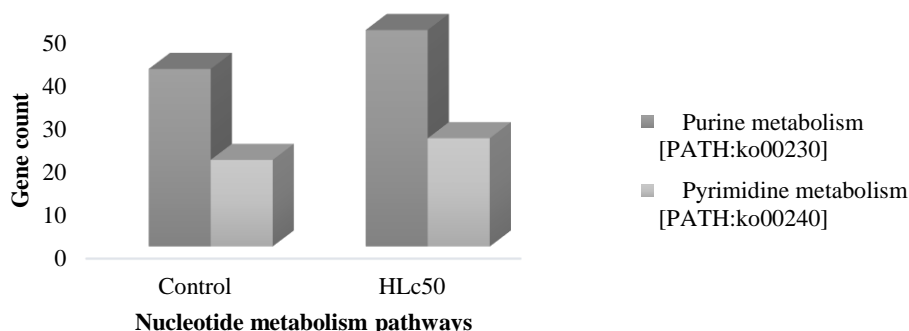


Figure 3.21: Depicts gene count involved in different pathways of Nucleotide Metabolism

Table 3.25: Gene count involved in Metabolism of terpenoids and polyketides: Pathway analysis

Metabolism of terpenoids and polyketides	Control	HLc50
Terpenoid backbone biosynthesis [PATH: ko00900]	14	20
Insect hormone biosynthesis [PATH: ko00981]	8	8
Limonene degradation [PATH: ko00903]	1	1
Pinene, camphor and geraniol degradation [PATH: ko00907]	2	2
Biosynthesis of ansamycins [PATH: ko01051]	1	1
Zeatin biosynthesis [PATH: ko00908]	0	1

Metabolism of terpenoids and polyketides

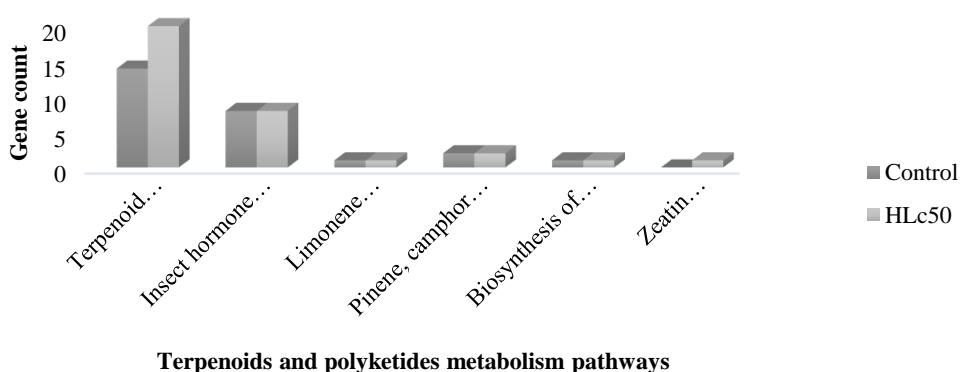


Figure 3.22: Depicts Gene count involved in different pathways of Metabolism of terpenoids and polyketides

Table 3.26: Gene count involved in Xenobiotics biodegradation and metabolism: Pathway analysis

Xenobiotics biodegradation and metabolism	Control	HLc50
Benzoate degradation [PATH: ko00362]	2	2
Aminobenzoate degradation [PATH: ko00627]	3	3
Chloroalkane and chloroalkene degradation [PATH: ko00625]	2	2
Styrene degradation [PATH: ko00643]	3	3
Caprolactam degradation [PATH: ko00930]	5	5
Naphthalene degradation [PATH: ko00626]	1	1
Metabolism of xenobiotics by cytochrome P450 [PATH: ko00980]	6	6
Drug metabolism - cytochrome P450 [PATH: ko00982]	5	5
Drug metabolism - other enzymes [PATH: ko00983]	16	19

Xenobiotic biodegradation and metabolism

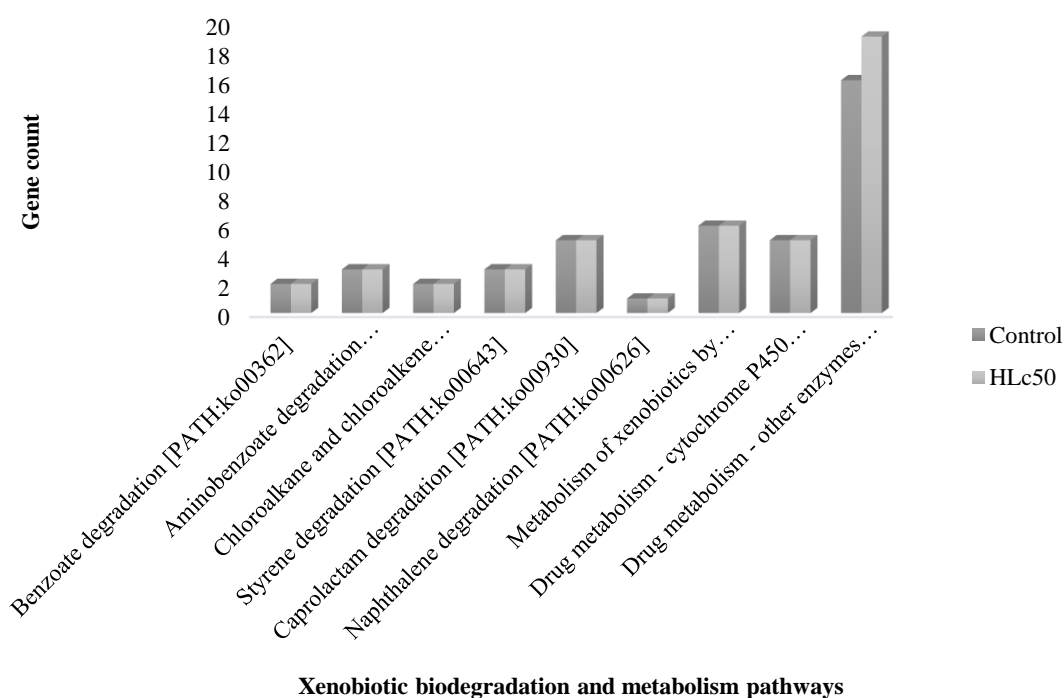


Figure 3.23: Depicts gene count involved in different pathways of Xenobiotics biodegradation and metabolism

Genetic processing information

The study conducted revealed a noteworthy and continuous trend of elevated gene counts in the treated group as compared to the control group in all pathways associated with the processing of genetic information (**Table 3.27 & Fig. 3.24**). Moreover, upon closer examination of particular pathways, a notable and significant rise in the number of genes was detected within the **transcriptional** machinery of the treated group in comparison to the control group (**Table 3.28**). The findings of the study revealed that within the control group, the gene counts for RNA polymerase, Basal transcription factors, and Spliceosome were 17, 20, and 77, respectively. In contrast, the numbers observed in the treated group were comparatively higher, namely 22 for RNA polymerase, 28 for Basal transcription factors, and 95 for Spliceosome (**Fig. 3.25**). The results concerning the **translational** machinery reveal a substantial overall rise in the number of genes in the treated group, in comparison to the gene count in the control group. Moreover, the findings also provide insights into gene count present in five prominent pathways associated with translation: Ribosome, Aminoacyl-tRNA biosynthesis, Nucleocytoplasmic transport, mRNA surveillance route, and Ribosome biogenesis (**Table 3.29**). Among the pathways examined, it was observed that the Ribosome pathway exhibited the largest number of genes. Specifically, the control group had a slightly greater gene count (99) in comparison to the treatment group (97). The observed disparity in gene count between the two groups was particularly notable in the domain of Nucleocytoplasmic transport, where the treated group exhibited a count of 75 genes, while the control group had a count of 40 genes (**Fig. 3.26**). The results pertaining to **Replication and repair** reveal a significant overall increase in gene count within the treated group as compared to the control group (**Table 3.30**). Furthermore, the findings emphasise the gene counts pertaining to Replication and repair among seven prominent pathways. It is noteworthy that the Nucleotide excision repair pathway had the greatest gene count, with 39 genes identified in the treatment group and 26 genes in the control group. On the contrary, the pathway exhibiting the least number of genes was non-homologous end-joining, with a count of 4 genes in the control group and 8 genes in the treatment group (**Fig. 3.27**). The results relating to **protein folding, sorting, and degradation** reveal a significant rise in the gene count in the treated group as compared to the control group. Moreover, the findings offer valuable insights on the gene counts

pertaining to seven prominent pathways that are closely linked to with these processes (Table 3.31). Among these pathways, the highest gene count was observed in Protein processing in the endoplasmic reticulum, with 97 genes in both the treated and control groups. It is worth noting that there is a discernible increase in the number of genes seen in the treated group. In contrast, it was observed that the Sulphur relay system had the lowest gene count, including 2 genes in the control group and 3 genes in the treatment group (Fig. 3.28).

Table 3.27: Identified gene counts which are involved in genetic processing information

Genetic Information Processing	Control	HLc50
Transcription	133	179
Translation	249	350
Folding, sorting and degradation	251	347
Replication and repair	54	124

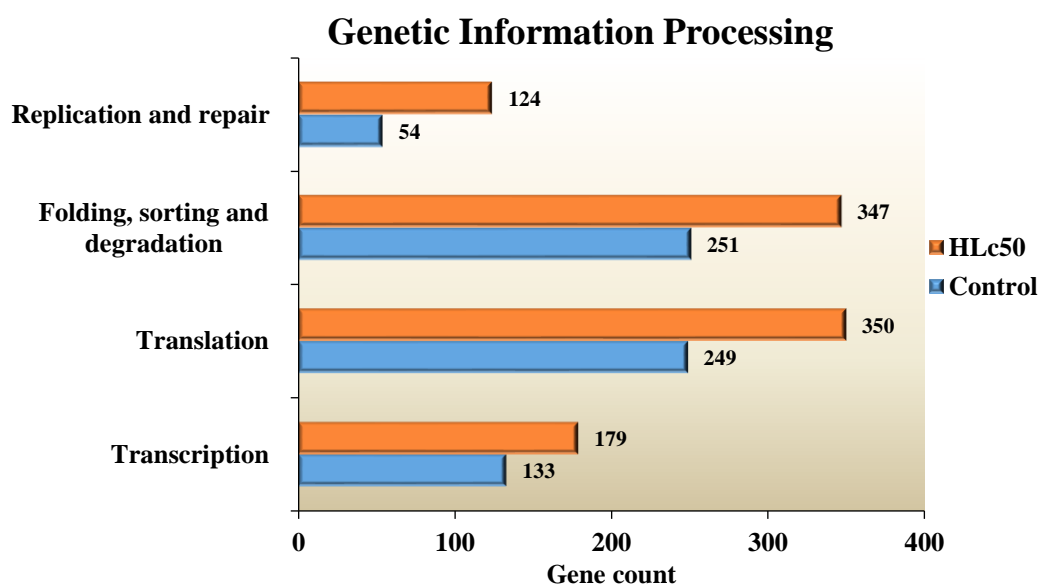


Figure 3.24: Depicts gene count involved in different pathways of the genetic processes.

Table 3.28: Gene counts involved in Transcription: Pathway analysis

Transcription	Control	HLc50
RNA polymerase [PATH: ko03020]	17	22
Basal transcription factors [PATH: ko03022]	20	28
Spliceosome [PATH: ko03040]	77	95

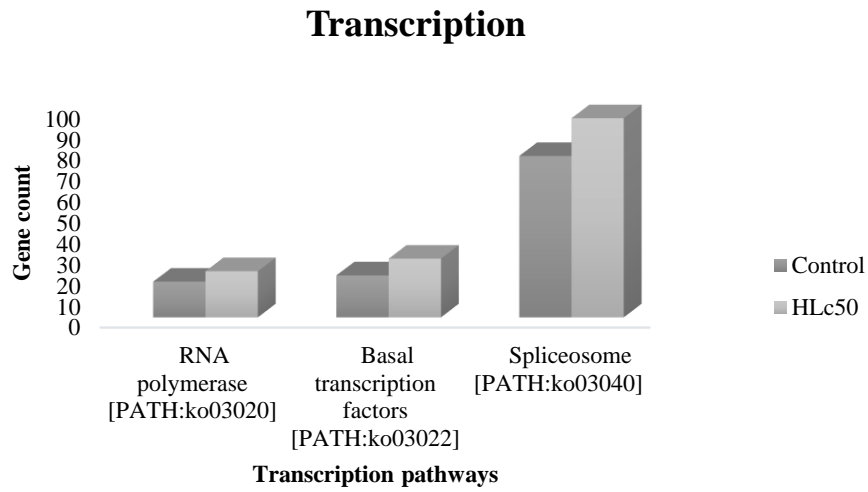


Figure 3.25: Depicts gene counts involved in different pathways of Transcription

Table 3.29: Gene count involved in Translation: Pathway analysis

Translation	Control	H _{Le50}
Ribosome [PATH: ko03010]	99	97
Aminoacyl-tRNA biosynthesis [PATH: ko00970]	22	27
Nucleocytoplasmic transport [PATH: ko03013]	40	75
mRNA surveillance pathway [PATH: ko03015]	43	56
Ribosome biogenesis in eukaryotes [PATH: ko03008]	43	61

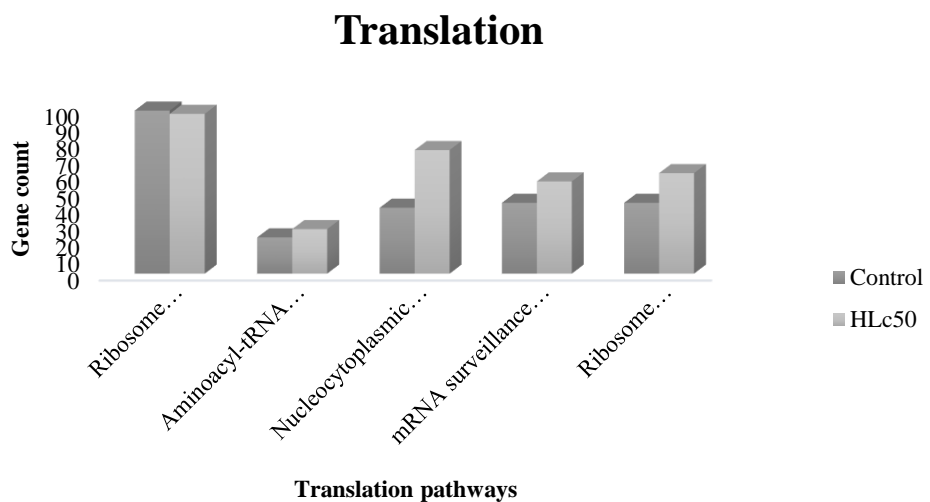


Figure 3.26: Depicts gene count involved in different pathways of Translation

Table 3.30: Gene count involved in Replication and repair: Pathway analysis

Replication and repair	Control	HLc50
DNA replication [PATH: ko03030]	14	30
Base excision repair [PATH: ko03410]	15	26
Nucleotide excision repair [PATH: ko03420]	26	39
Mismatch repair [PATH: ko03430]	9	17
Homologous recombination [PATH: ko03440]	9	24
Non-homologous end-joining [PATH: ko03450]	4	8
Fanconi anaemia pathway [PATH: ko03460]	10	27

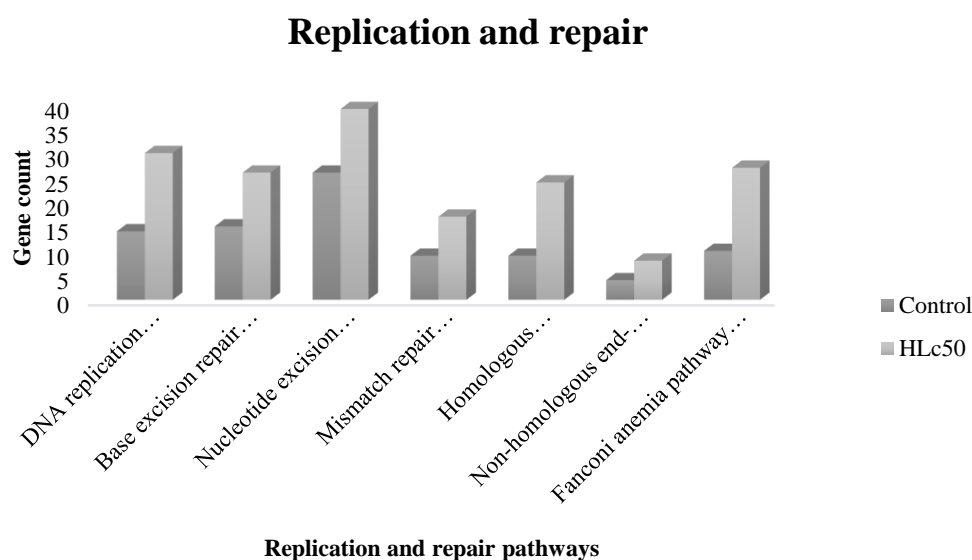


Figure 3.27: Depicts gene count involved in different pathways of Replication and repair

Table 3.31: Gene count involved in Folding, sorting and degradation: Pathway analysis

Folding, sorting and degradation	Control	HLc50
Protein export [PATH: ko03060]	15	17
Protein processing in endoplasmic reticulum [PATH: ko04141]	72	97
SNARE interactions in vesicular transport [PATH: ko04130]	16	18
Ubiquitin mediated proteolysis [PATH: ko04120]	49	83
Sulfur relay system [PATH: ko04122]	2	3
Proteasome [PATH: ko03050]	34	36
RNA degradation [PATH: ko03018]	31	48

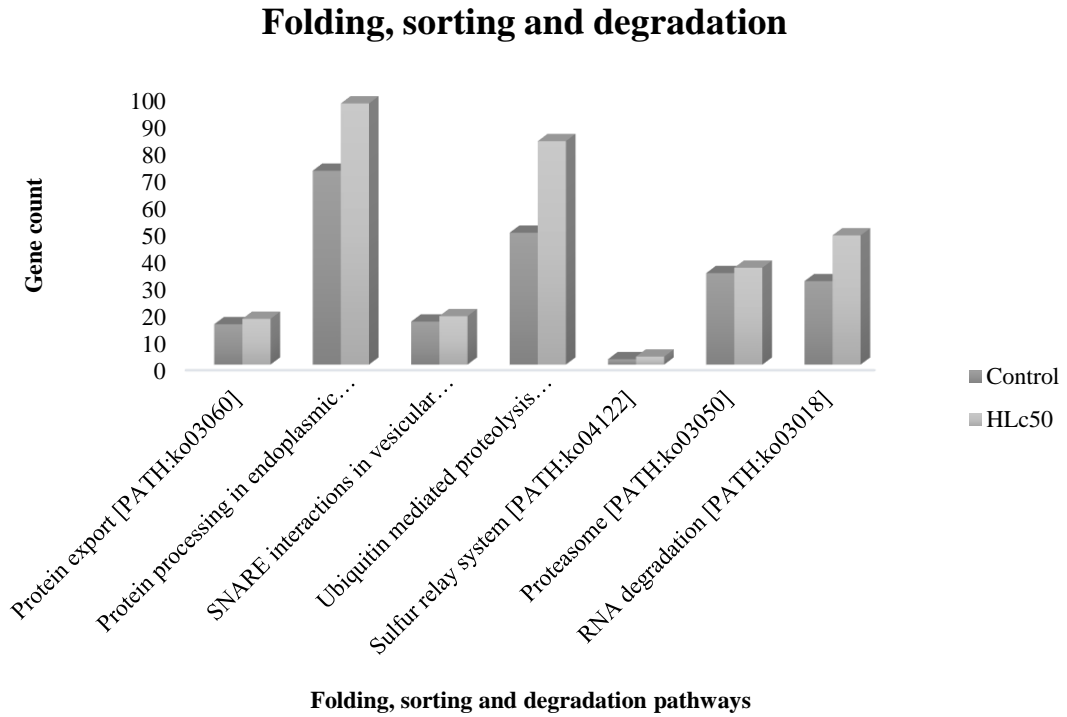


Figure 3.28: Depicts gene count involved in different pathways of Folding, sorting and degradation

Environmental Information Processing

The study revealed a consistent and noteworthy pattern of elevated gene counts in the treated group as compared to the control group, across all pathways associated with the processing of environmental information (**Table 3.32 & Fig. 3.29**). The findings of the **Membrane transport** study revealed a significant increase in the overall number of genes in the treatment group as compared to the control group (**Table 3.33**). Moreover, the results underscored the significance of two notable routes, namely ABC transporters and Bacterial secretion system. Significantly, there was a notable disparity in gene count within the ABC transporters pathway, as the treated group displayed 15 genes while the control group only had 6 genes. In contrast, the number of genes included in the secretion system pathway exhibited stability, since both groups had 2 genes (**Fig. 3.30**). The **Signal transduction** analysis yielded significant findings, showcasing a substantial increase in gene count within the treated group in comparison to the control group. Furthermore, the investigation identified a total of 25 major pathways involved in Signal transduction (**Table 3.34**). Among these pathways, the mTOR signaling pathway displayed the highest gene count, with 60 genes in the treated group and 37 in the control group. Similarly, the MAPK signaling pathway exhibited a consistent trend, with 50 genes in the treated group and 20 in the control group. In contrast, the JAK-STAT signaling pathway had the lowest gene count in the control group (2 genes) compared to the treated group (13 genes), while the Two-component system pathway showed an equal gene count of 7 genes in both groups (**Fig. 3.31**). The findings from the **Signalling molecules and interaction** analysis have highlighted a substantial increase in the overall gene count within the treated group when compared to the control group. Additionally, the investigation identified four major pathways in the Signalling molecules and interaction category, namely Neuroactive ligand-receptor interaction, Cytokine-cytokine receptor interaction, ECM-receptor interaction, and Cell adhesion molecules (**Table 3.35**). The pathway of neuroactive ligand-receptor interaction had the largest number of genes, with 13 genes seen in the treated group and 6 genes in the control group. In contrast, the pathway involving the interaction between cytokines and cytokine receptors exhibited the smallest number of genes, with a total of two genes (one in the control group and one in the treated group). It is significant that the control group exhibited a

complete absence of Cell adhesion molecules, whereas the treated group showed the presence of 9 genes (Fig. 3.32).

Table 3.32: Gene count involved in the Environmental Information Processing

Environmental Information Processing	Control	HLc50
Membrane transport	8	29
Signal transduction	278	572
Signalling molecules and interaction	20	50

Environmental Information Processing

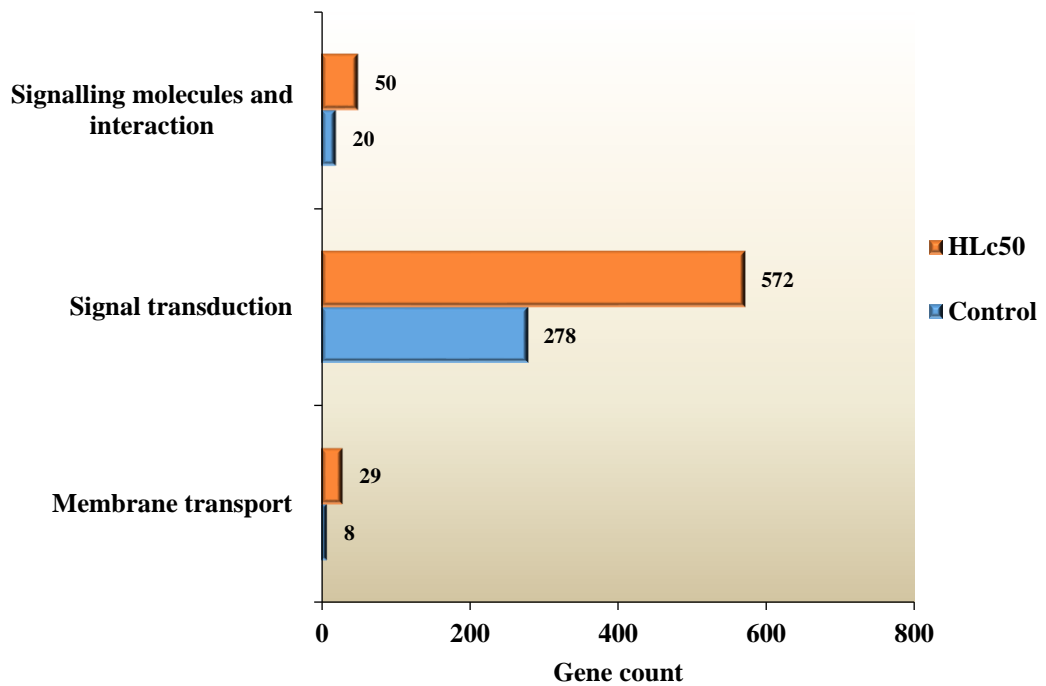


Figure 3.29: Depicts the gene count involved in the Environmental Information Processing

Table 3.33: Gene count involved in Membrane transport: Pathway analysis

Membrane transport	Control	HLc50
ABC transporters [PATH: ko02010]	6	15
Bacterial secretion system [PATH: ko03070]	2	2

Membrane transport

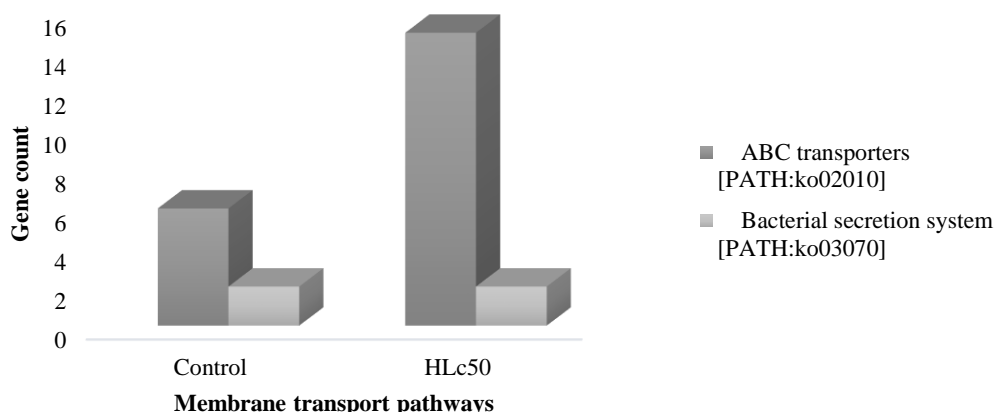


Figure 3.30: depicts gene count involved in different pathways of Membrane transport

Table 3.34: Gene count involved in Signal transduction: Pathway analysis

Signal transduction	Control	HLc50
Two-component system [PATH: ko02020]	7	7
MAPK signaling pathway - fly [PATH: ko04013]	20	50
ErbB signaling pathway [PATH: ko04012]	6	20
Ras signaling pathway [PATH: ko04014]	15	36
Rap1 signaling pathway [PATH: ko04015]	13	36
Wnt signaling pathway [PATH: ko04310]	19	42
Notch signaling pathway [PATH: ko04330]	4	13
Hedgehog signaling pathway - fly [PATH: ko04341]	11	17
TGF-beta signaling pathway [PATH: ko04350]	11	27
Hippo signaling pathway - fly [PATH: ko04391]	13	28
VEGF signaling pathway [PATH: ko04370]	7	11
Apelin signaling pathway [PATH: ko04371]	18	33
JAK-STAT signaling pathway [PATH: ko04630]	2	13
NF-kappa B signaling pathway [PATH: ko04064]	8	17
TNF signaling pathway [PATH: ko04668]	15	24
HIF-1 signaling pathway [PATH: ko04066]	21	31
FoxO signaling pathway [PATH: ko04068]	17	32

Calcium signaling pathway [PATH: ko04020]	18	30
Phosphatidylinositol signaling system [PATH: ko04070]	17	27
Phospholipase D signaling pathway [PATH: ko04072]	13	30
Sphingolipid signaling pathway [PATH: ko04071]	20	34
cAMP signaling pathway [PATH: ko04024]	24	41
cGMP-PKG signaling pathway [PATH: ko04022]	19	30
PI3K-Akt signaling pathway [PATH: ko04151]	29	57
AMPK signaling pathway [PATH: ko04152]	27	41
mTOR signaling pathway [PATH: ko04150]	37	60

Signal transduction

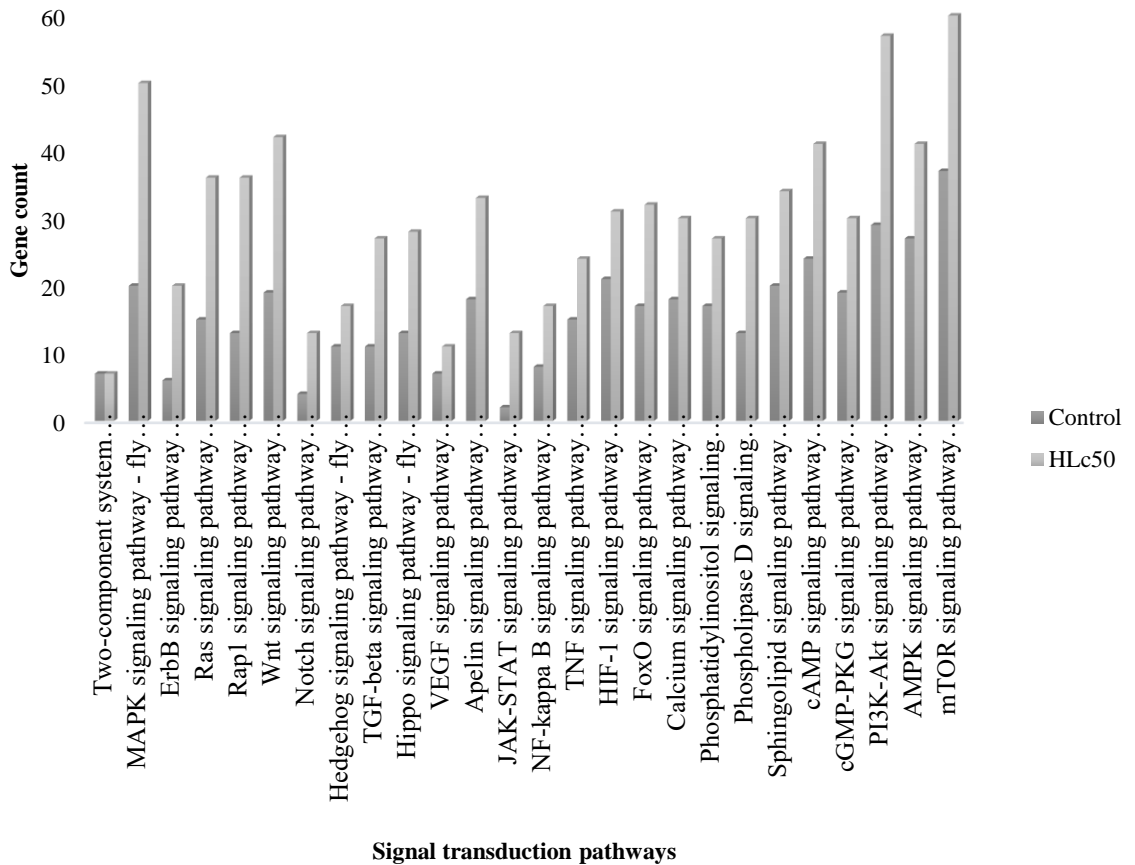


Figure 3.31: Depicts gene count involved in different pathways of Signal transduction

Table 3.35: Gene count involved in Signalling molecules and interaction: Pathway analysis

Signalling molecules and interaction	Control	HLe50
Neuroactive ligand-receptor interaction [PATH: ko04080]	6	13
Cytokine-cytokine receptor interaction [PATH: ko04060]	1	2
ECM-receptor interaction [PATH: ko04512]	2	9
Cell adhesion molecules [PATH: ko04514]	0	9

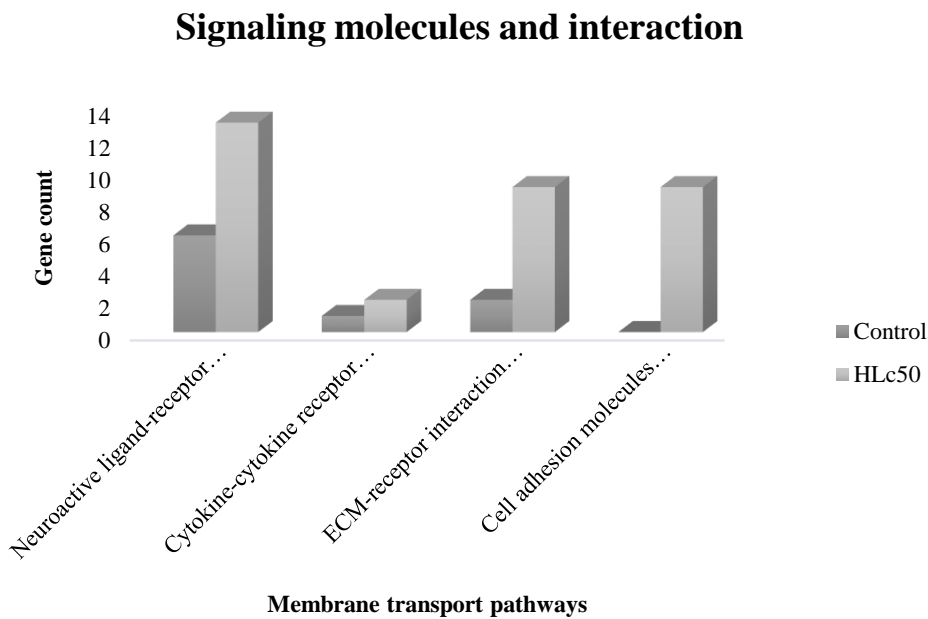


Figure 3.32: Depicts gene count involved in different pathways of Signalling molecules and interaction

Cellular Process

The research findings indicated a significant and notable pattern of increased gene counts in the treated group as compared to the control group. The aforementioned pattern was discerned throughout all **cellular process** pathways (**Table 3.36& Fig. 3.33**). The **Cell organelle process** analysis revealed a substantial rise in gene counts within the treated group when compared to the control group. Additionally, six primary pathways related to the Cell organelle process were identified (**Table 3.37**). In all six pathways, the treated group exhibited a higher gene count than the control group. Notably, the Endocytosis pathway showed the maximum gene count in the treated group (96) compared to the control group (46), while the Mitophagy pathway had the lowest gene count in the control group (21) compared to the treated group (27) (**Fig. 3.34**). The findings derived from the study of the **Cell division and senescence** pathways demonstrate a significant increase in the number of genes within the treated group in comparison to the control group. In addition, we have found ten significant pathways that are connected with the processes of cell division and senescence (**Table 3.38**). Among the pathways examined, the **Cell cycle** pathway exhibited the highest number of genes, with the treated group exhibiting a significant rise of 84 genes compared to the control group, which only showed 27 genes. In contrast, the Cell cycle - Caulobacter pathway had the lowest gene count (2) in both the control and treated groups (**Fig. 3.35**). The results obtained from the analysis of the Cell division and senescence pathways demonstrate a substantial rise in the total gene count within the treated group when compared to the control group (**Table 3.39**). Additionally, when examining five key pathways related to **Cell Communications**, the Tight junction pathway exhibited the highest gene count, with 21 genes in the control group and a notable increase to 43 genes in the treated group compared to the control. Similarly, a minimum gene count was observed in the treated group of Gap junction pathway, with 15 genes compared to the control group, which had 7 genes (**Fig. 3.36**). The results of the Cell motility analysis reveal a significant increase in the total number of genes in the treated group compared to the control group. In addition, two pathways were found in the context of Cell motility: Motor proteins and Regulation of actin cytoskeleton (**Table 3.40**). In each of these pathways, a higher number of genes were identified to be implicated in the treated group (52 and 45) compared to the control group (32 and 20) respectively (**Fig. 3.37**).

Table 3.36: Gene count involved in cellular processes.

Cellular Processes	Control	H _{Lc50}
Cell organelle process	278	462
Cell division and senescence	150	289
Cellular communications	54	143
Cell motility	66	131

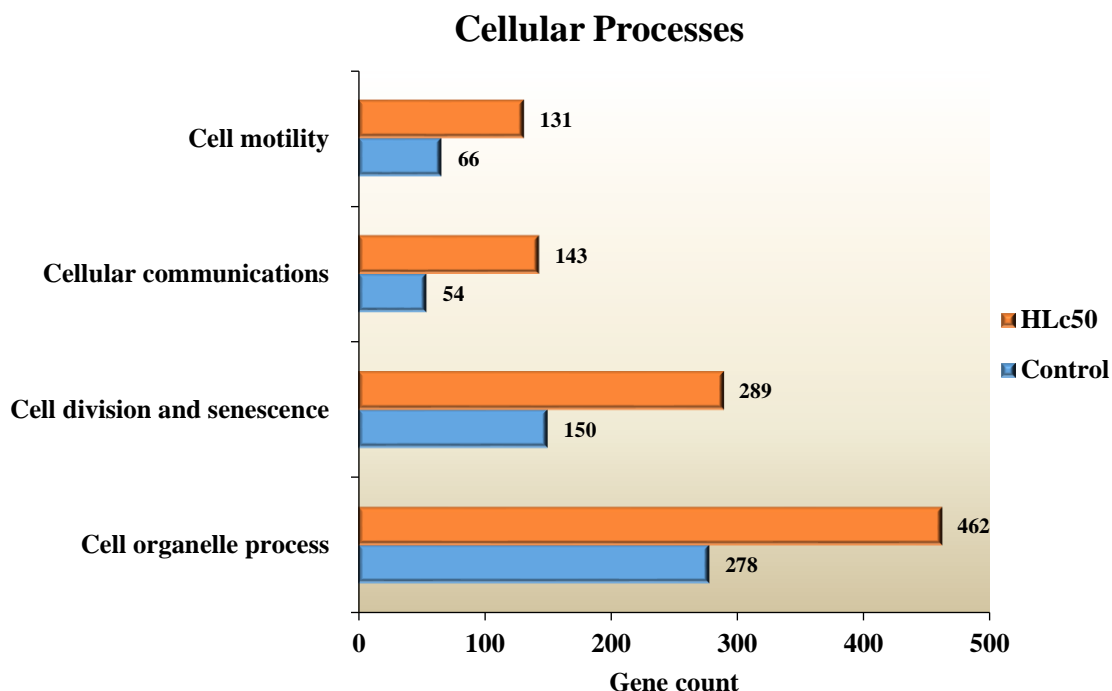


Figure 3.33: Depicts the gene count involved in cell organelle process

Table 3.37: Gene count involved in cell organelle process: Pathway analysis

Cell organelle process	Control	H _{Lc50}
Endocytosis [PATH: ko04144]	46	96
Phagosome [PATH: ko04145]	28	35
Lysosome [PATH: ko04142]	45	61
Peroxisome [PATH: ko04146]	32	45
Autophagy [PATH: ko04140]	39	61
Mitophagy [PATH: ko04137]	21	27

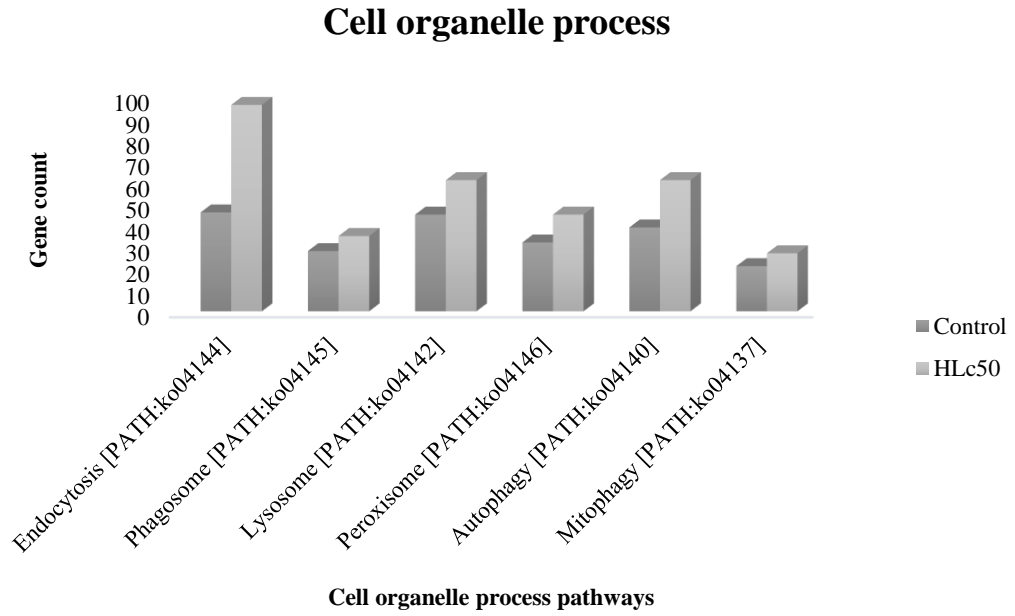


Figure 3.34: Depicts gene count involved in different pathways of Cell organelle process

Table 3.38: Gene count involved in Cell division and senescence: Pathway analysis

Cell division and senescence	Control	HLc50
Cell cycle [PATH: ko04110]	27	84
Cell cycle - Caulobacter [PATH: ko04112]	2	2
Meiosis [PATH: ko04113]	13	41
Oocyte meiosis [PATH: ko04114]	25	44
Apoptosis [PATH: ko04210]	25	36
Apoptosis - fly [PATH: ko04214]	21	34
Ferroptosis [PATH: ko04216]	13	16
Necroptosis [PATH: ko04217]	20	31
p53 signaling pathway [PATH: ko04115]	13	20
Cellular senescence [PATH: ko04218]	20	46

Cell division and senescence

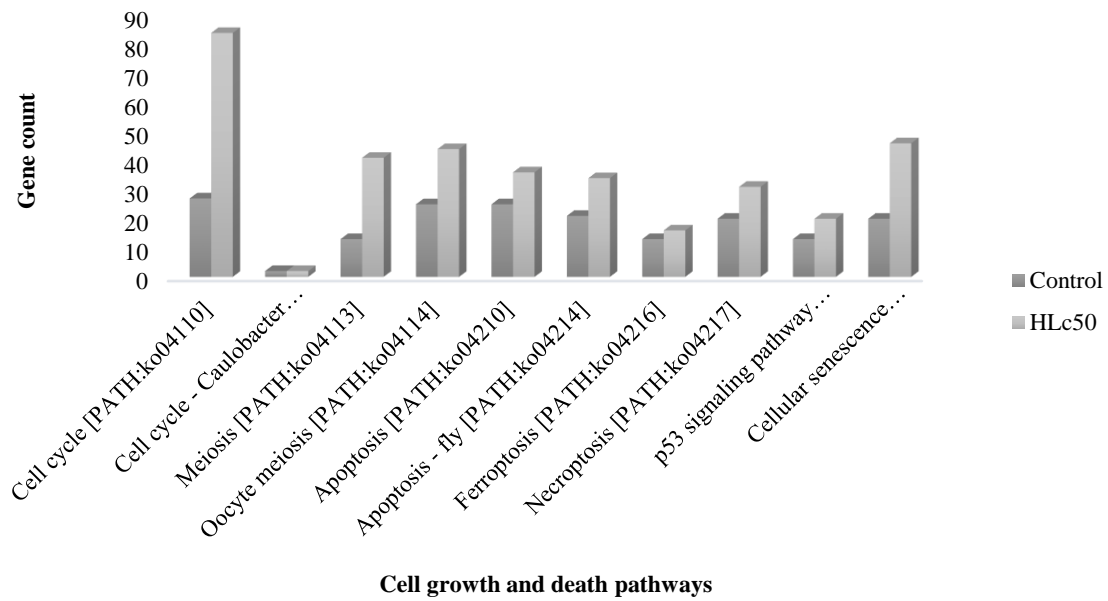


Figure 3.35: Depicts gene count involved in different pathways of Cell division and senescence: Pathway analysis

Table 3.39: Gene count involved in Cell Communications: Pathway analysis

Cell Communications	Control	HLe50
Focal adhesion [PATH: ko04510]	17	42
Adherens junction [PATH: ko04520]	12	28
Tight junction [PATH: ko04530]	21	43
Gap junction [PATH: ko04540]	7	15
Signaling pathways regulating pluripotency of stem cells [PATH: ko04550]	7	26

Cell Communications

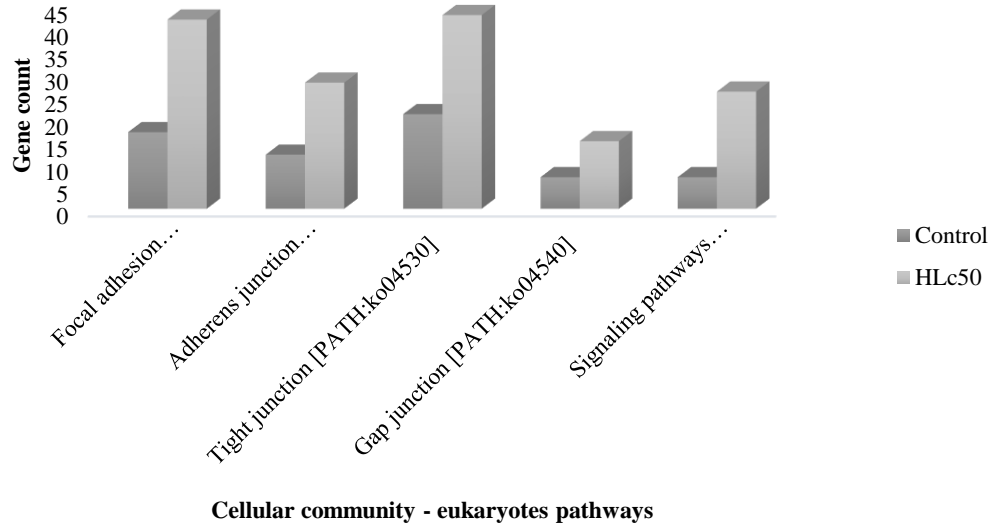


Figure 3.36: Depicts gene count involved in different pathways of Cell communications

Table 3.40: Gene count involved in Cell motility: Pathway analysis

Cell motility	Control	HLc50
Motor proteins [PATH: ko04814]	32	52
Regulation of actin cytoskeleton [PATH: ko04810]	20	45

Cell motility

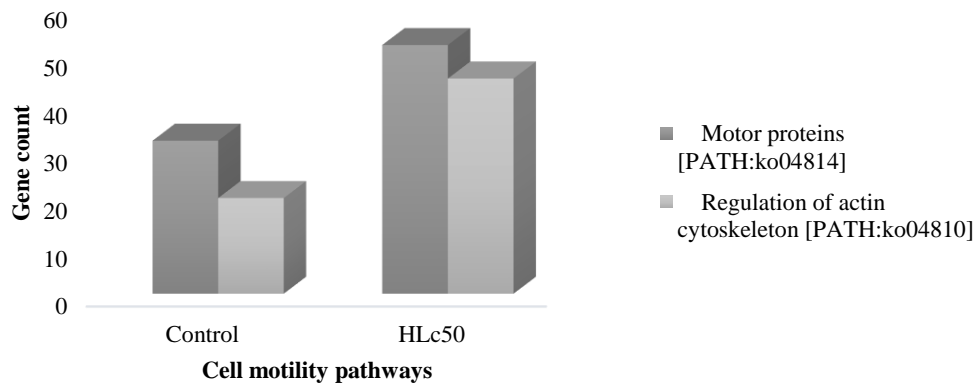


Figure 3.37: Depicts gene count involved in different pathways of Cell motility

Organismal System

The research findings revealed a significant and noteworthy trend of higher gene counts in the treated group as compared to the control group of the **Organismal Systems**. The pattern was seen throughout all pathways of the within the Organismal systems (**Table 3.41 and Fig. 3.38**). The findings related to the **Circulatory system** demonstrate a noteworthy increase in the overall gene count within the treated group when compared to the control group. Furthermore, we identified three major pathways: Cardiac muscle contraction, Adrenergic signaling in cardiomyocytes, and Vascular smooth muscle contraction (**Table 3.42**). In each of these pathways, there was an observed higher gene count in the treated group (21, 30 and 24) compared to the control group (20, 18 and 12) respectively (**Fig. 3.39**). The outcomes obtained from the analysis of **Development and regeneration** point to a significant increase in the total gene count within the treated group when contrasted with the control group. Furthermore, we identified four major pathways: Dorso-ventral axis formation, Axon guidance, Axon regeneration, and Osteoclast differentiation (**Table 3.43**). The highest gene count was observed in the Axon guidance pathway within the treated group (33 genes) compared to the control group (9 genes). Conversely, the lowest gene count was found in the control group for the Dorso-ventral axis formation pathway (5 genes) compared to the treated group (14 genes) (**Fig. 3.40**).

The findings regarding gene counts related to the **Digestive system** indicate a substantial increase in the treated group compared to the control group. We identified a total of ten pathways associated with the digestive system (**Table 3.44**). Among these, the highest number of genes were found in the treated group, with 21 genes in the Hepato-Pancreatic secretion pathway, compared to the control group. Conversely, the lowest gene count was observed in the control group for the Vitamin digestion and absorption pathway, with just 3 genes, as opposed to the 6 genes present in the treated group (**Fig. 3.41**). The results obtained from the RNA-seq analysis indicated a noteworthy increase in gene count within the treated group as compared to the control group in the context of the **Endocrine system**. Specifically, we observed gene counts from a substantial number of pathways (23) related to the endocrine system (**Table 3.45**). Among these pathways, the highest gene count was registered in the Insulin-like signaling pathway, with a significantly higher number in the treated group (45 genes) in comparison to the control group (28 genes). Likewise, the minimum gene

count was also observed, indicating that the control group of the Ovarian-like steroidogenesis pathway had only 2 genes, whereas the treated group had 4 genes (**Fig. 3.42**).

The results of the **Excretory system** demonstrate a significant rise in the number of genes in the treated group in comparison to the control group. In addition, we have discovered five primary routes that are linked to the excretory system (**Table 3.46**). Within the examined pathways, the treated group exhibited the greatest number of genes, namely 15 genes, in the Vasopressin-regulated water reabsorption pathway. In contrast, the control group had a lower gene count of 10. In a similar vein, the control group had the lowest gene count for the Aldosterone-regulated sodium reabsorption pathway, consisting of just 3 genes, in contrast to the treated group which displayed a higher count of 6 genes (**Fig. 3.43**). The RNA sequencing results revealed a significant augmentation in the genes counts in the treated group as compared to the control group of the **Immune system**. A comprehensive analysis was conducted on a significant number of pathways, namely 17, that are associated with the immune system (**Table 3.47**). In the present study, it was observed that the treated group exhibited the greatest gene count in two pathways, namely the NOD-like receptor signalling route and the Chemokine signalling network. Specifically, both pathways displayed a gene count of 35 in the treated group, whereas the control group exhibited a gene count of 25 for the NOD-like receptor signalling pathway and 15 for the Chemokine signalling pathway. On the contrary, the control group of the Natural killer cell-mediated cytotoxicity pathway exhibited the lowest number of genes in the, totalling just 3 genes, whereas the treated group had a higher count of 12 genes (**Fig. 3.44**).

The findings related to the **Nervous system** indicate a noteworthy increase in the overall gene count within the treated group when compared to the control group. We identified a total of ten pathways associated with the Nervous system (**Table 3.48**). Among these pathways, the highest gene count was observed in the treated group, with 35 genes in the Retrograde endocannabinoid signaling pathway, compared to the control group with 33 genes. Conversely, the lowest gene count was recorded in the control group for the Long-term depression pathway, which had only 5 genes, while the treated group had 11 genes (**Fig. 3.45**). The findings related to the **Sensory system** demonstrate a significant rise in the total gene count of the treated group compared to

the control group. Additionally, we have discovered four significant pathways in our study: Phototransduction in flies, Olfactory transduction, Taste transduction, and the modulation of TRP channels by inflammatory mediators (**Table 3.49**). Among these pathways, the highest gene count (12) was observed in the Inflammatory mediator regulation of TRP channels pathway's treated group, in contrast to the control group, which had (6) gene count. Conversely, the lowest gene count was reported in the control group for the Taste transduction pathway, with only (2), whereas the treated group had (5) (**Fig. 3.46**).

The findings regarding Environmental adaptation highlight a notable increase in the overall gene count within the treated group when compared to the control group. We identified a total of five major pathways associated with Environmental adaptation, and interestingly, four of these pathways exhibited a relatively low gene count (**Table 3.50**). However, a significant contrast was observed in the Thermogenesis pathway, with 86 genes in the control group and slightly more, totalling 100 genes, in the treated group. On the other hand, the least number of genes were found in the control group of the Circadian rhythm – fly pathway, with only 3 genes, while the treated group had 8 genes (**Fig. 3.47**).

Table 3.41: Gene count involved in the different organismal system

Organismal Systems	Control	H_{Lc50}
Immune system	144	252
Endocrine system	157	286
Circulatory system	49	74
Digestive system	95	161
Excretory system	41	57
Nervous system	115	175
Sensory system	12	30
Development and regeneration	41	101
Environmental adaptation	120	158

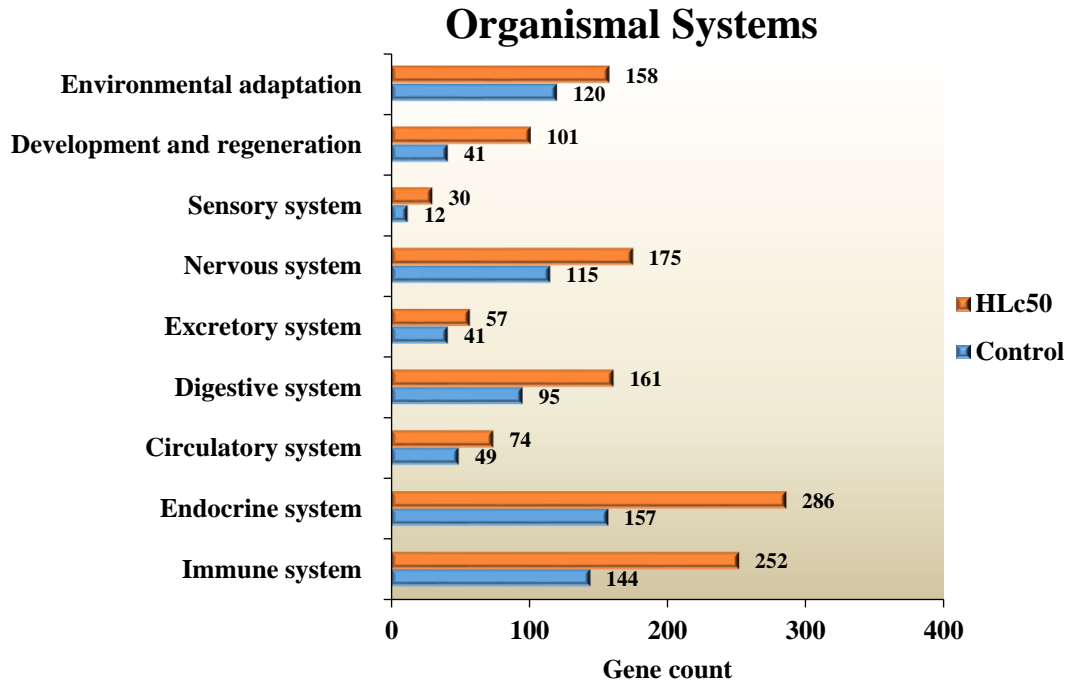


Figure 3.38: Depicts the gene count involved in the different organismal system.

Table 3.42: Gene count involved in Circulatory system: Pathway analysis

Circulatory system	Control	H _{LC50}
Cardiac muscle contraction [PATH: ko04260]	18	21
Adrenergic signaling in cardiomyocytes [PATH: ko04261]	20	30
Vascular smooth muscle contraction [PATH: ko04270]	12	24

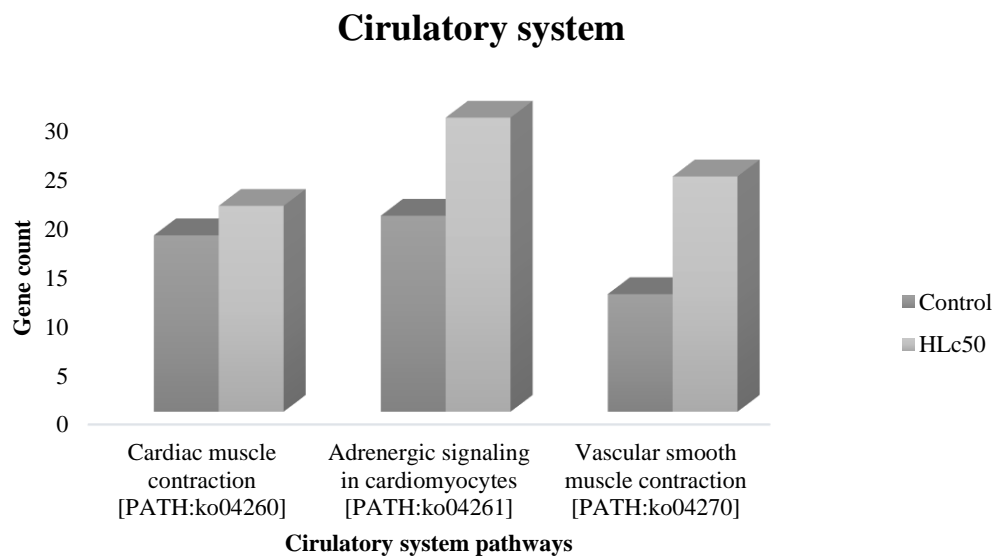


Figure 3.39: Depicts gene count involved in different pathways of Circulatory system: Pathway analysis

Table 3.43: Gene count involved in Development and regeneration: Pathway analysis

Development and regeneration	Control	H _{Lc50}
Dorso-ventral axis formation [PATH: ko04320]	5	14
Axon guidance [PATH: ko04360]	9	33
Axon regeneration [PATH: ko04361]	14	29
Osteoclast differentiation [PATH: ko04380]	11	15

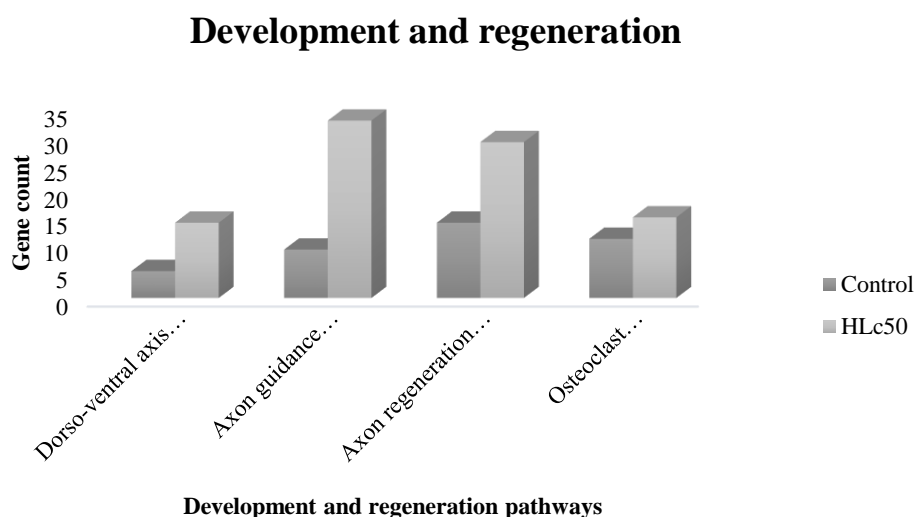


Figure 3.40: Depicts gene count involved in different pathways of development and Regeneration

Table 3.44: Gene count involved in Digestive system: Pathway analysis

Digestive system	Control	H _{Lc50}
Salivary secretion [PATH: ko04970]	8	15
Gastric acid secretion [PATH: ko04971]	6	11
Hepato-Pancreatic secretion [PATH: ko04972]	14	21
Bile secretion [PATH: ko04976]	9	12
Carbohydrate digestion and absorption [PATH: ko04973]	5	8
Protein digestion and absorption [PATH: ko04974]	7	12
Fat digestion and absorption [PATH: ko04975]	10	13
Cholesterol metabolism [PATH: ko04979]	12	13
Vitamin digestion and absorption [PATH: ko04977]	3	6
Mineral absorption [PATH: ko04978]	6	10

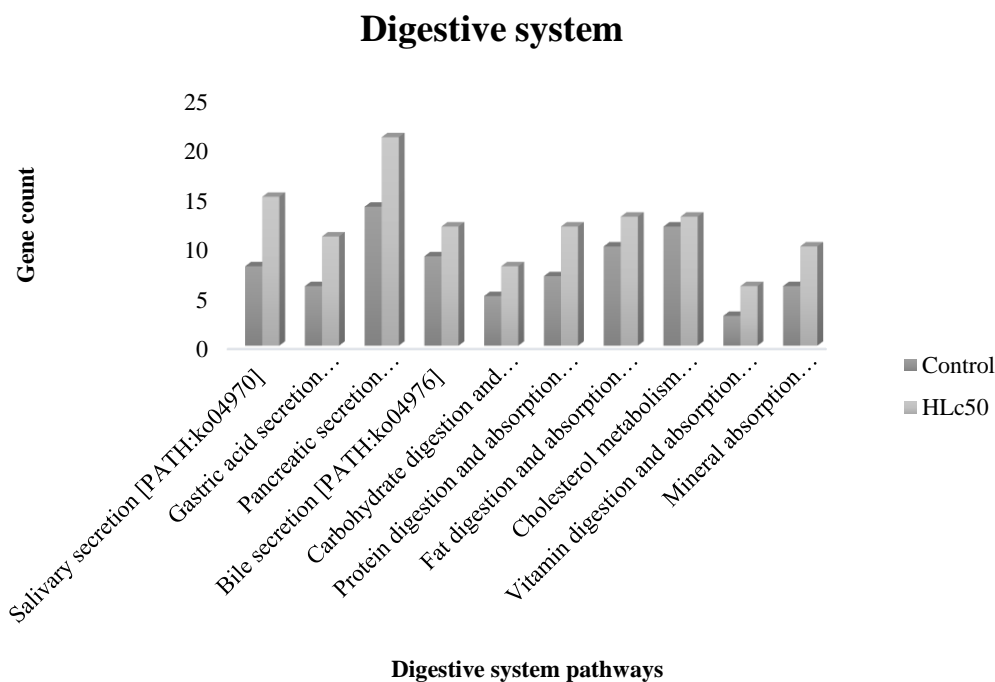


Figure 3.41: Depicts gene count involved in different pathways of Digestive system

Table 3.45: Gene count involved in Endocrine system: Pathway analysis

Endocrine system	Control	HLc50
Insulin like secretion [PATH: ko04911]	9	15
Insulin like signaling pathway [PATH: ko04910]	28	45
Glucagon like signaling pathway [PATH: ko04922]	27	31
Regulation of lipolysis in adipocytes [PATH: ko04923]	5	8
Adipocytokine signaling pathway [PATH: ko04920]	11	17
PPAR signaling pathway [PATH: ko03320]	16	18
GnRH secretion [PATH: ko04929]	5	8
GnRH signaling pathway [PATH: ko04912]	10	21
Ovarian like steroidogenesis [PATH: ko04913]	2	4
Estrogen like signaling pathway [PATH: ko04915]	16	24
Progesterone like mediated oocyte maturation [PATH: ko04914]	16	37
Prolactin like signaling pathway [PATH: ko04917]	7	15
Oxytocin signaling pathway [PATH: ko04921]	18	30
Relaxin signaling pathway [PATH: ko04926]	13	23
Growth hormone synthesis, secretion and action [PATH: ko04935]	12	27

Thyroid like hormone synthesis [PATH: ko04918]	9	16
Thyroid like hormone signaling pathway [PATH: ko04919]	21	38
Parathyroid like hormone synthesis, secretion and action [PATH: ko04928]	8	23
Melanogenesis [PATH: ko04916]	7	15
Renin secretion [PATH: ko04924]	8	13
Renin-angiotensin system [PATH: ko04614]	6	6
Aldosterone synthesis and secretion [PATH: ko04925]	12	18
Cortisol synthesis and secretion [PATH: ko04927]	6	13

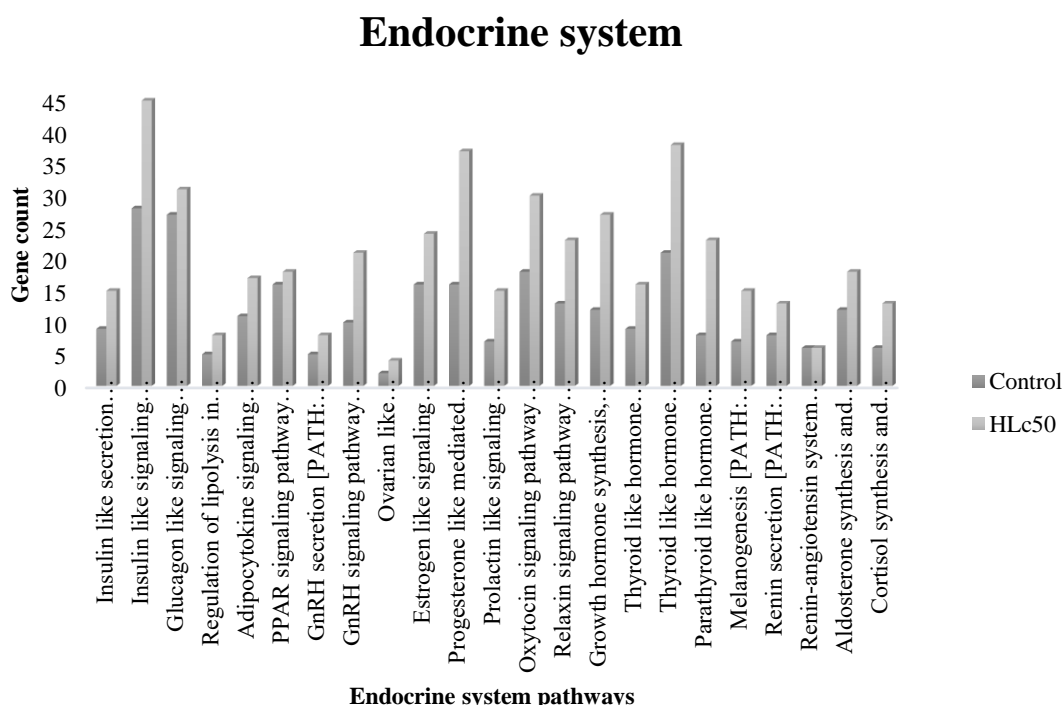


Figure 3.42: Depicts gene count involved in different pathways of Endocrine system

Table 3.46: Gene count involved in Excretory system: Pathway analysis

Excretory system	Control	H _{Lc50}
Vasopressin-regulated water reabsorption [PATH: ko04962]	10	15
Aldosterone-regulated sodium reabsorption [PATH: ko04960]	3	6
Endocrine and other factor-regulated calcium reabsorption [PATH: ko04961]	7	11
Proximal tubule bicarbonate reclamation [PATH: ko04964]	5	7
Collecting duct acid secretion [PATH: ko04966]	9	10

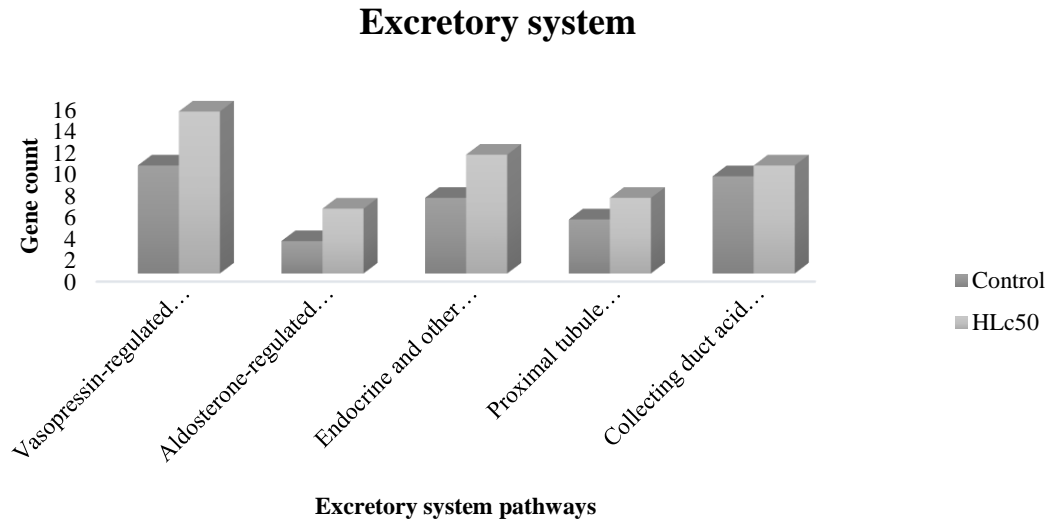


Figure 3.43: Depicts gene count involved in different pathways of Excretory system

Table 3.47: Gene count involved in Immune system: Pathway analysis

Immune system	Control	HLc50
Neutrophil extracellular trap formation [PATH: ko04613]	19	26
Toll-like receptor signaling pathway [PATH: ko04620]	16	22
NOD-like receptor signaling pathway [PATH: ko04621]	25	35
RIG-I-like receptor signaling pathway [PATH: ko04622]	11	14
Cytosolic DNA-sensing pathway [PATH: ko04623]	20	23
C-type lectin receptor signaling pathway [PATH: ko04625]	12	18
Natural killer cell mediated cytotoxicity [PATH: ko04650]	3	12
Antigen processing and presentation [PATH: ko04612]	11	13
T cell receptor signaling pathway [PATH: ko04660]	17	26
Th1 and Th2 cell differentiation [PATH: ko04658]	7	10
Th17 cell differentiation [PATH: ko04659]	8	13
IL-17 signaling pathway [PATH: ko04657]	13	19
B cell receptor signaling pathway [PATH: ko04662]	9	14
Fc epsilon RI signaling pathway [PATH: ko04664]	7	12
Fc gamma R-mediated phagocytosis [PATH: ko04666]	13	26
Leukocyte transendothelial migration [PATH: ko04670]	7	20
Chemokine signaling pathway [PATH: ko04062]	15	35

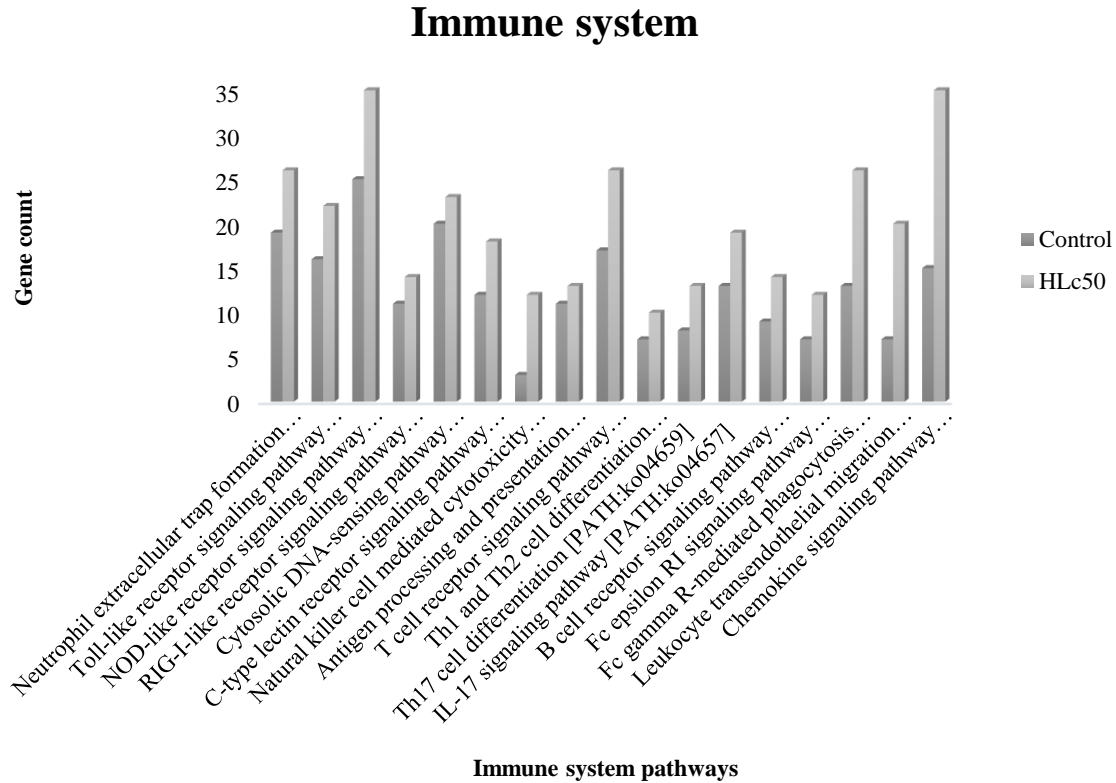


Figure 3.44: Depicts gene count involved in different pathways of Immune system

Table 3.48: Gene count involved in Nervous system: Pathway analysis

Nervous system	Control	HLe50
Glutamatergic synapse [PATH: ko04724]	6	16
GABAergic synapse [PATH: ko04727]	7	15
Cholinergic synapse [PATH: ko04725]	8	16
Dopaminergic synapse [PATH: ko04728]	18	27
Serotonergic synapse [PATH: ko04726]	8	15
Long-term potentiation [PATH: ko04720]	8	13
Long-term depression [PATH: ko04730]	5	11
Retrograde endocannabinoid signaling [PATH: ko04723]	33	41
Synaptic vesicle cycle [PATH: ko04721]	19	29
Neurotrophin signaling pathway [PATH: ko04722]	21	34

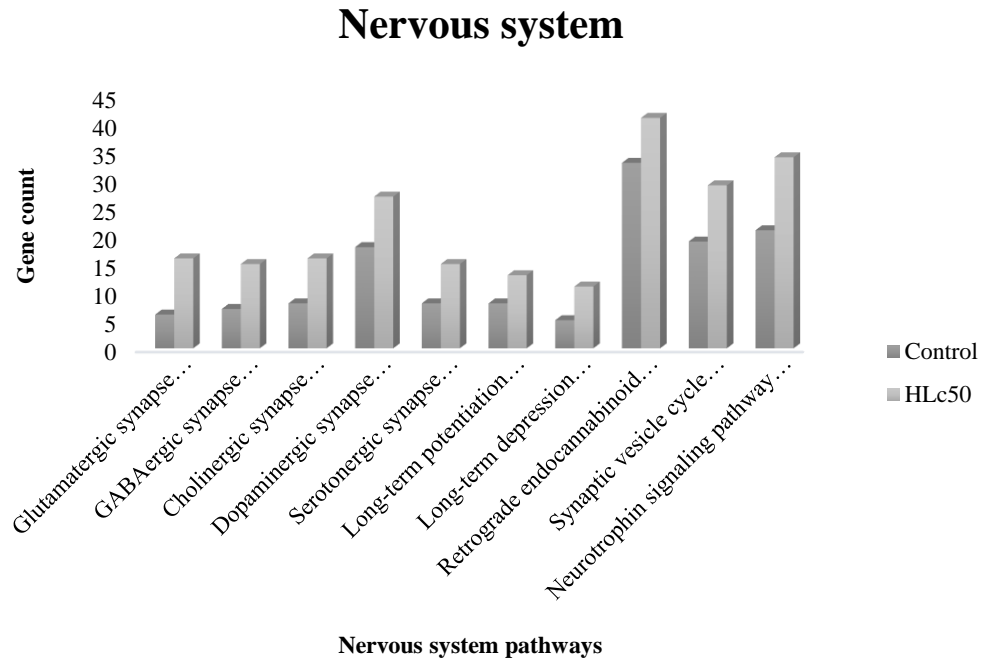


Figure 3.45: Depicts gene count involved in different pathways of Nervous system

Table 3.49: Gene count involved in Sensory system: Pathway analysis

Sensory system	Control	HLC50
Phototransduction - fly [PATH: ko04745]	3	9
Olfactory transduction [PATH: ko04740]	4	9
Taste transduction [PATH: ko04742]	2	5
Inflammatory mediator regulation of TRP channels [PATH: ko04750]	6	12

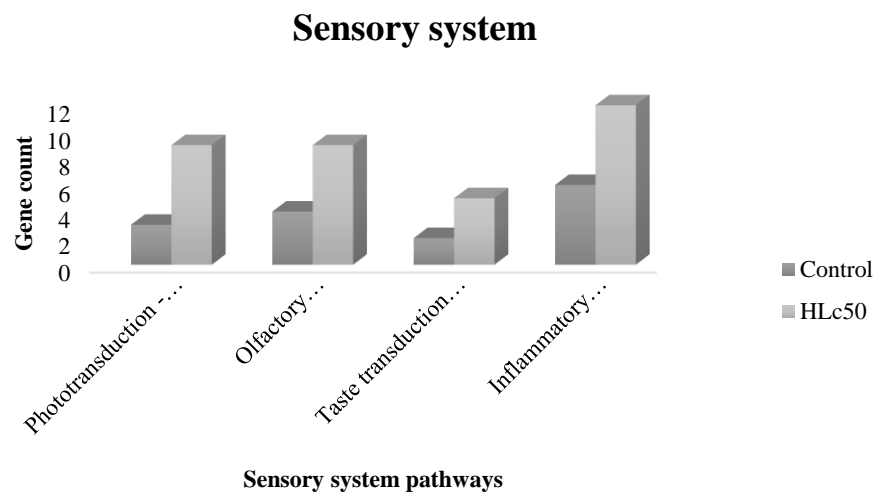


Figure 3.46: Depicts gene count involved in different pathways of Sensory system

Table 3.50: Gene count involved in Environmental adaptation: Pathway analysis

Environmental adaptation	Control	HLc50
Circadian rhythm [PATH: ko04710]	6	11
Circadian entrainment [PATH: ko04713]	7	20
Circadian rhythm - fly [PATH: ko04711]	3	8
Thermogenesis [PATH: ko04714]	86	100
Plant-pathogen interaction [PATH: ko04626]	8	8

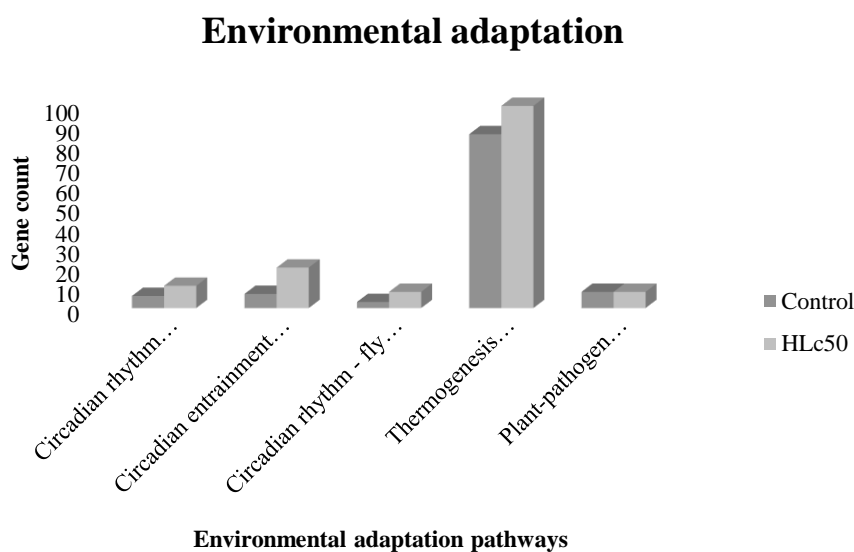


Figure 3.47: Depicts gene count involved in different pathways of Environmental adaptation

Validation of the Gene expression

The metabolic detoxification enzymes of phases I, II, and III and cuticular penetration gene are crucial in the insects to attain insecticide resistance. The current work involved the assessment of phases I, II, III and cuticular penetration gene expressions in order to get insights into the Deltamethrin induced resistance on *C. chinensis*. The findings of this study demonstrated a statistically significant increase ($p < 0.01$) in the mRNA expression levels of Phase I CYP450 genes, including *cyp6bq9*, *cyp4g7*, and *cyp4c3*, as well as the *cnc* transcriptomic factor (Table 3.51 and Fig. 3.48). In a similar vein, the mRNA expression levels of genes such as *gst*, *gstd2*, *gstd3*, *cest4*, *sult1*, and *gpx* were seen to be elevated during Phase II (Table 3.52 and Fig. 3.49). In contrast, the downregulation of Phase I and II genes, such as *sod* and *pdi*, is seen (Table 3.53 and Fig. 3.50). The genes *abc9* and *abc10*, which are associated with

Phase III ATP-binding cassette (ABC) transporters, reported rise in the expression levels (Table 3.54 and Fig. 3.51). An overexpression of cuticular penetration genes, like lac2 and chs2, was also observed (Table 3.55 and Fig.3.52).

Table 3.51: Phase I gene expression *(p<0.05); **(p<0.01).

Gene name	Gene symbol	Control	H _{Lc50}
Cap n Collar (Transcriptomic factor)	cnc	1±0.051	72.17±0.86**
CytochromeP450 6bq9	cyp6bq9	1±0.056	25.98±0.62**
CytochromeP450 4g7	cyp4g7	1±0.045	155.67±0.84**
CytochromeP450 4c3	cyp4c3	1±0.064	81.23±0.51**

Phase I: Upregulated Genes

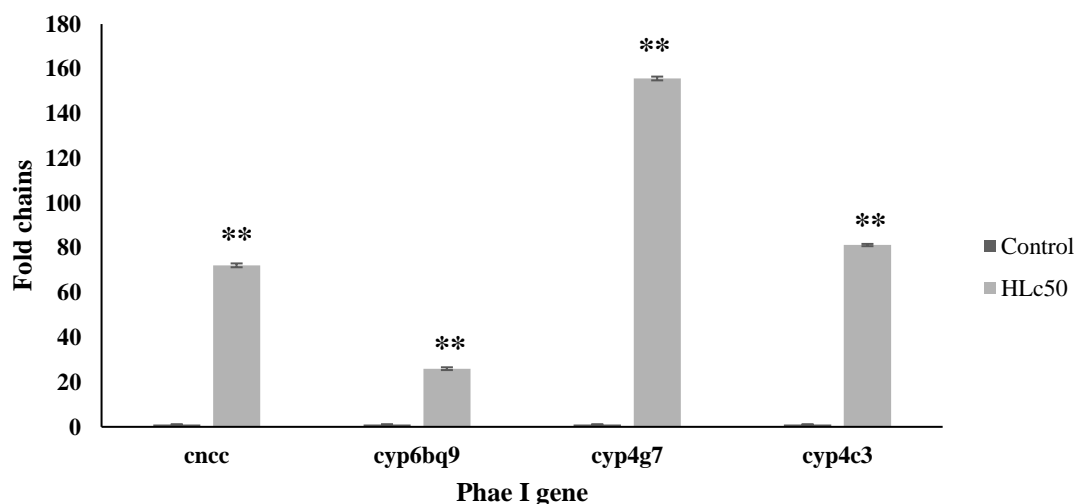


Figure 3.48: Depicts gene expression of the Phase I upregulated genes *(p<0.05); **(p<0.01).

Table 3.52: Phase II gene expression *(p<0.05); **(p<0.01).

Gene name	Gene symbol	Control	H _{Lc50}
glutathione s-transferase	gst	1±0.074	8.56±0.54*
glutathione s-transferase delta 2	gstd2	1±0.038	189.51±0.61**
glutathione s-transferase delta 3	gstd3	1±0.032	70.17±0.56**
carboxylesterase 4	cest4	1±0.075	271.91±0.75**
cytosolic sulfotransferase 1	sult1	1±0.032	84.68±0.86**
glutathione peroxidase	gpx	1±0.050	7.88±0.57*

Phase II: Upregulated Genes

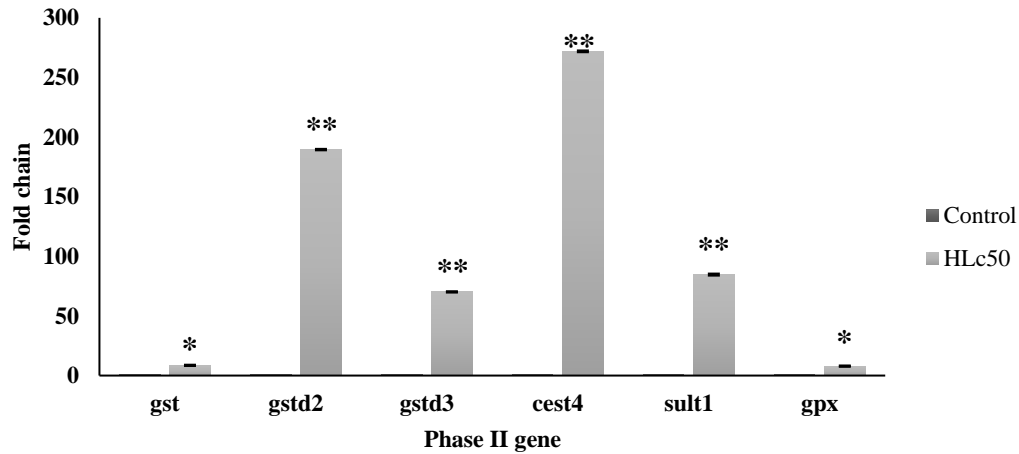


Figure 3.49: Depicts gene expression of the Phase II upregulated genes *(p<0.05); ***(p<0.01).

Table 3.53: Phase I and II downregulated gene expression *(p<0.05); ***(p<0.01).

Gene name	Gene symbol	Control	HLc50
Sodium dismutase	sod	1±0.070	0.02±0.006*
protein disulfide isomerase (p4hb)	pdi	1±0.013	0.12±0.0079*

Phase I and II: Downregulated Genes

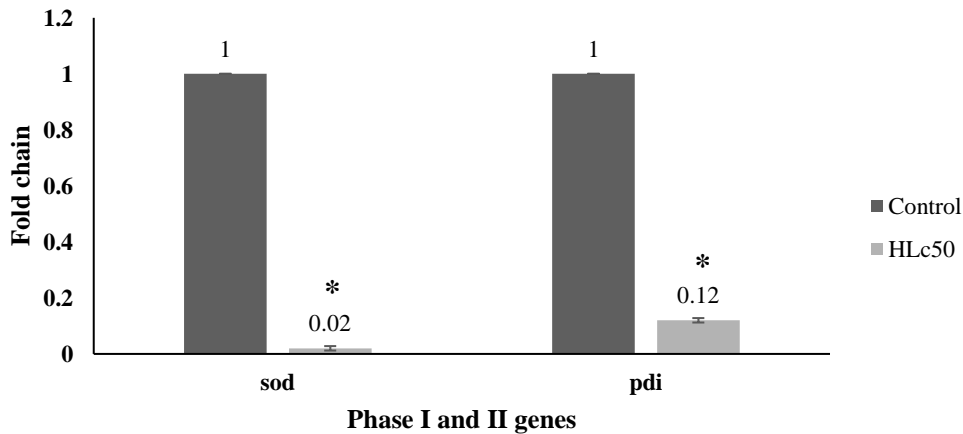


Figure 3.50: Depicts gene expression of the Phase I and II downregulated genes *(p<0.05); ***(p<0.01).

Table 3.54: Phase III gene expression *(p<0.05); **(p<0.01)

Gene name	Gene symbol	Control	H _{Lc50}
ATP-binding cassette (ABC) transporters 9	abc9	1±0.075	39.19±0.36**
ATP-binding cassette (ABC) transporters 10	abc10	1±0.049	20.53±0.50**

Phase III: Upregulated Genes

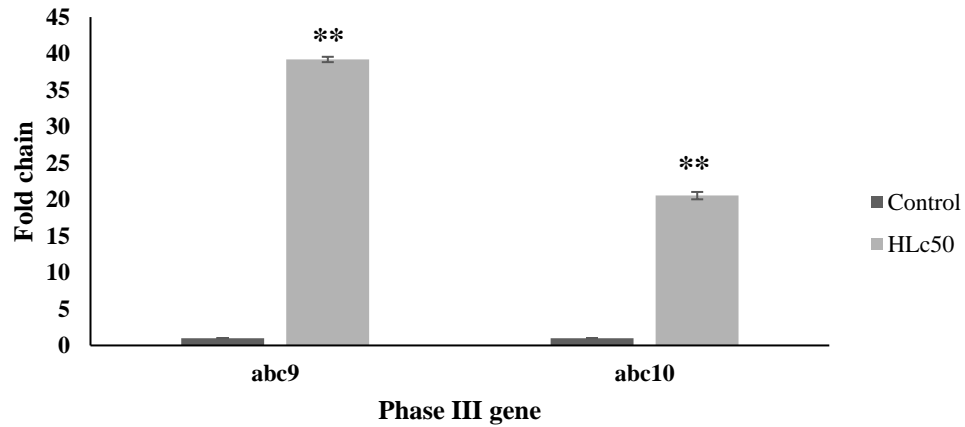


Figure 3.51: Depicts gene expression of the Phase III genes *(p<0.05); **(p<0.01).

Table 3.55: Cuticle penetration genes expression *(p<0.05); **(p<0.01).

Gene name	Gene symbol	Control	H _{Lc50}
laccase2	lac2	1±0.058	15.63±0.66*
chitin synthase 2	chs2	1±0.047	148.86±0.60**

Cuticle Penetration Genes

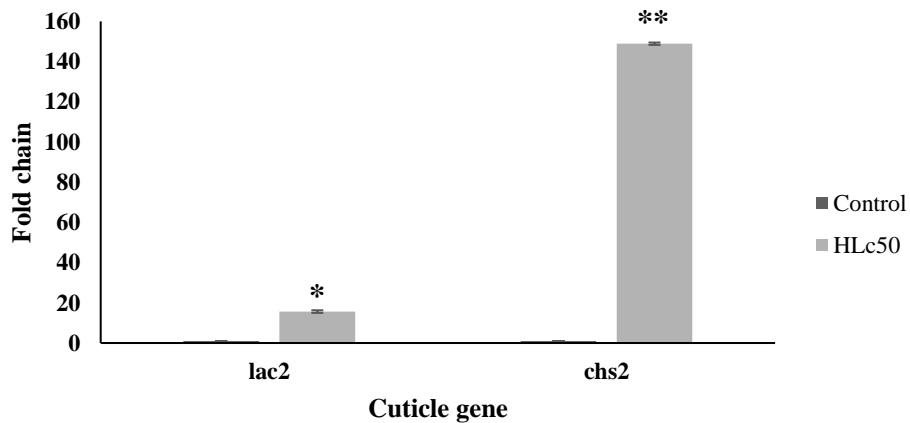


Figure 3.52: Depicts gene expression of the cuticles *(p<0.05); **(p<0.01).

Table 3.56: Summary of the few important differentially expressed genes (DEGs) involved in different pathways.

KEGG pathway	Upregulated genes	Downregulated genes
Amino acid metabolism	trypsin; methyltransferase; serine protease; carboxypeptidase; dehydrogenase; transmembrane protease; aminotransferase; esterase E4; dehydrogenase; amino acid transporter; aminopeptidase	glutamate decarboxylase; amino acid transporter; acid decarboxylase; aminoacylase; serine carboxypeptidase; amino acid oxidase; dehydrogenase; L-aminoadipate-semialdehyde dehydrogenase-phosphopantetheinyl transferase
Carbohydrate metabolism	triosephosphate isomerase; carboxylate transporter; glucosamine-6-phosphate isomerase; chitinase; glycerate kinase; UTP-glucose-1-phosphate uridylyltransferase; acid phosphatase; pyruvate kinase; UDP-galactose transporter; L-galactose dehydrogenase; 1-acyl-sn-glycerol-3-phosphate acyltransferase alpha.	phosphoglucomutase; phosphoglycerate kinase; carboxylate transporter; glucose-6-phosphate isomerase; glycogen phosphorylase; acetylgalactosamine kinase; inorganic phosphate cotransporter; glyceraldehyde-3-phosphate dehydrogenase 2; pyruvate dehydrogenase E1; galactokinase; malate dehydrogenase.
Lipid metabolism	fatty acid synthase; lipase; fatty acyl-CoA reductase; triacylglycerol lipase; inositol-3-phosphate synthase; acyl-CoA synthetase; lipoprotein lipase; pancreatic lipase-related protein 3; desaturase;	fatty acid-binding protein; acyl-CoA-binding protein; acyl-CoA dehydrogenase; carboxylesterase; acyl carrier protein; juvenile hormone esterase; monooxygenase; aminopeptidase N; fatty acids protein; phosphatidylserine synthase
Energy metabolism	ATP synthase; glycerophosphodiester	cytochrome c; ATP synthase; mitochondrial

	phosphodiesterase; NADH dehydrogenase; cytochrome b5; phosphate carrier protein;	glutamate carrier; adenylate cyclase; NADH-cytochrome b5 reductase 3
Xenobiotics metabolism	cytochrome P450; esterase; glutathione-S-transferase; UDP-glycosyltransferase; ATP-binding cassette transporter; Cap n Collar transcriptomic factor; Sulfotransferase	Sodium dismutase; protein disulfide isomerase
Information processing Signal transduction mechanisms	tyrosine-protein kinase receptor; G-protein coupled receptor; MAP kinase-interacting serine/threonine-protein kinase; insulin-like receptor; serine/threonine-protein kinase; tyrosine-protein kinase; scavenger receptor; Rho GTPase-activating protein	mitogen-activated protein kinase 4, nuclear receptor-binding protein; glutamate receptor-interacting protein; mTOR signalling
Post translational modification, protein turnover, chaperones	Hsp70-6; serine protease; Hsp68;	heat shock 70; co-chaperone protein daf-41; chaperone 2; BAG family molecular chaperone regulator 5;

3.4 Discussion

Callosobruchus chinensis is considered a significant pest in the context of pulse crops. Until now, multiple research efforts have focused on exploring the biological and ecological aspects of *C. chinensis*. Effects of lethal concentrations of pyrethroid against stored grain pest have been extensively studied (Vuiez et al., 2017; Shakoori et al., 2018; Karimzadeh et al., 2021; Ortega et al., 2021); however, studies on the toxic effects of pyrethroid are limited. Hence, understanding the mechanisms of insecticide action and effects on the target insect, including potential resistance, is required. Numerous research has been conducted to investigate the impact of pyrethroids on stored grain pests such as *Tribolium*, *R. dominica*, *S. oryzae*, and others. However, a significant gap exists in the literature about studies specifically focused on *C. chinensis*. Therefore, the *C. chinensis* were subjected to deltamethrin exposure, and subsequent analysis of transcriptional alterations was conducted using Rna-seq. A comparative transcriptome study was conducted to compare the gene expression profiles of treated and control *C. chinensis*. The comprehensive examination of the transcriptome of *C. chinensis* resulted in the identification of 58,120 transcripts, of which 25,343 were classified as unigenes. Among these, a total of 13,614 transcripts were determined to be the final coding sequences. The items were classified into distinct functional categories according to their homologous blast results in publicly available databases. The results indicate that 82% of the CDS exhibited a greater degree of similarity with the CDS of *C. maculatus*, a closely related species. This finding has significance as it can serve as a good point of reference for future investigations into gene function characterisation (Sayadi et al., 2016).

In the present work a total of 330 significant differentially expressed genes (DEGs) Out which the top 50 genes were shortlisted and represented in the heatmap form. Previous studies conducted by multiple scientists have reported significant variations in the total differentially expressed genes (DEGs) of various insect pests, such as *S. zeamais*, *P. koraiensis*, *S. frugiperda*, *T. aestivum* and *Sitotroga cerealella* (Liao et al., 2016; Ma et al., 2017; Huang et al., 2018; Hou et al., 2021; Lv et al, 2023) when exposed to insecticides like spinosad, pyrethroid, chlorantraniliprole etc. The discovery and characterization of differentially expressed genes (DEGs) implicated in the action and detoxification of deltamethrin in *C. chinensis* can offer a viable

molecular foundation for understanding the processes behind the toxic effects of insecticide-induced physiological alterations. The findings of the gene ontology (GO) analysis of differentially expressed genes (DEGs) indicated a notable enrichment of "metabolic processes" under deltamethrin exposure. Furthermore, Kyoto Encyclopaedia of Genes and Genomes (KEGG) analysis performed to make predictions about the intricate biological functions of the genes that were altered (either up-regulated or down-regulated). This analysis successfully revealed numerous crucial metabolic pathways, such as carbohydrate, amino acid, lipid, energy, and xenobiotic metabolism. The correlation study conducted between GO and KEGG revealed a significant association between certain critical pathways and the hazardous effects induced by deltamethrin. Additionally, gene counts associated with signal transduction and post-translational modifications, under the category of "information processing," exhibited substantial alterations.

Carbohydrate and energy metabolisms provide the primary source of energy/substrates for daily insect activities. Earlier studies have reported exposure of insecticide results into upregulation (Meng et al., 2019) or downregulation (Gao et al., 2020) of the key players in the metabolism of carbohydrate, which suggests that insecticide treatment may have different effects on the carbohydrate metabolism. In our study, we speculate that carbohydrate may play a vital role in the defence against deltamethrin stress. Numerous studies have been conducted on the impact of insecticide treatments on energy metabolism in insects. For example, Sagri et al. (2014) observed that the energy metabolism in resistant olive flies may play a crucial role in facilitating their detoxification process (needs to be checked), hence suggesting a potential association with insecticide resistance.

The significance of ATPase in ATP synthesis has been well established (Wu et al., 2019). It has been shown that the expression levels of ATPase are influenced by insecticide treatment. Consequently, ATPase expression may lead to heightened resistance to insecticides. NADPH dehydrogenase and COX, which are integral constituents of the mitochondrial respiratory chain, have been identified as prominent targets of numerous insecticides (Luo et al., 2018). Our investigation revealed that the gene expression levels of ATPase and NADH dehydrogenase was significantly downregulated in *C. chinensis* upon exposure to deltamethrin, indicating its impact on energy metabolism. Our finding is in agreement with earlier reported work conducted

by Meng et al. (2019), where they have confirmed a decrease in the energy metabolism components ATPase, NADH dehydrogenase, and COX. These reductions had a negative effect on the growth of the insects.

The metabolism of amino acids plays a crucial role in the synthesis of proteins and the provision of nonessential amino acids and cellular energy. The current study demonstrated a significant enrichment in the metabolic pathways of glycine, serine, threonine, arginine, and proline. These pathways were shown to be related with the enzyme's dehydrogenase, serine protease, and argininosuccinate synthase. Furthermore, the metabolic pathways of glycine, serine, and threonine, as well as the degradation routes of valine, leucine, and isoleucine, exhibited enrichment. These pathways were shown to be connected with dehydrogenases and acetyltransferases according to David et al., (2010) and Wilkins (2017). The outcomes of our study exhibited resemblance to the results obtained by Meng et al. (2019) in their research on *C. suppressalis* subjected to chlorantraniliprole treatment. Differential expression of genes associated with amino acid metabolism was observed in insecticide-resistant and -susceptible strains, indicating a potential role in the establishment of insecticide resistance.

Lipid metabolism is the enzymatic process involved in the digestion, absorption, synthesis, and breakdown of fats with the purpose of generating energy (Jiang et al., 2020). Significantly, it has been documented that alterations in lipid metabolism have an impact on the growth, development, and reproductive processes of insects (Huang et al., 2016; Peng et al., 2018). In the present work the KEGG analysis of control vs treated group revealed that the pathways directly involved in lipid metabolism were enriched in Glycerolipid metabolism, Glycerophospholipid metabolism and Fatty acid degradation. Based on the findings of our study, it is postulated that the exposure to deltamethrin induces notable alterations in lipid metabolism and exerts a substantial impact on the growth, development, and reproductive processes of *C. chinensis*. Additional research is required to provide a comprehensive understanding of the correlation between lipid metabolism and deltamethrin.

Insects have developed complex detoxification mechanisms to metabolise xenobiotics, such as insecticides. These mechanisms are often categorised into three steps (Nakata et al. 2006). During the early phase of the system, cytochrome P450 monooxygenases (P450s) and esterases have a direct role in targeting lipophilic

xenobiotics. These enzymes assist the incorporation of a polar group through oxidation and hydrolysis processes (Hattori et al., 2008). The process of conjugating intermediate metabolites produced by the phase I system with various hydrophilic moieties in order to produce metabolites that are more soluble in water is facilitated by enzymes known as uridine diphosphate (UDP)-glycosyltransferases (UGTs) and glutathione S-transferases (GSTs) in the phase II system (Nakata et al., 2006). The present study categorised DEGs related to the synthesis, transportation, and breakdown of secondary metabolites primarily as P450 enzymes. These enzymes were shown to be enriched in pathways such as "metabolism of xenobiotics by cytochrome P450" and "drug metabolism-cytochrome P450" in both groups. Indeed, the genes *gst*, *gstd2*, *gstd3*, *cest4*, *sult1*, and *gpx* were shown to be significantly ($p < 0.01$) upregulated. The current results are consistent with previous studies conducted by Miah et al. (2019), Simma et al. (2019), and Nagar et al. (2021), which have documented the upregulation of several isoforms of cytochrome P450 enzymes and glutathione-S-transferases in response to deltamethrin.

The ATP-binding cassette (ABC) transporters in the phase III system employ the energy derived from ATP hydrolysis to facilitate the transport of water-soluble metabolites across cellular membranes, ultimately facilitating their excretion from the organism (Meng et al., 2021). In the present study, the ABC transporters, *abc9* and *abc10* exhibited significant ($p < 0.01$) upregulation. This finding aligns with the research conducted by Rösner and Merzendorfer (2020) as well as Liu et al. (2021), both of whom observed upregulation of ABC transporters in response to pesticide exposure. Several studies have proven the correlation between insecticide resistance and three prominent categories of genes responsible for encoding metabolic enzymes, namely P450s, esterases, and GSTs. However, emerging evidence has indicated that the upregulation of genes encoding UGTs and ABC transporters also plays a role in the development of insecticide resistance (Dermauw and Van-Leeuwen, 2014; Meng et al., 2021; Rösner and Merzendorfer, 2020).

The alteration of receptor and kinase expression involved in signal transduction was observed in *C. chinensis* upon exposure to deltamethrin. The differentially expressed genes (DEGs) implicated in signal transduction were mostly categorised under the domain of "environmental information processing" and exhibited enrichment in the "mTOR signalling pathway and MAPK signalling pathway-fly". The Mitogen-

Activated Protein Kinase (MAPK) pathway serves as a fundamental mechanism for the transmission of signals from the extracellular environment to the intracellular space. It is primarily involved in mediating stress responses, such as the cellular reactions to various insecticides (Hotamisligil and Davis, 2016). In our study, several significant signalling mediators' transcripts were detected, such as serine/threonine-protein kinase, insulin-like receptor, MAP kinase-interacting serine/threonine-protein kinase 1, mitogen-activated protein kinase 4, G-protein coupled receptor, tyrosine-protein kinase, nuclear receptor-binding protein, glutamate receptor-interacting protein, ryanodine receptor, and Rho GTPase-activating protein. Additional research pertaining to single cell RNA seq is required to investigate the roles and mechanisms of action associated with these putative signal transduction genes in resistance mechanism.

Posttranslational modifications play a crucial role in maintaining the functionality of proteins, while protein turnover represents the overall outcome of the ongoing processes of protein synthesis and degradation, which are necessary for the maintenance of properly functioning proteins (Mohan, 2009). Moreover, chaperones aid in the folding and assembly of proteins, thereby contributing to the maintenance of cellular homeostasis in both stressed and unstressed cells (Mathangasinghe et al., 2021). Highly sensitive proteins (Hsps) serve as molecular chaperones and exhibit prompt synthesis in reaction to many environmental stressors, such as cold shock, herbicides, and heavy metals (Lu et al., 2017). Hence, it is imperative to do more research on the functioning of Heat Shock Proteins (Hsps) in the context of deltamethrin exposure. Posttranslational changes are of paramount importance in preserving the functioning of proteins. The maintenance of proteins that function optimally necessitates protein turnover, which encompasses the continuous processes of protein synthesis and degradation (Leithe et al., 2018). Moreover, chaperones aid in the folding and assembly of proteins, thereby contributing to the maintenance of cellular homeostasis in both stressed and unstressed cells (Takeuchi et al., 2015). In the present study posttranslational modifications, protein turnover, and chaperones were also impacted by deltamethrin exposure as their total gene count in treated were increased compared to control. Many heat shock proteins (Hsps) like Hsp70-6; Hsp68 were upregulated while heat shock 70; co-chaperone protein daf-41; chaperone 2; BAG family molecular chaperone regulator 5 were downregulated. (Hsps) serve as

molecular chaperones and exhibit prompt synthesis in reaction to many environmental stressors, such as cold shock, herbicides, and heavy metals (Lu et al., 2017). Hence, it is imperative to do more research on the functioning of (Hsps) in the context of deltamethrin exposure.

The present study represents a significant advancement in our understanding of how gene expression can impact various organismal systems. It has shed light on changes occurring within crucial pathways associated with several fundamental aspects of an organism's life, including digestion, development and regeneration, the immune system, circulatory system, excretory system, nervous system, and sensory system. These findings, however, leave us with intriguing questions about the specific roles and consequences of these alterations. The potential link between these gene expression alterations and the emergence of insecticide resistance is particularly intriguing. Investigating this connection is of utmost importance, as it can help us develop more effective strategies for managing insect populations and mitigating the spread of resistance. In conclusion, the findings of this study have opened up exciting avenues for research, emphasizing the need for further investigation into the functions and consequences of these alterations within various organismal systems. This deeper understanding will not only advance our knowledge of basic biology but also have practical implications for fields such as pest control and public health.

The metabolic detoxification system is the major resistance mechanism observed in insects. This mechanism allows insects to efficiently break down or isolate xenobiotics, hence accelerating their degradation process and mitigating their harmful impact. The aforementioned resistance mechanism enables insects to enhance the production of enzymes, including cyp450s, CarEs, GSTs and ABC transporters as a means to counteract the harmful impacts of insecticides (Wang et al., 2016; Bavithra et al., 2023; Tan et al., 2023; Siddiqui et al., 2023). Prior research has indicated a positive association between the levels of P450 expression and the extent of pesticide resistance. In particular, populations that exhibit resistance tend to exhibit an upregulation of many P450 genes (Li et al., 2007). In invertebrates, particularly insects, the homologous counterpart of Nrf2, known as cap 'n' collar isoform C (cncc), assumes a crucial function in defending the organism from oxidative stress. This is achieved through the regulation of several stress-responsive genes, while also contributing to resistance to xenobiotics (Kalsi & Palli, 2017; Pan et al., 2020). The

supergene family of metabolic enzymes known as cyp450s has been the subject of substantial research into the overexpression of cyp genes mediated by several pesticides (Liang et al., 2015). In this study, an observation was made regarding the significant ($p < 0.01$) overexpression of the cyp450 genes, which aligns with previous research findings like, the findings of Zhu et al. (2010) indicate that the upregulation of cyp plays a substantial role in the insect's ability to metabolise insecticides. Similarly, Liang et al. (2015) discovered that three out of the eight selected cyp genes displayed significant expression levels when the insects were exposed to four different insecticides: cypermethrin, permethrin, cyhalothrin, and lambda imidacloprid. The current study has identified the cncc transcription factors as crucial regulators in the activation of cyp genes and the development of deltamethrin resistance. The observed overexpression of cncc in this study aligns with previous findings by Kalsi and Palli, (2017a and 2017b), who reported that cncc functions in a cascade manner when insects are exposed to xenobiotics. The overexpression of cncc leads to the upregulation of phase I cytochrome P450 genes. The results of this study provide additional support for the potential involvement of cyp6bq9, cyp5g7, and cyp4c3 in the detoxification and metabolism of deltamethrin in *C. chinensis*. However, further investigation is required to validate these findings. The complete understanding of the molecular processes underlying the overexpression of P450 genes in insecticide-resistant populations remains limited. Hence, it is imperative to comprehend the regulatory network that orchestrates the expression of genes involved in detoxification response in order to overcome resistance.

GSTs are diverse group of enzymes that plays important role in Phase II detoxification process. The insecticides are metabolised by enzymes through a conjugation process with reduced glutathione, resulting in the formation of hydrophobic xenobiotics. These enzymes then generate water-soluble metabolites that may be readily eliminated. The classification of insect GSTs was determined according to their cellular localization, namely in the cytosol, microsomes, and mitochondria (Liu et al., 2019; Park et al., 2019). These GSTs belong to several protein classes in arthropods, including Delta, Epsilon, Sigma, Theta, Omega, and Zeta (Dai et al., 2016; Han et al., 2016). In the present work, *gst*, *gstd2* and *gstd3* were analysed, notably, all three genes exhibited significant ($p < 0.01$) upregulation following exposure to deltamethrin. The present study aligns with prior research, as,

Song et al. (2020) observed in their study an upregulation in the expression levels of *gstd2* and *gstd3* subsequent to the exposure of phoxim and lambda-cyhalothrin exposed *Tribolium castaneum*. Understanding the process of detoxification mediated by glutathione S-transferase (*gst*) is crucial in identifying resistance at an early stage, eliminating the specific insecticide prior to the fixation of resistance alleles within populations, and facilitating the development of efficacious insecticide molecules.

Carboxylesterases are enzymes that are widely distributed across several biological systems and play a crucial role in the process of detoxifying xenobiotics that contain ester groups. The enzymes belong to the esterase family and have been discovered in several organisms. They are engaged in hydrolytic processes, wherein they catalyse the conversion of carboxyl esters into carboxylic acids and alcohols. The process of hydrolyzing the ester bond encompasses the hydrolysis of many ester substrates, such as phospho, thio, carboxylic, and other esters (Hatfield et al., 2016; Ma et al., 2018; Li et al., 2020; Ding et al., 2022). According to Gong et al. (2014), the level of carboxylesterase expression was shown to be notably higher in the *Aphis gossypii* species that exhibited resistance to organophosphorous (OP) compounds, as compared to the susceptible species. Zhang et al. (2017) observed an increase in carboxylesterase activity and expression in the pyrethroid-resistant species of *Musca domestica*. Additionally, the heightened activity of the CarE enzyme was shown to be associated with the development of tolerance to cypermethrin in *Musca domestica*. In a similar vein, the heightened level of CarE activity seen in both the OP-resistant and susceptible strains of *Nilaparvata lugens*, together with the corresponding upregulation of CarE mRNA expression, indicates a potential association between CarE mRNA and OP resistance in *Nilaparvata lugens*. The present study investigated the expression of *cest4/cest6* in response to deltamethrin exposure. The results demonstrated a significant increase in expression, consistent with previous research by Wei et al., (2019) who has reported the induction of *Tcest4/Tcest6* gene expression following treatment with carbofuran or dichlorvos insecticides. These findings support the notion that *cest4/cest6* play a crucial role in detoxification and contribute to insecticide resistance, as further confirmed by RNA interference experiments targeting *cest4* and *cest6*.

Sulfotransferases (*sults*) are enzymes involved in phase II detoxification processes. They facilitate the sulfonate conjugation of xenobiotics by using 3'-phosphoadenosine

5'-phosphosulfate (PAPS) as the sulfonate donor (Hemmerich et al., 2004; Paul et al., 2012). The sulfs can be categorised into two groups based on their subcellular localization: membrane-associated sulfs and cytosolic sulfs. The metabolism of xenobiotics and small endogenous substrates, including biological amines and hormones, is primarily carried out by cytosolic sulfs. On the other hand, membrane-coupled sulfs are believed to be involved in the sulfonation of macromolecular substances, such as proteins and peptides. This distinction between cytosolic and membrane-coupled sulfs has been discussed in studies by Alnouti and Klaassen (2008) and Paul et al. (2012). The process of sulfoconjugation, which is facilitated by SULT enzymes, plays a significant role in the metabolic conversion of several medications in mammals (Hemmerich et al., 2004; Gamage et al., 2006; Hattori et al., 2008; Suiko et al., 2017). In the present study, we examined the expression of the *sult1* gene and determined that it exhibits a significant ($p < 0.01$) upregulation in response to deltamethrin exposure. In recent years, an increasing amount of evidence has been gathered indicating that the transcriptional factor *cnc* plays a pivotal role in regulating the expression of the genes responsible for encoding enzymes and transporters involved in insecticide detoxification and metabolic resistance (Hirotsu et al., 2012; Deng and Kerppola, 2013; Kalsi and Palli, 2015; Wilding, 2018; Palli, 2020). The present finding has once again provided the same confirmation.

Glutathione peroxidase is recognised for its ability to neutralise various organic hydroperoxides that are generated during lipid peroxidation (LPO), converting them into their respective hydroxyl molecules (Kolawole and Kolawole, 2014). This process involves the utilisation of glutathione (GSH) and other reducing equivalents. According to Xiong et al. (2013), the enzyme glutathione peroxidase serves as a protective mechanism for cells when exposed to mild oxidative stress. The observed significant ($p < 0.01$) upregulation in glutathione peroxidase activity in the current investigation may be attributed to the increased concentration of deltamethrin. The process of detoxifying reactive oxygen species (ROS) and hydroperoxides involves the oxidation of reduced glutathione (GSH) to its oxidised form, glutathione disulfide (GSSG), by the enzyme glutathione peroxidase. GSSG is then converted to GSH by the action of GR, utilising NADPH as a source of energy (Narayanankutty et al., 2019). The observed inverse relationship between the activities of Glutathione

peroxidase (GPx) and GR in the stressed bruchid aligns with the pattern observed in the presence of insecticides.

Superoxide dismutase (sod) plays a vital role as an enzymatic component in insects, fulfilling various functions including modulation of immune response, mitigation of damage caused by free radicals, and protection of cellular integrity against adverse environmental factors (Dubovskiy et al., 2008; Piedrafita et al., 2015; Sharmen et al., 2023). Prior research has established that the use of abamectin led to elevated levels of superoxide dismutase (sod) activities in *Harmonia axyridis*, as compared to the control group (Wang et al., 2011). Nevertheless, as time elapsed, this sod activities exhibited a gradual restoration towards their initial levels (Cao et al., 2019). The current study observed a significant ($p < 0.05$) reduction in the expression of the sod gene following exposure to deltamethrin. This finding is consistent with the previous study done by Shan et al. (2020), which found a negative correlation between pesticide concentration and superoxide dismutase (sod) activity.

Protein disulphide isomerase (pdi) is a crucial participant in several physiological processes due to its oxidoreductase activity and molecular chaperone function (Meng et al., 2021a). The enzyme pdi has the ability to facilitate the creation of disulfide bonds in substrate proteins by means of its oxidoreductase activity. Additionally, pdi is capable of rearranging improperly generated disulfide bonds through its isomerase activity (Fu et al., 2020). Furthermore, pdi exhibits molecular chaperone functionality, hence enhancing the efficiency of protein oxidative folding and mitigating protein aggregation. It is worth mentioning that the molecular chaperone activity of pdi is contingent upon the maintenance of redox equilibrium (Tsai et al., 2001; Nakamura, & Lipton, 2011; Meng et al., 2021a). The phenomenon of pdi has been widely investigated in various organisms, particularly yeast and humans. However, there is a scarcity of relevant research on insects. In this study, we examined the expression of pdi in response to deltamethrin and our findings indicate a significant ($p < 0.05$) downregulation of pdi. Based on the findings of our study, it can be inferred that the pdi enzyme may have implications in the antioxidant properties exhibited by *C. chinensis*.

ABC transporters are involved in phase III processes and use the energy derived from the hydrolysis of ATP to transport a diverse range of physiological metabolites and Xenobiotics (Merzendorfer, 2014). Insecticide resistance has been associated with

certain members of these families, namely within subfamilies B and C (Dermauw and van Leeuwen, 2014). The probable involvement of genes encoding ABC transporters in the process of water solubilization and excretion of pesticides in pests has been described in studies conducted by Gott et al. (2017) and Huang et al. (2018). The role of ABC transporter genes in conferring resistance to insecticides has been investigated in *S. frugiperda* and several other insect species (Merzendorfer, 2014; Chen et al., 2016a). The current study reveals a significant ($p < 0.05$) rise in the expression levels of *abc9* and *abc10*. The present discovery aligns with prior research conducted by Kalsi and Palli (2017a), who identified four ABC transporters in a strain that demonstrated resistance to pyrethroids like tefluthrin. Moreover, Rösner and Merzendorfer (2020) has substantiate the participation of ABC transporters in the detoxifying mechanism of the chitin synthesis inhibitor DFB.

Chitin, a polysaccharide composed of N-acetyl-b-D-glucosamine monomers is present in several tissues and organs of insects, including the epidermis, trachea, and peritrophic membrane (Arquette & Rodriguez, 2013; Zhuo et al., 2014). Chitin has a vital role in maintaining the structural integrity of insects and protecting them from stresses from the outside (Merzendorfer, 2011; Wang et al., 2012). The phenomenon of chitin production is distinguished by a state of dynamic equilibrium between chitin synthase (*chs*) and chitinase, an enzymatic catalyst accountable for the degradation of chitin (Toprak et al., 2016; Alvarenga et al., 2016). The enzyme known as *chs* plays a pivotal part in the intricate process in chitin formation and is an essential need for the growth and development of insects (Van Leeuwen et al., 2012). The genes responsible for encoding *chs* belong to a gene family and are commonly classified as *chs1* and *chs2*.

The enzyme *chs1* has been identified as the primary catalyst for chitin production in the cuticle and cuticular lining of the foregut, hindgut, and trachea in *Anopheles gambiae* (Zhang et al., 2012), *T. castaneum* (Arakane et al., 2008), and *Locusta migratoria* (Liu et al., 2012). In contrast, *chs2* has been found to have a specialised role in chitin synthesis inside the peritrophic matrix in many species, including *A. gambiae* (Zhang et al., 2012), *T. castaneum* (Arakane et al., 2005b), *Ostrinia nubilalis* (Khajuria et al., 2010), *L. migratoria* (Liu et al., 2012), and *Culex*. In the present study, the expression of *chs2* was shown to be significant ($p < 0.01$) upregulated. This finding aligns with the earlier investigation conducted by Zhang et al. (2012),

whereby they quantified the expression of *chs2* across different anatomical regions and tissues. The abdominal region had the highest degree of expression, followed by the midgut region which displayed a following level of expression. The heightened degree of manifestation observed in the abdominal area might potentially be linked to the existence of gastrointestinal tissue within this anatomical locality. The results suggest that *chs2* may play a significant role in the morphogenesis of gastrointestinal tissue. Our results are consistent with the documented roles of *chs2* in the formation of the peritrophic membrane, as reported in previous research (Bolognesi et al., 2005). To get a more complete comprehension of the biological mechanisms linked to chitin synthesis, it is crucial to undertake a systematic study of chitin synthase genes across a diverse array of insect species.

Insects acquire resistance to external factors by modifying the thickness or composition of their cuticular barriers (Lilly et al., 2016; Balabanidou et al., 2018). Additionally, they also remodel the cuticle through the abundant presence of cuticular proteins. The presence of laccase enzyme is facilitated the defence mechanism by promoting the synthesis of a more substantial cuticle, so impeding the penetration of insecticide into the insect's body (Dubovskiy et al., 2013; Ding et al., 2022). Prior research has established that the increased expression of *laccase2* is associated with changes in cuticle composition (Ye et al., 2021), hence augmenting insects' ability to withstand insecticides in their surroundings. Arkane et al. (2005a) demonstrated the correlation between cuticle tanning and the expression profile of *lac2* throughout the developmental stages from pupation to adult eclosion. The findings of this study align with the reported mode of action and its association with resistance. Specifically, the significant ($p < 0.01$) upregulation of *lac2* has been observed to facilitate changes in the cuticle composition, leading to a decrease in penetration and acting as a protective mechanism against deltamethrin (Julio et al., 2017). Therefore, the future research of cuticular proteins can establish a solid basis for the identification of key contributors to the cuticular resistance mechanism. This, in turn, can facilitate the formulation of novel methods for managing resistance.

3.5 Conclusion

The complete study of genomic and transcriptomic data has successfully revealed the important genes responsible for producing detoxifying enzymes, including *cyp450s*, *gst*, and *caes*. Additionally, genes associated with cuticle penetration, such as *chs2* and *lac2*, have also been found. Nevertheless, the verification of the majority of genes' contributions still necessitates substantial genetic investigation, such as RNA interference (RNAi) and gene functional characterization. The downregulation of overexpressed detoxifying genes in *C. chinensis* has the potential to uncover and clarify the activities of these genes, as well as offer insights into the causes contributing to the resistance of *C. chinensis*. The experimental approach utilising double-stranded RNA interference (RNAi) can serve as a valuable tool in elucidating the underlying processes responsible for resistance development. Collectively, RNA-seq technology proves to be a proficient instrument for investigating the molecular pathways behind the adverse effects of sub-lethal dosages of pesticide in *C. chinensis*. The study of the transcriptome revealed that differentially expressed genes (DEGs) were found to be considerably enriched in pathways related to metabolism and information processing. These findings suggest that these pathways may be involved in insecticide detoxing mechanisms. The findings of our study indicate that sublethal exposures to deltamethrin can lead to the upregulation or downregulation of *cyp450s*, *cest*, *gsts*, *abc* transporters along with the cuticular genes. These findings hold particular importance in enhancing our comprehension of the activities of detoxification-related genes in *C. chinensis*. The data presented in this study elucidate the systematic toxicity processes triggered by deltamethrin. These findings have significant implications for the evaluation of hazards and risks associated with the environmental management of this particular insecticide.